"TIQXMMI" NATIONAL RESEARCH UNIVERSITY INSTITUTE OF
FUNDAMENTAL AND APPLIED RESEARCH

UDC: 530.12:531.51

BOBUR VALENTINOVICH TURIMOV

ENERGETIC PROPERTIES OF BLACK HOLES IN SCALAR-TENSOR-VECTOR GRAVITY

01.04.02 - THEORETICAL PHYSICS

01.03.01 - ASTRONOMY

DISSERTATION OF THE DOCTOR OF SCIENCES (DSc)
IN PHYSICS AND MATHEMATICS

Scientific advisors:

BOBOMURAT J. AHMEDOV

doctor of sciences in physics and mathematics, academician

AHMADJON A. ABDUJABBAROV

doctor of sciences in physics and mathematics, professor

TASHKENT - 2026

When asked "Dr. Einstein, why is it that when the mind of man has stretched so far as to discover the structure of the atom we have been unable to devise the political means to keep the atom from destroying us?" That is simple, my friend. It is because politics is more difficult than physics.

Albert Einstein

Contents

Introduction **8**

I Scalar-Tensor-Vector Gravity **21**

1.1 Introduction 22

1.2 Background spacetime and particle dynamics 29

1.3 Massless particle motion 32

1.3.1 Strong Gravitational Lensing 32

1.3.2 Weak Gravitational Lensing 36

1.4 Massive particle motion 38

1.4.1 Orbital precession of S2 star 42

1.5 Conclusion 49

II Penrose process in the vicinity Kerr-MOG black hole **51**

2.1 Introduction 51

2.2 Axially-symmetric black hole solution 55

2.3 Penrose process 62

2.4 Collision of two massive particles near Kerr-MOG black hole 66

2.5 Conclusions 72

III Gravitational synchrotron radiation and radiation reaction **76**

3.1 Introduction 77

3.2 Gravitational synchrotron radiation 79
3.3 Gravitational radiation reaction 82
3.4 Conclusion 87

IV Black hole perturbations in STVG **89**

4.1 Introduction 89
4.2 Thermodynamic properties of black hole 94
4.3 Black hole perturbations 99
4.4 Scalar perturbations 101
4.5 Electromagnetic perturbations 104
4.6 Gravitational perturbations 106
4.6.1 Axial gravitational perturbations and Regge-Wheeler equation 109
4.7 Method and Results 113
4.8 Conclusion 117

Main results and conclusions **119**

Acronyms

STVG	**S**calar-**T**ensor **V**ector **G**ravity
MOG	**MO**dified **G**ravity
GR	**G**eneral **R**elativity
BD	**B**rans–**D**icke
ISCO	**I**nnermost-**S**tabe **C**ircular **O**rbit
PDE	**P**artial **D**ifferential **E**quation
ODE	**O**rdinary **D**ifferential **E**quation
DM	**D**ark **M**atter

Some experimental and observational data

Electron rest mass	$m_e \simeq 9.109 \times 10^{-34}$ g
Elementary charge	$e \simeq 1.602 \times 10^{-19}$ C
Solar mass	$M_\odot \simeq 1.9 \times 10^{33}$g

Physical constants & other definitions

Newtonian gravitational constant	$G_N \simeq 6.672 \times 10^{-8}$ cm^3 g^{-1} s^{-2}
Speed of Light	$c \simeq 2.998 \times 10^{10}$ cm $\cdot$ s^{-1}
Reduced Plank constant	$\hbar = h/2\pi \simeq 1.054 \times 10^{-27}$ g cm^2 s^{-1}
Boltzman constant	$k_{\rm B} \simeq 1.608 \times 10^{-16}$g $\cdot$ cm^2 $\cdot$ s^{-2} $\cdot$ K^{-1}

1 parsec = 1 pc = 3.26 ly = 3.08×10^{18} cm

1 eV = 1.6×10^{-19}J = 1.6×10^{-12} erg

1 Gauss = 1 G = 10^{-4} T

Introduction

Topicality and demand of the theme of the dissertation. Modified theories of gravity represent extensions of general relativity (GR) that are gaining substantial attention in cosmology and astrophysics. These theories are being developed for several reasons, such as explaining the Universe's accelerating expansion, examining the foundational principles of GR, and addressing long-standing issues within these fields including singularity and non-compatibility with quantum field theory. Currently, modified gravity theories are a focal point of research, as they may offer new insights into both the fundamental aspects of gravity and the universe's structure. However, classical gravity presents considerable obstacles when attempting to unify quantum fields with quantized gravity. In this context, the scalar-tensor-vector gravity (STVG) emerges as a compelling alternative. This approach considers gravity not as a fundamental force, but as an interaction that arises from different types of fields. Inspired by the differences between GR's description of gravity and the behavior of other fundamental forces, the concept of STVG is an area of active research and discussion, with the potential to reveal new perspectives on the universe's underlying structure and the nature of gravity.

In STVG, gravity is generated by introducing additional field generating spacetime curvature. This theory, also known as Modified Gravity (MOG), is one of the simplest extensions of general relativity that seeks to address certain cosmological and astrophysical challenges, such as the need for dark matter. STVG introduces

additional fields to general relativity, specifically scalar, tensor, and vector fields, to modify the behavior of gravity on large scales.

Radiation reaction is a phenomenon in physics where a charged particle slows down or speeds up due to the emission of electromagnetic radiation (photons) as it moves through space. This effect arises from the particle's interaction with its own electromagnetic fields, as described by classical electrodynamics. When a charged particle accelerates or decelerates, it generates changing electric and magnetic fields, which in turn produce electromagnetic radiation. This radiation carries away energy and momentum from the particle, causing it to lose kinetic energy and reduce its speed.

By modifying the fundamental gravitational principles, modified gravity theories seek to elucidate galactic rotation curves, gravitational lensing, and the dynamics of large-scale structures in the universe. A deeper comprehension of gravity on cosmic scales is vital for accurately interpreting astrophysical phenomena and advancing our understanding of the fundamental forces shaping the Universe. This work is devoted to analysis of the effect of radiation reaction in dynamical motion of test particle around the Schwarzschild-MOG black hole in STVG.

This research work corresponds to the tasks by the following state regulatory documents: Decree of the President of the Republic of Uzbekistan No. PD-4947 "On the Strategy of Actions for the Further Development of the Republic of Uzbekistan" dated February 07, 2017, Resolution of the President of the Republic of Uzbekistan No. PR-2789 "On measures for further improvement of the activities of the Academy of Sciences, organization, management and financing of research activities" dated February 18, 2017 and others.

Conformity of the research to the main priorities of science and technology development of the republic. The dissertation research has been carried

out in accordance with the priority areas of science and technology in the Republic of Uzbekistan: II. “Power, energy and resource-saving”.

The degree of knowledge of the problem The particle motion around compact gravitating object have been investigated by the different researcher worldwide (A. Ovgun, R. Pantig, G. Mustafa, F. Javed, A. zakharov, J.Schee, M. Kolos, B Ahmedov, N. Dadhich, S. Ghosh, P. Joshi, etc.). However, particle motion around black holes in scalar-tensor-vector gravity have not been systematically studied.

The null geodesic of the compact objects are properly studied by different authors (F. Atamurotov, A. de-Vries, L. Rezzolla, V. Bozza, Z. Stuchlik, A. Abdujabbarov, etc). The investigation of null geodesics and the associated optical properties of black holes, such as black hole shadows, have been remain an active topic of research in rotating black hole spacetimes and have been studied by various researchers (A. Belhaj, M. Benali, J. Luminet, etc.). However, the question of effect of MOG parameters of scalar-tensor-vector gravity on shadow and related phenomenon have not been studied yet.

Connection of the topic of the dissertation with the scientific works of scientific research organizations, where the dissertation was carried out. The dissertation was done in the framework of the scientific projects funded by the Ministry of Innovative Development. F-FA-2021-510 "Investigations of nuclear matter of neutron stars in modified gravity".

The aim of the research is the development and improvement of theoretical models based on scalar-tensor-vector gravity and corresponding solutions for the black holes.

The tasks of the research:

to study the thermodynamic properties of the Schwarzschild-MOG black hole in

STVG and to investigate several thermodynamic observational quantities of the black hole;

to formulate the first law of black hole thermodynamics in STVG;

to study the heat capacity of the Schwarzschild-MOG black hole, utilizing the isochoric heat capacity formula derived from thermodynamics principles;

to find the expression for the lifetime of the Schwarzschild-MOG black hole and a dependence on the MOG parameter;

to analyze the geodesic motion in the Schwarzschild-MOG spacetime, focusing on the effects of the MOG parameter;

to analyze photon motion around the black hole and find analytical expressions for the photon sphere and impact parameter;

to investigate the circular motion of massive particles in the Schwarzschild-MOG spacetime, specifically examining the innermost stable circular orbit (ISCO) and marginally bound orbit;

to find an exact analytical solution for the components of the vector potential of the electromagnetic field in the Schwarzschild-MOG background;

to explore the motion of charged particles around the Schwarzschild-MOG black hole in the presence of the asymptotically uniform magnetic field;

to study the circular motion in the equatorial plane and find the effective potential governing the motion of the massive particle in orbit around the Kerr-MOG black hole;

to study the gravitational radiation emitted by a massive particle falling radially onto a Kerr-MOG black hole with angular velocity;

to analyze the angular velocity of massive particles orbiting a Schwarzschild-MOG black hole, comparing it to the Keplerian angular velocity predicted by general relativity;

to investigate the gravitational counterpart of radiation reaction occurring when a stellar black hole orbits a supermassive black hole;

to test STVG with the Penrose process and analyze its impact on the energy extraction from a Kerr-MOG black hole;

to investigate the particle collision mechanism in the context of the Kerr-MOG black hole.

The objects of the research are astrophysical compact objects, black hole, modified gravity, scalar-tensor-vector gravity.

The subjects of the research are massive and massless particles motion, analytic solutions for the electromagnetic field, energetic processes around black holes, thermodynamics of the black holes. .

The methods of the research. are methods of computational mathematics, methods of theoretical astrophysics, modern methods of mathematical physics, analytical and numerical methods of calculating differential equations for field and particle motion.

The scientific novelty of the research is in the followings:

For the first time it has been found the exact formulation of the first law of black hole thermodynamics in STVG including the additional term arising from the presence of scalar-vector-tensor field. It has been shown that the Hawking temperature decreases due to the influence of the MOG parameter. It has been observed that the positive nature of the MOG parameter ensures that the temperature of the Schwarzschild-MOG black hole is consistently smaller than that predicted in the Schwarzschild spacetime.

It is shown that entropy of the Schwarzschild-MOG black hole is always greater than the entropy of the Schwarzschild black hole.

The consistency between the area law and the first law of black hole thermody-

namics enhances our understanding of the entropy of Schwarzschild-MOG black holes and contributes valuable insights to the broader field of gravitational physics.

It has been shown that the heat capacity for the Schwarzschild-MOG black hole is negative. It has been concluded that within the context of the STVG theory, the fractional heat capacity of the black hole increases with the augmentation of the MOG parameter.

The results prompt a reevaluation of the thermodynamic properties of black holes within the Schwarzschild-MOG framework, challenging the conventional expectations derived from general relativity.

It has been stated that the black hole's lifetime is longer in the context of STVG. It has been shown that both the photon sphere and the size of the black hole shadow increase due to the presence of MOG.

Practical results of the research are as follows:

It has been also shown that in the presence of MOG parameter the characteristic radii of ISCO orbits are larger compared to those in the pure Schwarzschild spacetime. Furthermore, it was obtained that the maximum energy efficiency of test particles around the Schwarzschild-MOG black hole can reach up to approximately 8.14 It has been shown that the magnetic field exhibits a non-uniform behavior in the vicinity of the Schwarzschild-MOG black hole, with denser field lines compared to the pure Schwarzschild case. It was estimated that for a typical SMBH with a mass of 10^9 $M_\odot$ and black hole with mass 10 $M_\odot$ orbiting around it, the intensity of the radiation takes the value 2.43×10^{39} erg.

For the first time the gravitational analogue of radiation reaction experienced by a massive particle orbiting a Schwarzschild-MOG black hole has been developed. Within this model the equation of motion has been simplified by discarding high-order terms concerning damping time.

It has been demonstrated that the maximum center-of-mass energy of a colliding pair of particles depends on the disparity in the specific energy values of the individual particles. Moreover, it remains independent of the vector field, and the effect of STVG emerges solely from the spacetime geometry.

Reliability of the research results is provided by applying modern proven methods of mathematical physics, computational mathematics, and relativistic astrophysics. The results were obtained strictly within the mathematical apparatus of general relativity and theoretical physics. Modern numerical and analytical methods of calculation are also used, and the results are compared with available observational data and the results of other authors. The structured conclusions of the thesis correspond to the basic rules of astrophysics of compact objects.

Scientific and practical significance of the research results. The scientific significance of the research results is determined by the following. The ongoing exploration of the research results not only contributes to our understanding of black hole physics but also underscores the intricate interplay between gravitational theories and thermodynamics, paving the way for further advancements in our comprehension of the fundamental nature of the cosmos.

The practical significance of the research results is that the positive nature of the MOG parameter ensures that the temperature of the Schwarzschild-MOG black hole is consistently smaller than one predicted in the Schwarzschild spacetime, providing valuable insights into the thermal behavior of black holes in the context of Modified Gravity.

Application of the research results.

The developed theoretical models of the photon and particle motion in the MOG theory have been applied to the followings:

scientific results obtained on the motion of particles and photons have been used

by scientists from Fudan University (FU) in Shanghai (FU, China, November 4, 2024 reference);

For the first time the thermodynamics of the MOG black hole, including entropy, Hawking temperature, Gibbs free energy, specific heat and lite time of the black hole have been explored in detail. For the first dipole gravitational radiation has been investigated. Black hole perturbation has been studied within STVG theory. Results on the dynamics of particles have been used in the works of foreign researchers, in foreign journals with a high impact factor (Physics Letters B, Volume 854, id.138758, Web-Sc, IF-4.4; Communications in Theoretical Physics, Volume 76, Issue 8, id.085402, Web-Sc, IF-2.4; Pramana, Volume 98, Issue 3, id.92, Web-Sc, IF-2.219 and others) are used in more than 30 published scientific papers to describe the effects of particles around a black hole.

Approbation of the research results. The research results were reported in the form of reports and tested at 5 international and local scientific conferences.

The main results of the study were tested at the scientific seminars of the Institute of Fundamental and Applied Research (2023), Astronomical Institute (2020-2022), of the Department of Theoretical Physics of Samarkand State University of Uzbekistan (2019), Department of Chemistry-Physics in Basque Country Universit (Spain, 2017-2018), Department of Theoretical Physics in University of Zurich (Switzerland, 2016) etc.

Publication of the research results. On the dissertation theme there were published 15 scientific works, including 11 scientific papers in international journals with high impact factors and recommended by the Supreme Attestation Commission of the Republic of Uzbekistan for publishing basic scientific results of doctoral theses.

Volume and structure of the dissertation. The dissertation consists of an

introduction, four chapters, a conclusion, an appendix and a bibliography. The size of the dissertation is 143 pages.

List of publications.

Part I

1. B. Turimov, "Comment on Orbital precession of the S2 star in scalar–tensor–vector gravity", Monthly Notices of the Royal Astronomical Society, Oxford University Press (United Kingdom), Volume 516, Issue 1, Pages 434–436 (2022). Doi:10.1093.mnras.stac2113 (Impact Factor: 5.1)

2. B. Turimov, H. Alibekov, P. Tadjimurodov, A. Abdujabbarov, "Gravitational synchrotron radiation and Penrose process in STVG theory", Physics Letters B, Elsevier (Netherlands), Volume 843, article id.138040 (2023). Doi:10.1016/j.physletb.2023.138040 (Impact Factor : 4.5)

3. B. Turimov, A. Abdujabbarov, B. Ahmedov, Z. Stuchlík, "Exact charged traversable wormhole solution", Physics Letters B, Elsevier (Netherlands), Volume 868, article id.139800, (2025). Doi:10.1016/j.physletb.2025.139800 (Impact Factor : 4.5)

4. B. Turimov, S. Usanov, "On exact massless spinor quasibound states of Schwarzschild black hole", Physics Letters B, Elsevier (Netherlands), Volume 867, article id.139617, (2025). Doi:10.1016/j.physletb.2025.139617 (Impact Factor : 4.5)

5. A. Errehymmy, Y. Khedif, M. Daoud, K. Myrzakulov, B. Turimov, T. Myrzakul, "Quantum corrections to Dymnikova-Schwinger black holes in Einstein-Gauss-Bonnet gravity", Physics Letters B, Elsevier (Netherlands), Volume 870, article id.139617, (2025). Doi:10.1016/j.physletb.2025.139915 (Impact Factor : 4.5)

6. B. Turimov, A. Nosirov, A. Abdujabbarov "Gravitational analogue of radiation

reaction in STVG", Physics of the Dark Universe, Elsevier (Netherlands), Volume 42, article id.101375, (2023). Doi:10.1016/j.dark.2023.101375 (Impact Factor : 6.4)

7. B. Turimov, S. Usanov, Y. Khamroev, "Particles acceleration by Bocharova–Bronnikov–Melnikov–Bekenstein black hole", Physics of the Dark Universe, Elsevier (Netherlands), Volume 48, article id.101876, (2025). Doi:10.1016/j.dark.2023.101876 (Impact Factor : 6.4)

8. B. Turimov, O. Rahimov, A. Davlataliyev, P. Tadjimurodov, Sh. Rahimova, "Analyzing geodesic motion in Bocharova-Bronnikov-Melnikov-Bekenstein spacetime", Physics of the Dark Universe, Elsevier (Netherlands), Volume 48, article id.101855, (2025). Doi:10.1016/j.dark.2023.101855 (Impact Factor : 6.4)

9. B. Turimov, B. Toshmatov, B. Ahmedov, Z. Stuchlík, "Quasinormal modes of magnetized black holes", Physical Review D, American Physical Society (USA), Volume 100, article id.084038 (2019). Doi:10.1103/PhysRevD.100.084038 (Impact Factor : 5.3)

10. B. Turimov, J. Rayimbaev, A. Abdujabbarov, B. Ahmedov, Z. Stuchlík, "Test particle motion around a black hole in Einstein-Maxwell-scalar theory", Physical Review D, American Physical Society (USA), Volume 102, article id. 064052 (2020). Doi: 10.1103/PhysRevD.102.064052 (Impact Factor : 5.3)

11. B. Turimov, A. Davlataliyev, A. Abdujabbarov, B. Ahmedov, "Influence of scalar field in massive particle motion in JNW spacetime", Physical Review D, American Physical Society (USA), Volume 110, article id. 084053 (2024). Doi:10.1103/PhysRevD.110.084053 (Impact Factor : 5.3)

12. B. Turimov, M. Boboqambarova, B. Ahmedov, Z. Stuchlík, "Distinguishable feature of electric and magnetic charged black hole: Acceleration of charged particle in Reissner–Nordström spacetime", European Physical Journal Plus, Springer

(Germany), Volume 137, article id. 222 (2022). Doi: 10.1140/epjp/s13360-022-02390-7 (Impact Factor : 2.9)

13. B. Turimov, S. Shaymatov, Sh. Hayitov, "Collisions of particles near Kerr-MOG black holes", European Physical Journal Plus, Springer (Germany), Volume 138, article id. 1022 (2023). Doi:10.1140/epjp/s13360-023-04618-6 (Impact Factor : 2.9)

14. B. Turimov, I. Smolyaninov "Curved spacetime as a dispersive multiferroic medium for an electromagnetic wave: Polarization and magnetization vectors in the Schwarzschild spacetime", Chinese Journal of Physics, Elsevier (Netherlands), Volume 85, pp.186-195 (2022). Doi:10.1016/j.cjph.2023.06.006 (Impact Factor: 4.6)

15. B. Turimov, A. Davlataliyev, B. Ahmedov, Z. Stuchlík, "Exploring a novel feature of Ellis spacetime: Insights into scalar field dynamics", Chinese Journal of Physics, Elsevier (Netherlands), Volume 94, pp. 807-819 (2025). Doi:10.1016/j.cjph.2024.09.030 (Impact Factor: 4.6)

16. B. Turimov, M. Boboqambarova, A. Abdujabbarov, "Particle motion around Schwarzschild-MOG black hole", Modern Physics Letters A, World scientific (Singapore) Volume 38, Issue 10, article id.2350071 (2023). Doi:10.1142/S0217732323500712 (Impact Factor: 1.6)

17. A. Errehymmy, B. Turimov, A. Syzdykov, K. Myrzakulov, N. Alesss, A. H. Abdelaty "Dymnikova-Schwinger GUP-corrected wormholes in f(R,L,T) gravity", Nuclear Physics B, Elsevier (Netherlands), Volume 1090, article id.117116, (2025). Doi:10.1016/j.nuclphysb.2025.117116 (Impact Factor : 2.8)

18. A. Errehymmy, O. Donmes, B. Turimov, K. Myrzakulov, N. Alesss, A.-H. Abdel-Aty, "Dehnen-type dark matter wormholes in the f(R,L,T) action", Annals of Physics, Elsevier (Netherlands), Volume 481, article id.170164, (2025).

Doi:10.1016/j.aop.2025.170164 (Impact Factor : 3.0)

19. B. Turimov, B. Ahmedov, "Observable Properties of Thin Accretion Disk in the γ-Spacetime", Symmetry, MDPI (Switzerland) Volume 15, Issue 10, 1858 (2023). Doi:10.3390/sym15101858 (Impact Factor : 2.2)

20. B. Turimov, B. Ahmedov, "Zipoy-Voorhees Gravitational Object as a Source of High-Energy Relativistic Particles", Galaxies, MDPI (Switzerland) Volume 9, Issue 3, 59 (2021). Doi: 10.3390/galaxies9030059 (Impact Factor : 2.2)

Part II

21. B. Turimov, "Perihelion precession and deflection of light by the gravitational object in general relativity" Journal of Fundamental and Applied Research, Volume 1, Issue 1, (2021), https://www.jfar.uz/volumes/2021/1/articles/turimov20210005.pdf

22. B. Turimov, A.Mamadjanov, "Particle acceleration by electromagnetic wave in the presence of radiation reaction force", Journal of Fundamental and Applied Research, Volume 3, Issue 1, (2022), https://www.jfar.uz/volumes/2023/1/articles/20230004/04.pdf

23. S. Tojiyev, B. Turimov, Sh. Hayitov, "Black hole thermodynamics in Scalar-Tensor-Vector-Gravity model", Journal of Fundamental and Applied Research, Volume 5, Issue 2, (2025), https://www.jfar.uz/volumes/2025/2/articles/20250012/06.pdf

24. B. Turimov, "Propagation of Electromagnetic Wave in de Sitter Cosmology", Journal of Fundamental and Applied Research, Volume 4, Issue 3, (2024), https://www.jfar.uz/volumes/2024/3/articles/20240014/03.pdf

25. B. Turimov, "Distinguishable feature of electric and magnetic charges of black hole", Journal of Fundamental and Applied Research, Volume 4, Issue 3, (2024),

https://www.jfar.uz/volumes/2024/3/articles/20240015/04.pdf

26. Y. Khamroev, B. Turimov, “BBMB qora tuynigi atrofida skalyar maydon ta‘sirida zarralar to‘qnashuvini o‘rganish”, Xalqaro amaliy anjuman “UZLUKSIZ TA‘LIM JARAYONIDA FIZIKA, MATEMATIKA VA INFORMATIKA FANLARINING DOLZARB MUAMMOLARI VA YECHIMLARI” Samarqand O’zbekiston, Oktabr 24-25, 2025, pp. 16-19.

27. B. Turimov, Sh. Qarshiyev, Sh. Hayitov, “Quasinormal modes of black holes”, Materials of conference “Modern Problem in physics of semiconductors and dielectrics” Dushanbe, Tajiki-stan, April 30, 2025, pp.267-268.

28. B. Turimov, “Energetic properties of black hole in Scalar-Tensor-Vector gravity”, 4-Hradec Kralove international Physics days: 9–15 Oct., 2025, Faculty of Science University of Hradec Kralove, Czech Republic

29. B. Turimov, “Black holes perturbation in general relativity”, Materials of conference "Recent advances in photonic and quantum optics: new optoelectronic technologies, quantum communications and quantum computers", Urgench, Uzbekistan, September 29-30, 2025

30. B. Turimov, “Maxwell equations in curved spacetime”, Materials of conference "ICTPA-2025 International Conference on Theoretical Physics and Astrophys-ics", Tashkent, Uzbekistan, September 13-17, 2024

Chapter I

Scalar-Tensor-Vector Gravity

Width of life is more important than the length of life.

Avicenna

1.1 Introduction

Albert Einstein proposed his theory of general relativity in 1915, revolutionizing our understanding of gravitation. Prior to this, gravity was described within the framework of Newtonian mechanics, which had dominated physics since the publication of *Philosophic Naturalis Principia Mathematica* by Isaac Newton in 1687. In Newtonian gravity, the gravitational force between two masses is described by the inverse-square law,

$$\mathbf{F} = -G_N \frac{Mm}{r^2}\hat{\mathbf{r}},$$

where G_N is the gravitational constant, and M and m are the masses separated by a distance r and $\hat{\mathbf{r}}$ is the unit vector along the radius vector. This formulation successfully explained a wide range of physical phenomena, including planetary orbits, the motion of falling objects, and tidal effects. It formed the basis of celestial mechanics and was extraordinarily successful in predicting the motion of bodies within the solar system.

However, as observational precision increased and more subtle phenomena were discovered, it became clear that Newtonian gravity was not sufficient to fully describe the behavior of gravitating systems, especially in strong gravitational fields or at relativistic speeds. This gap led to the development of Einstein's general relativity, a geometric theory in which gravity is not a force but a manifestation of the curvature of spacetime caused by mass-energy. The Einstein field equations are given by

$$R_{\mu\nu} - \frac{1}{2}g_{\mu\nu}R = \frac{8\pi G_N}{c^4}T_{\mu\nu}\,,$$

where $R = g^{\mu\nu}R_{\mu\nu}$ is the Ricci scalar, and $R_{\mu\nu}$ is the Ricci tensor, which is constructed from the spacetime metric $g_{\mu\nu}$. The quantity $T_{\mu\nu}$ represents the energy-momentum tensor that characterizes the matter and energy content of spacetime.

On the right-hand side of the Einstein field equations, two fundamental constants appear: the speed of light c and Newton's gravitational constant G_N. These constants serve to relate the geometry of spacetime (left-hand side) with the distribution of matter and energy (right-hand side).

Einstein's theory has been subjected to numerous experimental and observational tests over the years with remarkable accuracy. Here are three key tests of general relativity, where classical Newtonian theory either fails or provides only an approximate explanation:

(i) *Gravitational Redshift* — One of the earliest and most famous tests of general relativity is the measurement of gravitational redshift. While Newtonian gravity has no mechanism to account for the change in the frequency of light in a gravitational field, general relativity predicts that light traveling upward against gravity loses energy, resulting in an increase in its wavelength. This effect was confirmed in the Pound-Rebka experiment in 1960, where gamma rays were emitted at the bottom of a tower and detected at the top. The observed redshift matched the predictions of general relativity [1].

(ii) *Gravitational Lensing* — According to Newtonian theory, light should not be affected by gravity, as it has no mass. However, in general relativity, the curvature of spacetime around massive objects causes the trajectory of light to bend. This effect, known as gravitational lensing, has been observed and confirmed through astronomical observations. A well-known example is the Hubble Space Telescope's observations of light bending around galaxy clusters, which allows the study of distant galaxies otherwise obscured. The deflection angle of a light ray passing by a mass M is given by [2]

$$\alpha = \frac{4G_N M}{c^2 b} \ ,$$

where b is the impact parameter.

(iii) *Perihelion Precession of Mercury* — Newtonian mechanics predicts an elliptical orbit for planets, but it cannot account for the full precession of Mercury's orbit. Observations showed that Mercury's perihelion precesses more than what is expected from Newtonian gravitational interactions with other planets. General relativity accurately accounts for the extra 43 arcseconds per century in the precession, thus providing one of its earliest confirmations [3]. The expression for the perihelion precession of a planet predicted by General Relativity is

$$\delta\phi = \frac{6\pi G_N M_\odot}{c^2 a(1-e^2)} \ ,$$

where $\delta\phi$ represents the angular shift of the perihelion per orbit (in radians), $M_\odot$ is the solar mass. The parameters a and e denote the semi-major axis and the eccentricity of the planet's orbit, respectively.

Despite its successes, general relativity is not a complete theory. It faces several challenges where it is either incomplete or fails to provide a full explanation of important problems in modern astrophysics and cosmology. These include: quantum gravity, the nature of singularities, and the phenomena of dark matter and dark energy. These limitations have motivated the development of alternative and extended theories of gravity.

One of the earliest and simplest such alternatives is the Brans–Dicke theory of gravitation, also known as the Jordan–Brans–Dicke theory or Scalar-Tensor Gravity (STG). This theory generalizes general relativity by introducing a dynamical scalar field φ, which effectively replaces the gravitational constant G, allowing it to vary with spacetime. This theory was developed in 1961 by Robert H. Dicke and Carl H. Brans [4], building upon earlier work by Pascual Jordan in 1959. Brans–Dicke theory is an example of a scalar–tensor theory of gravity, in which gravity is mediated not only by the spacetime metric but also by a scalar field. While the theory is generally consistent with observations, it remains a minority

viewpoint compared to general relativity. The action for the Scalar-Tensor Gravity (STG) by Brans–Dicke theory reads [4]

$$S_{BD} = \frac{1}{16\pi}\int d^4\sqrt{-g}\left[\varphi R - \frac{\omega}{2\varphi}\nabla_\mu\varphi\nabla^\mu\varphi + V(\varphi)\right] + S_M \ ,$$

where ω is a coupling constant, ∇_μ denotes the covariant derivative with respect to the coordinates x^μ, the quantity φ is the scalar field which is inversely proportional to the gravitational constant (i.e. $\varphi = 1/G$) and $V(\varphi)$ is the potential of the scalar field and S_M is the action for matter.

Exact solutions in Brans–Dicke (BD) theory refer to metric configurations and scalar fields that satisfy the coupled Einstein–Brans–Dicke field equations, which extend General Relativity by introducing a dynamical scalar field φ representing a variable gravitational constant. The field equations are [4]:

$$\begin{aligned} G_{\mu\nu} = {} & \frac{8\pi}{\varphi}T_{\mu\nu} + \frac{\omega}{\varphi^2}\left(\nabla_\mu\varphi\nabla_\nu\varphi - \frac{1}{2}g_{\mu\nu}\nabla_\alpha\varphi\nabla^\alpha\varphi\right) \\ & + \frac{1}{\varphi}\left(\nabla_\mu\nabla_\nu\varphi - g_{\mu\nu}\Box\varphi\right) - \frac{1}{2}g_{\mu\nu}V'(\varphi) \ , \end{aligned} \tag{1.1}$$

and the scalar field satisfies

$$\Box\varphi = \frac{8\pi}{3+2\omega}T + \frac{2V(\varphi) - \varphi V'(\varphi)}{3+2\omega} \ , \tag{1.2}$$

with $T = T^\mu_{\ \mu}$ the trace of the energy–momentum tensor of the matter. The first spherical symmetric vacuum solution (i.e., $T_{\mu\nu} = 0$) in the isotropic coordinates is found as [5]

$$ds^2 = -e^{\nu(r)}dt^2 + e^{\mu(r)}(dr^2 + r^2 d\theta^2 + r^2\sin^2\theta d\phi^2) \ , \tag{1.3}$$

with

$$e^{\nu(r)} = \left(\frac{1 - B/r}{1 + B/r}\right)^{2/\lambda} \ , \tag{1.4}$$

$$e^{\mu(r)} = \left(1 + \frac{B}{r}\right)^4\left(\frac{1 - B/r}{1 + B/r}\right)^{2(\lambda - C - 1)/\lambda} \ , \tag{1.5}$$

and

$$\varphi(r) = \varphi_0 \left(\frac{1 - B/r}{1 + B/r} \right)^{C/\lambda} , \tag{1.6}$$

where the parameters satisfy $\lambda^2 = (C+1)^2 - C\left(1 - \frac{\omega C}{2}\right)$ and B, C and φ_0 are integration constants. This is the most general spherically symmetric static vacuum solution in BD theory. When $\omega \to \infty$, the scalar field becomes constant $\varphi \to \varphi_0$, and the solution reduces to the Schwarzschild metric of General Relativity.

Other known exact solutions has been obtained in Bianchi type universe. For a spatially flat Friedmann–Robertson–Walker (FRW) metric [6, 7]

$$ds^2 = -dt^2 + a(t)^2(dx^2 + dy^2 + dz^2) , \tag{1.7}$$

the BD field equations yield power-law solutions:

$$a(t) \propto t^{\frac{2+2\omega}{4+3\omega}}, \quad \varphi(t) \propto t^{\frac{2}{4+3\omega}} . \tag{1.8}$$

Under the conformal transformation ($\tilde{g}_{\mu\nu} = \varphi g_{\mu\nu}$), the theory can be rewritten as GR with a canonical scalar field and a modified matter coupling.

More recently, BD theory has been further generalized by John Moffat [8] through the inclusion of a vector field, leading to the STVG theory, also known as Modified Gravity (MOG). This extension introduces new degrees of freedom to gravity and aims to address open questions such as the dark matter problem without invoking exotic particles. MOG modifies the gravitational interaction at large scales while reducing to general relativity in the appropriate limits.

In STVG, the gravitational interaction is characterized by the interplay of three distinct fields: a scalar field G, a vector field Φ_μ, and the metric tensor $g_{\mu\nu}$. The total action governing the dynamics of this system (in unit where $c = 1$) is given by [8]:

$$S = S_{EH} + S_V + S_S + S_M , \tag{1.9}$$

with

$$S_{EH} = \frac{1}{16\pi}\int d^4x\sqrt{-g}\frac{1}{G}\left(R + 2\Lambda\right) \ , \tag{1.10}$$

$$S_V = \int d^4x\sqrt{-g}\omega\left(-\frac{1}{4}B^{\mu\nu}B_{\mu\nu} + V(\Phi_\mu)\right) \ , \tag{1.11}$$

$$S_S = \int d^4x\sqrt{-g}\frac{1}{G}\Bigg[\frac{1}{G^2}\left(\frac{1}{2}\nabla_\mu G\nabla^\mu G - V(G)\right) + \left(\frac{1}{2}\nabla_\mu\omega\nabla^\mu\omega - V(\omega)\right) + \frac{1}{\mu^2}\left(\frac{1}{2}\nabla_\mu\mu\nabla_\mu\mu - V(\mu)\right)\Bigg] \ , \tag{1.12}$$

where $B_{\mu\nu} = \partial_\mu\Phi_\nu - \partial_\nu\Phi_\mu$ is the anti symmetric tensor, Λ denotes the cosmological constant, $V(\Phi_\mu)$ denotes a potential for the vector field Φ_μ, while $V(G), V(\omega)$ and $V(\mu)$ denote the three potentials associated with the three scalar fields G, ω and μ, respectively. Here, one has to emphasize that μ is mass of the vector field and ω is a coupling constant. For simplicity, we assume that ω and μ are constants, and the contribution of these fields vanish in equation of motion.

By varying the action (1.9), the field equations in STVG can be derived as

$$R_{\mu\nu} - \frac{1}{2}g_{\mu\nu}R + g_{\mu\nu}\Lambda + G(g_{\mu\nu}\nabla^\alpha\nabla_\alpha - \nabla_\mu\nabla_\nu)\frac{1}{G} = 8\pi G T_{\mu\nu} \ , \tag{1.13}$$

$$\nabla_\nu B^{\mu\nu} + \frac{dV(\Phi_\mu)}{d\Phi_\mu} = J^\mu \ , \qquad J^\mu = -\frac{1}{\sqrt{-g}}\frac{\delta S_M}{\delta\Phi_\mu} \ , \tag{1.14}$$

$$\nabla_\mu\nabla^\mu G + \frac{dV(G)}{dG} + \frac{3}{G}\left(\frac{1}{2}\nabla_\mu G\nabla^\mu G - V(G)\right) + \frac{G}{16\pi}(R + 2\Lambda + 8\pi G T) = 0 \ , \tag{1.15}$$

where $T = g^{\mu\nu}T_{\mu\nu}$ and the total energy-momentum tensor of the whole system is described by $T_{\mu\nu} = T_{M\mu\nu} + T_{V\mu\nu} + T_{S\mu\nu}$, where $T_{S\mu\nu}$, $T_{V\mu\nu}$ and $T_{M\mu\nu}$ denote the energy-momentum tensor of scalar field, vector field and ordinary matter. The energy-momentum tensor for the vector and scalar field can be written as

$$T_{V\mu\nu} = \omega\left[B_\mu{}^\alpha B_{\nu\alpha} - g_{\mu\nu}\left(\frac{1}{4}B^{\rho\sigma}B_{\rho\sigma} + V(\Phi)\right)\right] \ , \tag{1.16}$$

$$T_{S\mu\nu} = -\frac{1}{G^3}\left[\nabla_\mu G\nabla_\nu G - g_{\mu\nu}\left(\frac{1}{2}\nabla_\alpha G\nabla^\alpha G - V(G)\right)\right] \ . \tag{1.17}$$

As we mentioned before STVG theory is a modification of Einstein's theory GR that incorporates an additional scalar and vector field. The theory was first proposed as a possible alternative to GR that could address some of the shortcomings of the theory, such as the need for dark matter and dark energy [8]. In STVG, the scalar field is responsible for the expansion of the universe and is often associated with the Higgs boson. The vector field, on the other hand, is responsible for the gravitational interactions between particles and is often associated with the gauge bosons of the weak force and it is still an active area of investigation. Field equations in STVG are more complex than the field equations of GR, but they can be solved numerically to make predictions about the behavior of gravitational systems [8]. In later works MOG field equations were directly obtained from the least action principle and solutions of those equations were compared to cosmological and astrophysical observations [9]. The theory was successfully applied for explanation of galaxy rotation curves [10], cluster dynamics [11], gravitational lensing [12] and Solar system [12]. There is a proposed explanation for the behavior of part-time pulsars by effects of MOG [13]. MOG violates Birkhoff's theorem and some consequences of that were studied in [14]. Results of the study might provide a new insight to the nature of inertia.

Further studies on gravitational lensing in point source spherically symmetric spacetimes were concluded with results that can be applied for the cases of continuous distributions of mass and provide a possible explanation for Abel 520 merging clusters [15]. In [16, 17] authors continue the studies and show that MOG can be used to model acoustic power spectrum of the cosmic microwave radiation and apply it to model the peak of the spectrum. Angular powr spectrum was studied in [18]. Using the data of the HI Nearby Galaxy Survey catalogue of galaxies and the Ursa Major catalogue of galaxies a good fit to galaxy rotation curve was

obtained and it was shown that mass-to-light ratio derived during fitting process is correlated with the colors of galaxies [19, 20]. In [21, 22] authors model the shadows of static spherically symmetric black holes in MOG, which is then done for rotating black holes in [22] along with a construction of traversable wormhole solution. Black hole shadows in MOG were also investigated by [23] Other optical properties of black holes, such as gravitational lensing and gravitational delay were studied by [24–28] Fitting of gravitational wave data from LIGO-Virgo is performed in [29], theory wa also applied to Abell 1689 galaxy cluster in [30] and newtonian and modified newtonian dynamics are shown to not fit the acceleration data were MOG and Navarro-Frenk-White dark matter models do. Some other studies on galaxy clusters and acceleration data include [31, 31, 32]. There is a wide range of works on particle motion around compact gravitational objects in MOG focusing on different aspects, namely stable orbits' [33–35] and energy extraction [36]. Particle motion approach was also utilized to study the motion of S2 star on its orbit around Sagittarius A* SMBH [37–40], and constraints on parameters of the theory were discussed. Quasi-periodic oscillations in MOG were discussed by [36,41] and a new method for using QPO data to estimate alternative gravity theories parameters using QPOs was demonstrated using MOG by [42].

1.2 Background spacetime and particle dynamics

In order to find the semi-analytical black hole solution, action in STVG can be simplified. According to Refs. [21, 22], the scalar field is assumed to be constant i.e. $G = \text{const}$, then the action in STVG reduce to following simple form:

$$R_{\mu\nu} - \frac{1}{2} g_{\mu\nu} R = 8\pi G T_{\mu\nu} \ , \tag{1.18}$$

$$\nabla_\mu B^{\mu\nu} = 0 \ , \tag{1.19}$$

which is similar to Einstein-Maxwell system. The solution above system is rather simple. In the spherical coordinates $x^\alpha = (t, r, \theta, \phi)$, the simple solution to system above is given by the Schwarzschild-MOG spacetime which yields [21, 22]

$$ds^2 = -f(r)dt^2 + f(r)^{-1}dr^2 + r^2(d\theta^2 + \sin^2\theta d\phi^2) \ , \tag{1.20}$$

with

$$f(r) = \left(1 - \frac{2GM}{r} + \frac{G\tilde{Q}^2}{r^2}\right) \ ,$$

where M is a mass of a black hole, G is a modified gravitational constant related to Newtonian gravitational constant G_N as fallows $G = G_N(1+\alpha)$. The spacetime metric (1.20) is similar to the Reissner-Nordström spacetime, however, the quantity $\tilde{Q} = \sqrt{\alpha G_N}M$ is the coupling constant regarded to the external potential in STVG which is given as [21]

$$\Phi_\mu = \Phi_t(1,0,0,0) \ , \qquad \Phi_t = -\frac{\tilde{Q}}{r} = -\frac{\sqrt{\alpha G_N}M}{r} \ , \tag{1.21}$$

and α is positively defined MOG parameter. The radius of the outer and inner horizons of Schwarzschild-MOG black hole is located at

$$r_\pm = G_N M(1 + \alpha \pm \sqrt{1+\alpha}) \ .$$

Notice that the outer horizon r_+ is greater than the Schwarzschild radius for non-zero value of the MOG parameter, i.e. $r_+ \geq 2G_N M$ and dependence of the horizon from MOG parameter α is illustrated in Fig. 1.1 and r_- denotes the inner horizon.

We now examine the motion of a massive particle in the vicinity of a black hole within the framework of STVG. Unlike in general relativity and many other gravitational theories, in STVG massive particles do not follow geodesic paths [8]. The motion of test particle within STVG theory is described by the following

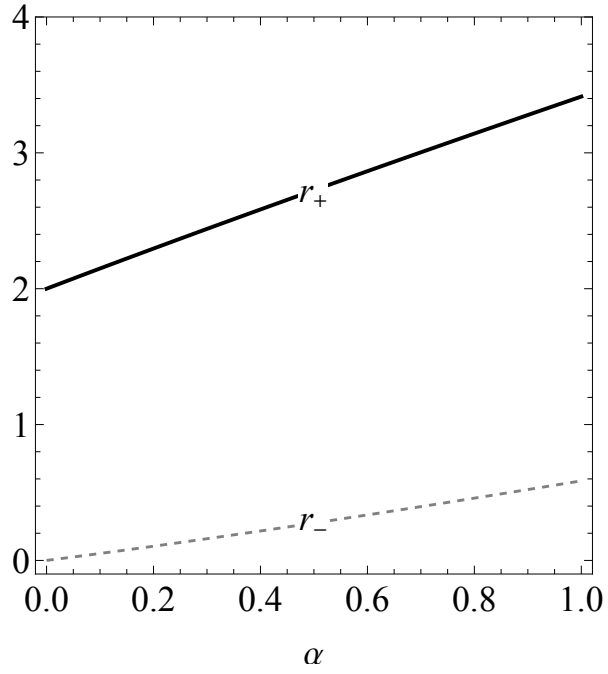


Figure 1.1: Dependence of the radius of the horizon of the Schwarzschild-MOG black hole on the MOG parameter α.

non-geodesic equation:

$$\frac{d^2x^\alpha}{ds^2} + \Gamma^\alpha_{\mu\nu}\frac{dx^\mu}{ds}\frac{dx^\nu}{ds} = \frac{\tilde{q}}{m}B^\alpha{}_\beta\frac{dx^\beta}{ds} \ , \qquad B_{\alpha\beta} = \partial_\alpha\Phi_\beta - \partial_\beta\Phi_\alpha \ , \tag{1.22}$$

which can be derived from the following Lagrangian:

$$\mathcal{L} = \frac{1}{2}g_{\mu\nu}\frac{dx^\mu}{ds}\frac{dx^\nu}{ds} + \frac{\tilde{q}}{m}\Phi_\mu\frac{dx^\mu}{ds} \ , \tag{1.23}$$

where m denotes the mass of the test particle, while $\tilde{q} = \sqrt{\alpha G_N}m$ represents the coupling strength between the particle and the vector field Φ_μ, $\Gamma^\alpha_{\mu\nu}$ are the Christoffel symbols and $\dot{x}^\alpha = dx^\alpha/ds$ is the 4-velocity of test particle normalized as $g_{\alpha\beta}\dot{x}^\alpha\dot{x}^\beta = -1$. The presence of the additional force term involving the field strength tensor $B^\mu_{\ \nu}$ indicates that massive particles in STVG are subject to a non-geodesic force analogous to a Lorentz force in electrodynamics, arising from their interaction with the vector field. However, motion of massless particle is described by null geodesic equation which we discuss in next section 1.3.

1.3 Massless particle motion

Let us consider the photon motion near a Schwarzschild-MOG black hole. Equation of motion for photon can be expressed as

$$\frac{d^2x^\alpha}{ds^2} + \Gamma^\alpha_{\mu\nu}\frac{dx^\mu}{ds}\frac{dx^\nu}{ds} = 0 \ , \tag{1.24}$$

We shall work with a system of units in which ($c = 1$). The equations for the radius r and for the angular ϕ and temporal t coordinates, which determine the orbit of the photon in the Schwarzschild-MOG metric, can be written as

$$\frac{dr}{d\lambda} = \sqrt{\frac{1}{b^2} - \frac{f(r)}{r^2}} \ , \tag{1.25}$$

$$\frac{d\phi}{d\lambda} = \frac{1}{r^2} \ , \tag{1.26}$$

$$\frac{dt}{d\lambda} = \frac{1}{bf(r)} \ , \tag{1.27}$$

where b is the impact parameter of photon and λ is an affine parameter normalized by the angular momentum of the photon.

1.3.1 Strong Gravitational Lensing

When the photon passes near the massive object, some part of the photon will be captured by the black hole and then will move along spherical orbits defining the boundary of the shadow of the lensing object. If photon moves along the spherical geodesics the radial equation satisfies the following conditions

$$\frac{dr}{d\lambda} = 0 \ , \qquad \frac{d^2r}{d\lambda^2} = 0 \ . \tag{1.28}$$

The first equation of (1.28) is responsible for the turning point of the light ray while second one is represents the radius of the spherical orbit.

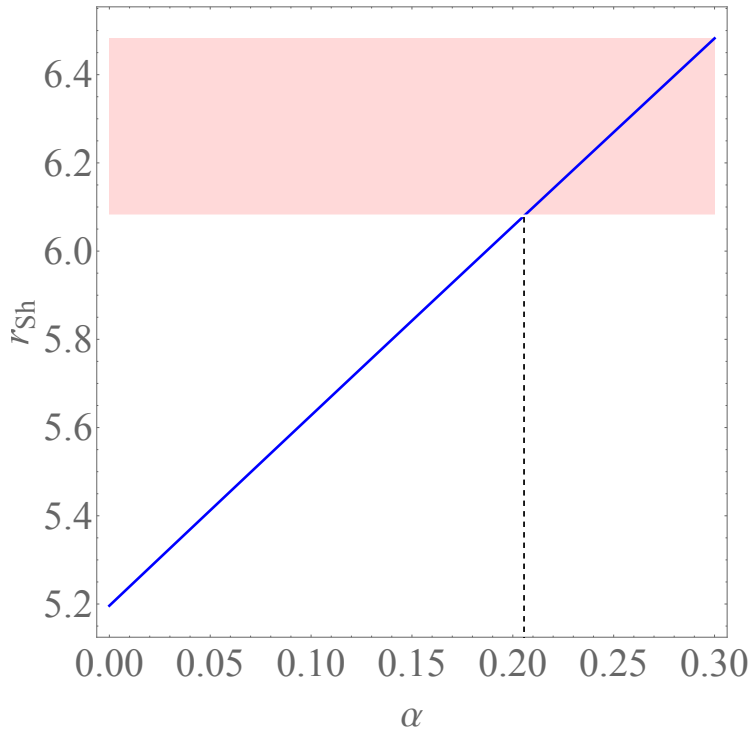


Figure 1.2: Capture cross section of photon by the black hole (shadow of the black hole) in the (x-z) plane for the different values of α parameter.

the radius of the photonsphere and the critical impact factor of photon is determined as

$$r_{\rm ph} = \frac{1}{2}\left[3(1+\alpha) + \sqrt{(1+\alpha)(9+\alpha)}\right] G_N M \ , \tag{1.29}$$

$$b = \frac{r_{\rm ph}}{\sqrt{f(r_{\rm ph})}} \ , \tag{1.30}$$

One can easily check that absence of α parameter above expressions will be $r_{\rm ph} = 3M$ and $b_0 = 3\sqrt{3}M$ corresponding to the photon-sphere and the critical impact parameter in the Schwarzschild space.

The capture cross section of photon by the black hole can be determined as $\sigma = \pi b_0^2$ and in the Schwarzschild-MOG metric it takes a form:

$$\sigma = \frac{2\pi\alpha M^2\left[3+3\alpha+\sqrt{(1+\alpha)(9+\alpha)}\right]^2}{\alpha+3+\sqrt{(1+\alpha)(9+\alpha)}} \ , \tag{1.31}$$

while in the Schwarzschild one it reduces to $\sigma = 27\pi M^2 \simeq 84.823 M^2$. To have

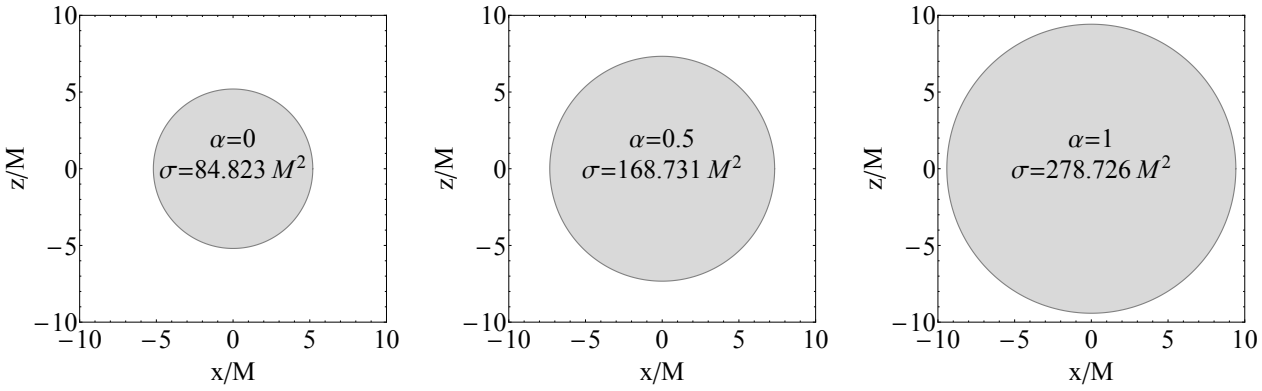


Figure 1.3: Capture cross section of photon by the black hole (shadow of the black hole) in the (x-z) plane for the different values of α parameter.

an idea about size of the black hole's shadow one can estimate cross section for the supermassive black hole (SMBH) with a million solar mass in the form:

$$\sigma \simeq 1.576 \times 10^{16} \left(\frac{M}{10^6 M_\odot}\right)^2 \text{km}^2 \ . \tag{1.32}$$

Note, that this large valued size of the shadow will have very small angular size due to the far distance to the super massive black hole from observer. More precise analyses can be presented in graphical way. Figure 1.3 illustrates capture cross section of photon by the black hole for different values of α parameter. Our analyses show that capture cross section in Schwarzschild-MOG space gets larger than that obtained in general relativity which is also found in Ref. [21].

Now we focus on the calculating the deflection angle of photon by the Schwarzschild-MOG black hole.

$$\hat{\alpha} = 2\Delta\phi - \pi \ , \tag{1.33}$$

where $\Delta\phi$ can be obtained from (1.25) as

$$\Delta\phi = \int_R^\infty \frac{dr}{r^2\sqrt{\frac{f(R)}{R^2} - \frac{f(r)}{r^2}}} \ , \tag{1.34}$$

Hereafter introducing new variable $u = R/r$ integral in (1.34) takes a form:

$$\Delta\phi = \frac{2R}{M\sqrt{\alpha(1+\alpha)(c-1)(a-b)}} F\left[\sin^{-1}\sqrt{\frac{a-b}{a(1-b)}}\middle|\frac{(c-a)(1-b)}{(a-b)(c-1)}\right] , \tag{1.35}$$

where $F(k|x)$ is the elliptic integral and a, b, c are solutions of cubic equation, respectively. In the case of weak field approximation $b \simeq R$ and the integral in (1.34) can be expanded as

$$\begin{aligned}
\Delta\phi \simeq & \int_0^1 \frac{du}{\sqrt{1-u^2}} \\
& + \frac{M(1+\alpha)}{b}\int_0^1 \frac{du}{\sqrt{1-u^2}}\frac{1-u^3}{1-u^2} \\
& + \frac{M^2\alpha(1+\alpha)}{2b^2}\int_0^1 \frac{du}{\sqrt{1-u^2}}\frac{1-u^4}{1-u^2} \\
& + \frac{3M^2(1+\alpha)^2}{2b^2}\int_0^1 \frac{du}{\sqrt{1-u^2}}\left(\frac{1-u^3}{1-u^2}\right)^2 \\
= & \frac{\pi}{2} + \frac{2M(1+\alpha)}{b} + \frac{M^2\alpha(1+\alpha)}{b^2} + \frac{(15\pi-16)(\alpha+1)^2M^2}{4b^2} ,
\end{aligned} \tag{1.36}$$

Finally, in the case of weak field approximation, the deflection angle is determined as

$$\hat{\alpha}_b = \frac{4(1+\alpha)M}{b} + \frac{(1+\alpha)[(15\pi-16)(\alpha+1)+8]M^2}{4b^2} , \tag{1.37}$$

Because the leading term already contains $1+\alpha$, observational constraints on the deflection angle from precise lensing measurements (e.g. light deflection near the Sun or strong-lens systems) primarily constrain α through that linear scaling. The second-order difference is numerically tiny for typical astrophysical lensing situations it scale $\mathcal{O}(M^2/b^2)$, but could be relevant in precision tests (e.g. very close grazing by compact objects or future high-precision astrometric missions). Therefore it is important to check which definition of b was used in the derivation

and to verify the expansion keeping consistent coordinate choices when comparing second-order coefficients to the canonical Schwarzschild result.

1.3.2 Weak Gravitational Lensing

It is well-known that gravitational lensing is one of the powerful tools to test GR versus alternate theories of gravity. According to GR theory the deflection of the light-ray around static spherically symmetric gravitational source with the total mass M is $\hat{\alpha} = 4M/b$, where b is the impact parameter of the light-ray. Here we study the weak gravitational lensing effect in the Schwarzschild-MOG spacetime. The one of simple approaches for studying gravitational lensing has been developed in [43–45], where the metric tensor can be expanded as $g_{\alpha\beta} \simeq \eta_{\alpha\beta} + h_{\alpha\beta}$ in the weak field approach, where $\eta_{\alpha\beta}$ is the metric tensor of a flat Minkowski spacetime and $h_{\alpha\beta}$ is a perturbation of the metric tensor. According to Ref. [43] the deflection angle of the light-ray can be expressed as

$$\hat{\alpha}_b = \frac{1}{2}\int_{-\infty}^{\infty} \frac{\partial}{\partial b}\left(h_{tt} + h_{zz}\right) dz \ . \tag{1.38}$$

Taking into account the above facts the spacetime metric (1.20) can be expanded as

$$\begin{aligned} ds^2 \simeq ds_0^2 &+ \frac{2M(1+\alpha)}{r}\left(1 - \frac{\alpha M}{2r}\right) dt^2 \\ &+ \frac{2M(1+\alpha)}{r}\left(1 + \frac{(3\alpha+4)M}{2r}\right) dr^2 \ . \end{aligned} \tag{1.39}$$

where $ds_0^2 = -dt^2 + dx^2 + dy^2 + dz^2$ is the line element in Minkowski spacetime. The perturbation for the components of the metric tensor are

$$h_{tt} = \frac{2M(1+\alpha)}{r}\left(1 - \frac{M\alpha}{2r}\right) \ , \tag{1.40}$$

$$h_{zz} = \frac{2M(1+\alpha)}{r}\left(1 + \frac{(3\alpha+4)M}{2r}\right)\cos^2\theta \ , \tag{1.41}$$

We assume that the light-ray approaches to the compact object along z-direction. Hereafter introducing the impact parameter of the light-ray, i.e., b, the radial coordinate takes a form $r = \sqrt{z^2 + b^2}$. Then the expression for the deflection angle takes a form:

$$\hat{\alpha}_b = \frac{4M}{b}(1+\alpha) + \frac{\pi M^2}{b^2}(1+\alpha)\left(1+\frac{\alpha}{4}\right) \ , \tag{1.42}$$

which is the exactly same expression as obtained in general relativity, however, the sign should be opposite. Since the deflection angle is vector quantity one can easily replace sign of expression (1.42).

It is known that the gravitational lens system contains three fragments: the source of the light-ray, gravitational object and observer. If these fragments are located in the same line then one can observe Einstein ring, otherwise one can observe two images of the source. According to the standard model of the gravitational lensing, the angular half-separation due to gravitational lensing between the images of the source is proportional to the Einstein deflection angle (1.42), and it can be expressed as [46]

$$\Theta_\alpha = \Theta_0\sqrt{1+\alpha} \ , \qquad \Theta_0 = \sqrt{\frac{4MD_{ds}}{D_sD_d}} \ , \tag{1.43}$$

where D_d is the distance between observer and lens, D_s is the distance between observer and source, and D_{ds} is the distance between the lens and source.

It is extremely interesting to study the observational consequences of the gravitational lensing, namely, the magnification of image sources. For this purpose, one can consider the lens equation $\beta = \theta - \Theta^2/\theta$, where the angle β is the real object from the observer-lens axis and angle θ is the apparent image of the object from the observer-lens axis, respectively. Finally, taking into account all facts, the total magnification of the images is determined as $\mu = |(\theta/\beta)(d\theta/d\beta)|$. The

magnification of the individual images can be determined as [46]

$$\mu_+ = \frac{1}{4}\left[2 + \frac{y}{\sqrt{y^2+4+4\alpha}} + \frac{\sqrt{y^2+4+4\alpha}}{y}\right] , \tag{1.44}$$

$$\mu_- = \frac{1}{4}\left[2 - \frac{y}{\sqrt{y^2+4+4\alpha}} - \frac{\sqrt{y^2+4+4\alpha}}{y}\right] , \tag{1.45}$$

where $y = \beta/\Theta$ and $\mu_\pm$ is responsible for the magnifications the main and secondary images of the source. The total magnification of the source is determined as $\mu = \mu_+ + |\mu_-|$. For the large values of β angle, the main magnification dominates and is simply equal to the total magnification. On the other hand, the time delay due to the gravitational field is determined as [46]

$$\Delta t = 4M(1+z)\left(\ln\frac{\sqrt{y^2+4+a\alpha}+y}{\sqrt{y^2+4+4\alpha}+y} + \frac{1}{2}y\sqrt{y^2+4+4\alpha}\right) , \tag{1.46}$$

where z is the red-shift factor.

1.4 Massive particle motion

Now we focus on investigating massive particle motion aroud the Schwarzschild-MOG black hole in STVG. As we mentioned before that massive particle follow Lorentz-like equation given in equation (1.22). For simplicity, we consider motion in the equatorial plane (i.e. $\theta = \pi/2$). Hereafter integrating (1.22), equation of motion of massive particle can be written as

$$\frac{dt}{ds} = \frac{1}{f}\left(\mathcal{E} - \frac{\alpha G_N M}{r}\right) , \tag{1.47}$$

$$\frac{d\phi}{ds} = \frac{\mathcal{L}}{r^2} , \tag{1.48}$$

$$\left(\frac{dr}{ds}\right)^2 = \left(\mathcal{E} - \frac{\alpha G_N M}{r}\right)^2 - f\left(1 + \frac{\mathcal{L}^2}{r^2}\right) , \tag{1.49}$$

with

$$f = 1 - \frac{2G_N M(1+\alpha)}{r} + \frac{(G_N M)^2\alpha(1+\alpha)}{r^2} ,$$

where $\mathcal{E}$ and $\mathcal{L}$ are the specific energy and specific angular momentum of test particle. For simplicity, we consider circular motion of test particle in the equatorial plane of the Schwarzschild-MOG black hole i.e., $\theta = \pi/2$ and $\dot{\theta} = 0$. The radial equation of motion can be derived as

$$\begin{aligned} \dot{r}^2 &= \left(\mathcal{E} - \frac{\alpha G_N M}{r}\right)^2 - f\left(1 + \frac{\mathcal{L}^2}{r^2}\right) \\ &= \left[\mathcal{E} - V_+(r)\right]\left[\mathcal{E} - V_-(r)\right] \ , \end{aligned} \tag{1.50}$$

where $V_\pm(r)$ is defined as

$$V_\pm(r) = \frac{\alpha G_N M}{r} \pm \sqrt{f\left(1 + \frac{\mathcal{L}^2}{r^2}\right)} \ . \tag{1.51}$$

The effective potential is a valuable tool for understanding how test particles move around black holes. Figure 1.4 shows the effective potential for massive particle for different values of the MOG parameter. By locating the minimum value of the effective potential, we can determine the position of the innermost stable circular orbit (ISCO) and understand how massive particles orbit around black holes without getting drawn into them or flung out into space. The ISCO is a significant location for astrophysical observations, as it affects the emission of radiation and matter falling onto the black hole. Additionally, studying the ISCO can provide insights into the properties of black holes and tests of general relativity, including alternative theories of gravity. The location of the ISCO depends on various factors such as the mass and spin of the black hole and the STVG parameter in the current research work.

In this study, we focus on finding the radius of the ISCO of massive particles around black holes in STVG and testing how it depends on the α parameter. To simplify the analysis, we consider the motion of massive particles in the equatorial plane, meaning that the effective potential depends on only the radial coordinate.

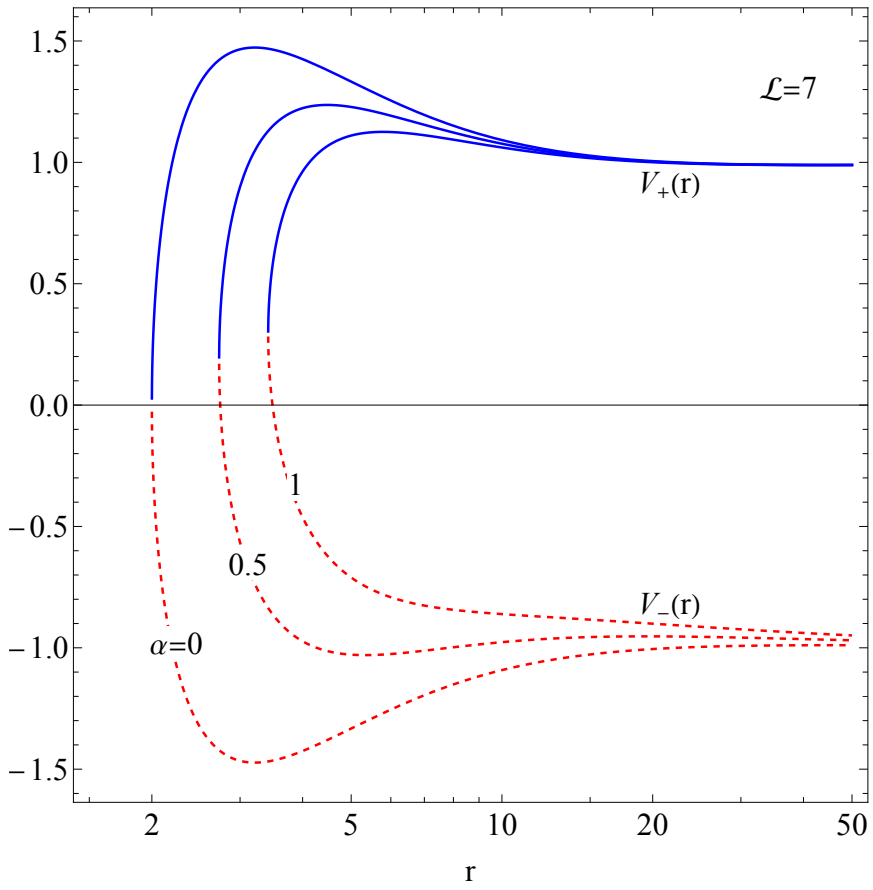


Figure 1.4: Dependence of the effective potential for massive particle orbiting the Schwarzschild-MOG black hole from the MOG parameter α.

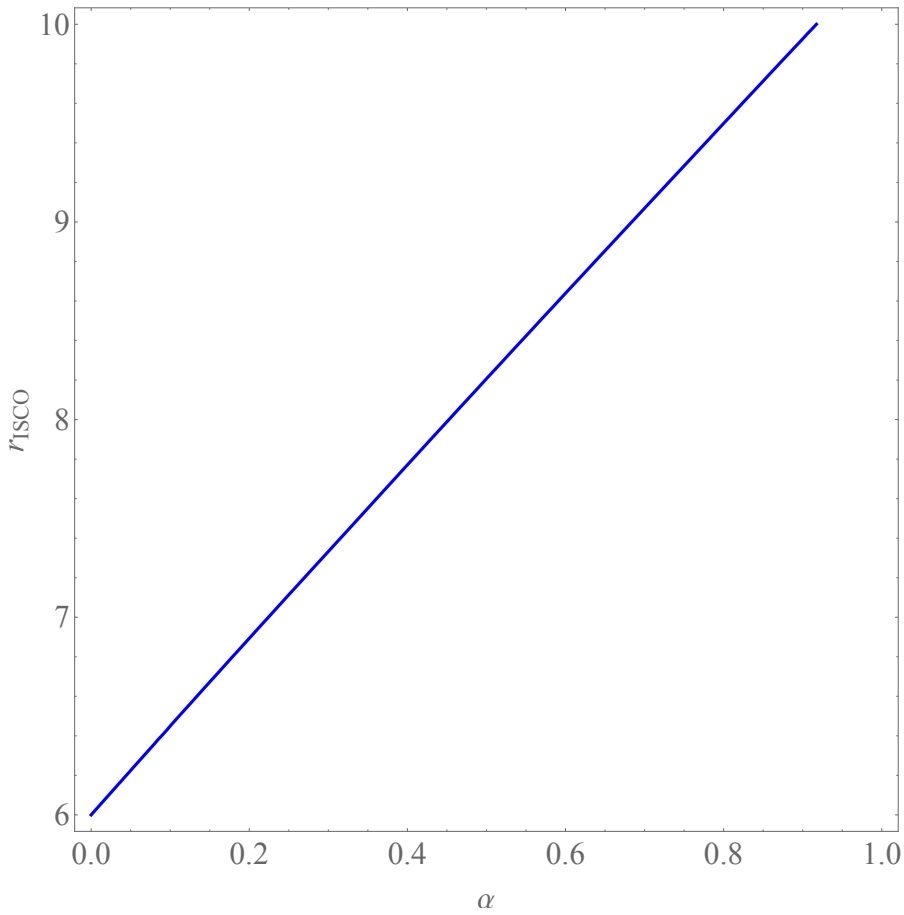


Figure 1.5: Dependence of the ISCO position for massive particle orbiting the Schwarzschild-MOG black hole from the MOG parameter α.

We can find the ISCO position using the standard method with the following conditions: $V_+(r) = \mathcal{E}$, $V'_+(r) = 0$, and $V''_+(r) \leq 0$. Analytical expressions can be obtained for the ISCO position, but careful numerical analyses are necessary to accurately determine its location.

Interestingly, our results indicate that the ISCO position gets larger due to the effect of STVG. Figure 1.5 illustrates the dependence of the ISCO position of massive particles orbiting around the Schwarzschild-MOG. These findings highlight the importance of considering the effects of STVG when studying the motion of massive particles around black holes.

From astrophysical point view the energy extraction from the black hole is quite

interesting problem. One of the simple model of the accreting matter onto the black hole is purposed in [47]. According to this model the matter flow onto black hole between innermost stable orbit and outer horizon, and the energy efficiency is related to the binding energy of the last stable orbit. The energy efficiency of test particle can be determined as $\eta = 1 - \mathcal{E}_{\rm ISCO}$, where $\mathcal{E}_{\rm ISCO}$ is the specific energy of particle at the ISCO position which depends on α parameter only. We do not present η here unless nature of its expression. However, one can determine the minimum and maximum value of the energy efficiency in the following form:

$$\lim_{\alpha\to 0}\eta = 1 - \frac{2\sqrt{2}}{3} \simeq 0.0572 \ , \qquad (5.72\%) \ , \tag{1.52}$$

$$\lim_{\alpha\to \infty}\eta = 1 - \frac{3}{4}\sqrt{\frac{3}{2}} \simeq 0.0814 \ , \qquad (8.14\%) \ . \tag{1.53}$$

1.4.1 Orbital precession of S2 star

A motion of S2-stars around the SMBH located in center of the Milky Way is quit interesting and important task to test the modified or/and alternative theories of gravity in both theoretical and astrophysical point view. It is well-known that the periastron expression of celestial object orbiting around central gravitational object in the framework of general relativity is determined as

$$\delta\phi_{\rm GR} = \frac{6\pi G_N M}{ac^2(1-e^2)} \ , \tag{1.54}$$

where a and e being the orbital semi-major axis and eccentricity, respectively. Here we are aimed to shown the derivation of the periastron precession of S2-star orbiting around SMBH in the STVG in the precise way. To do this we use the method formulated in the Ref. [48]. Taking into account equations (1.48), (1.49), and after introducing new variable $u = \mathcal{L}^2/G_N M r$, one can easily obtain

$$\left(\frac{du}{d\phi}\right)^2 = \frac{1}{\epsilon}\left(\mathcal{E} - \alpha\epsilon u\right)^2 - \left[1 - 2(1+\alpha)\epsilon u + \alpha(1+\alpha)\epsilon^2 u^2\right]\left(u^2 + \frac{1}{\epsilon}\right) \ , \tag{1.55}$$

where $\epsilon = (G_N M/\mathcal{L})^2 << 1$ is a small parameter. Notice that the solution of above equation represents the trajectory of celestial object orbiting around the SMBH. Hereafter differentiating the equation (1.55), one can get

$$u'' + u\,(1+\alpha\epsilon) = 1 + \alpha\delta + 3\epsilon(1+\alpha)u^2 - 2\epsilon^2\alpha(1+\alpha)u^3 \ , \tag{1.56}$$

where $\delta = 1 - \mathcal{E}$ and double primes denotes second order derivative with respect to the angle ϕ. Obviously, it is difficult to find exact solution to above equation. Therefore the semi-analytical approach can be performed to find approximate value of the periastron shift. Let's expand the solution in power of the small parameter in the form:

$$u(\phi) = u_0(\phi) + \epsilon u_1(\phi) + \mathcal{O}(\epsilon^2) \ . \tag{1.57}$$

Substituting the equation (1.57) into (1.56), the equations in the zeroth and first order approximations can be written as

$$u_0'' + u_0 = 1 + \alpha\delta \ , \tag{1.58}$$

$$u_1'' + u_1 = -\alpha u_0 + 3(1+\alpha)u_0^2 \ . \tag{1.59}$$

Our aim is to solve the above second order equations. As one can see that equation (4.43) looks similar to the classical expression for radial equation, however the terms proportional to α parameter are contribution due to STVG to Newtonian theory. The exact analytical solution to equation (4.43) reads $u_0 = 1+\alpha\delta+e\cos\phi$ which characterizes the elliptic motion of celestial object around the central object without periastron shift so that trajectory will be closed, i.e. $u_0(\phi) = u_0(\phi+2\pi)$. In order to obtain the periastron shift one needs to solve equation (4.46). Our analyses showed that the last term of the equation (4.46) is proportional to ϵ^2 therefore the contribution from this term is extremely small and can be safely removed from the expression. Hereafter substituting equation into (4.46) one can

obtain

$$u_1'' + u_1 = (1+\alpha\delta)\left[3+2\alpha+3\alpha(1+\alpha)\delta\right] + \frac{3(1+\alpha)e^2}{2} + \left[6+5\alpha+6\alpha(1+\alpha)\delta\right]e\cos\phi + \frac{3(1+\alpha)e^2}{2}\cos 2\phi \ . \tag{1.60}$$

The solution to equation (1.60) can be found as $u_1(\phi) = A + B\phi\sin\phi + C\cos 2\phi$, and

$$u_1'' + u_1 = A + 2B\cos\phi - 3C\cos 2\phi \ , \tag{1.61}$$

where A, B, and C are unknown constants found by comparing equations (1.60) and (1.61) in the form:

$$A = (1+\alpha\delta)\left[3+2\alpha+3\alpha(1+\alpha)\delta\right] + \frac{3(1+\alpha)e^2}{2} \ , \tag{1.62}$$

$$B = \left[3+\frac{5\alpha}{2}+3\alpha(1+\alpha)\delta\right]e \ , \tag{1.63}$$

$$C = -\frac{(1+\alpha)e^2}{2} \ . \tag{1.64}$$

Before proceeding the final result for u, one can use the following useful expression: $\cos[\phi(1-\epsilon)] \simeq \cos\phi + \epsilon\phi\sin\phi + \mathcal{O}(\epsilon^2)$ for small value of ϵ parameter. Consequently, taking into account all facts mentioned above, the solution (1.57) can rewritten as

$$u(\phi) \simeq 1+\alpha\delta+e\cos\phi\left[1-3\epsilon\left(1+\frac{5\alpha}{6}+\alpha(1+\alpha)\delta\right)\right] + \epsilon(1+\alpha)\left[(1+\alpha\delta)\left(\frac{3+2\alpha}{1+\alpha}+3\alpha\delta\right)+e^2(1+\sin^2\phi)\right] \ . \tag{1.65}$$

As we mentioned before that the trajectory of celestial body in Newtonian theory is closed and the position of test particle satisfied the following condition $u(\phi) = u(\phi+2\pi)$. However due to the general relativistic effect the position can be found $u(\phi) \simeq u(\phi+2\pi+\delta\phi)$ and the periastron precession in STVG theory reads

$$\delta\phi \simeq \delta\phi_{\rm GR}\left[1+\frac{5}{6}\alpha+\alpha(1+\alpha)\delta\right] \ . \tag{1.66}$$

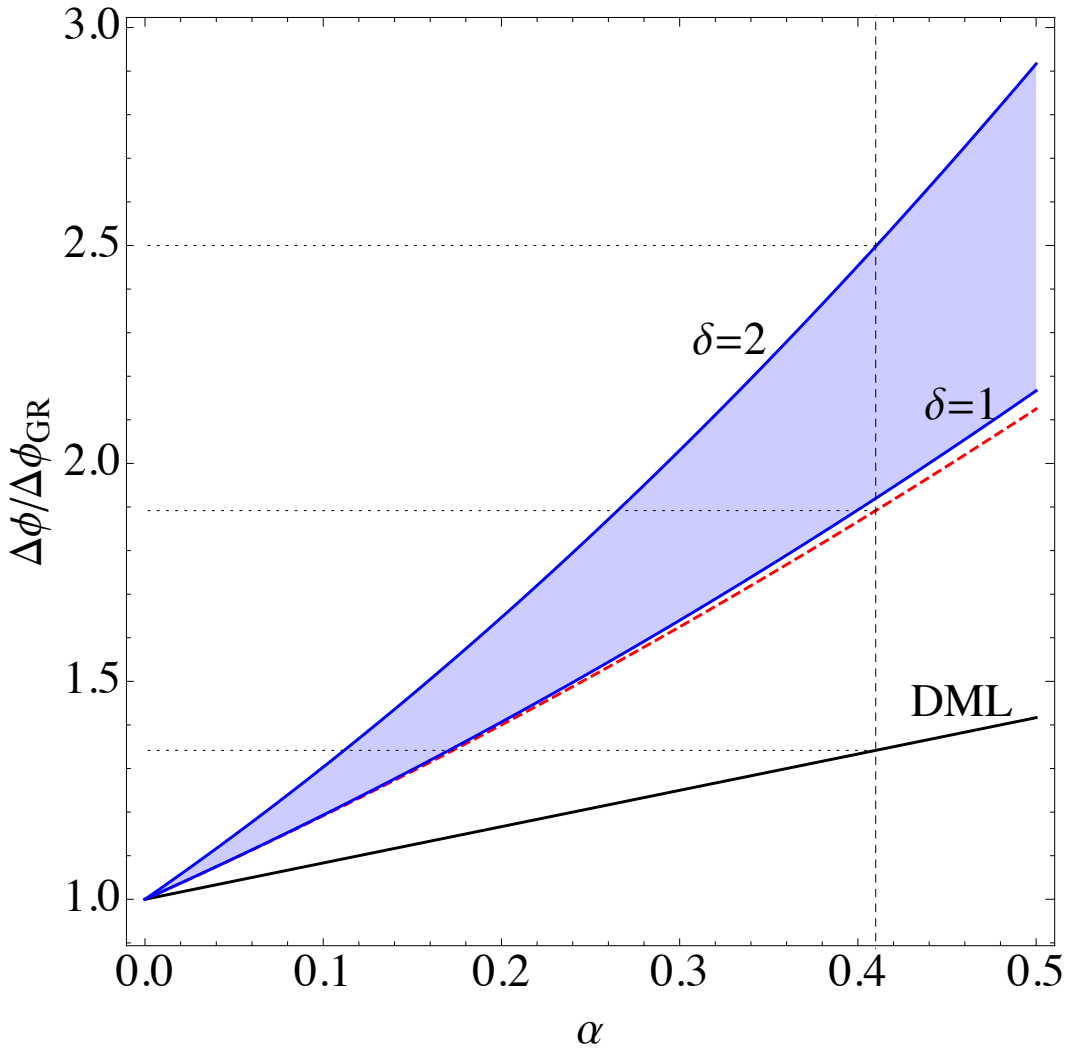


Figure 1.6: Fractional periastron precession of S2-star in STVG as a function α parameter in case when angular momentum in GR and STVG are the same, i.e. $L = L_{\rm GR}$. The lower black solid line DML represents the result in the paper [49], while the shaved area represents dependence of periastron precession from α parameter in the range of $1 \leq \delta \leq 2$ according to equation (1.66). The dashed red line is responsible for dependence of the periastron precession from STVG parameter without including the fifth interaction, i.e. $\kappa = 0$.

however according to [49], the expression for the periastron precession in STVG has been derived as

$$\delta\phi = \delta\phi_{\rm GR}\left(1+\frac{5}{6}\alpha\right)\ , \tag{1.67}$$

which can be easily obtained in the weak field approximation.

It is worth to noting that the paper [49] is well described and well written, in particular, statistical analyses on constraining the α parameter and cross correlations of the parameters by using Monte Carlo Markov Chain algorithm are nicely presented. It has been shown the upper limit for the STVG parameter is $\alpha \leq 0.41$ in CA and $\alpha \leq 0.58$ in QA approaches at 99.7% confidence level.

In order to get proper expression for the periastron shift in STVG one can estimate the parameter δ. Let's consider the energy of the star in the gravitational field including the fifth force. The energy expression for the star will be very similar to the energy of charged particle in the presence of the gravitational field and Coulomb potential (See for instance, [50]). Finally, the energy of star in STVG reads

$$E = \frac{mc^2\sqrt{g_{tt}}}{\sqrt{1-v^2/c^2}} - \frac{\alpha G_N M m}{r}\ , \tag{1.68}$$

so that

$$\delta = 1 + \frac{\sqrt{g_{tt}}}{\sqrt{1-v^2/c^2}} - \frac{\alpha G_N M}{c^2 r}\ . \tag{1.69}$$

where v is the three velocity of star measured by a local observer.

Taking into account all facts in the previous paragraph and using the observational data represented in the paper [49], the mass distance ratio for the S2 star can be estimated as $G_N M_\bullet/c^2 R_\bullet \simeq 6\times 10^{-12}$, where $M_\bullet$ is the mass of the SMBH and $R_\bullet$ is a distance from the SMBH to an observer. While the fractional velocity of the S2 star to speed of the light is $v/c \simeq 0.03$. So that the parameter δ is

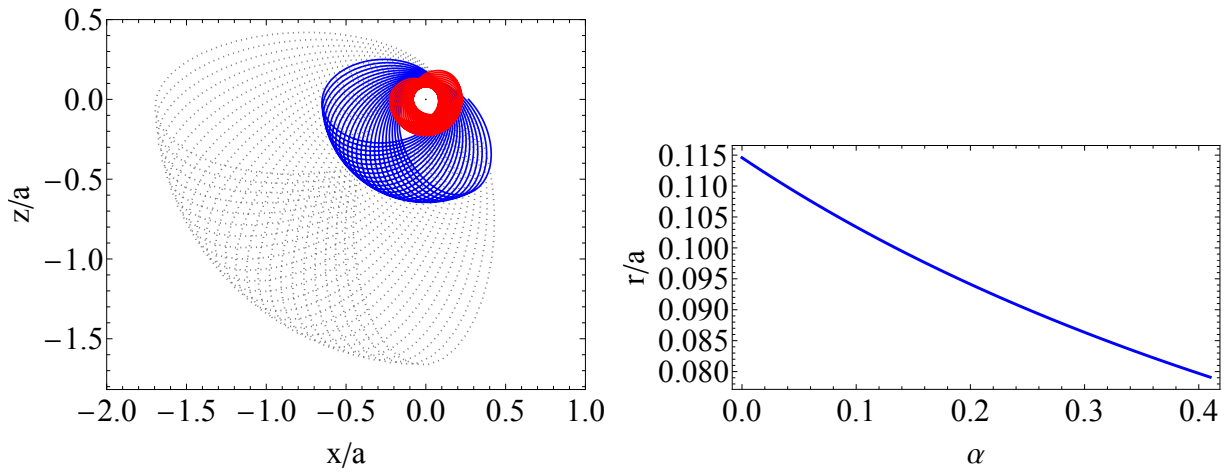


Figure 1.7: (Left) The trajectory of the S2 star around the SMBH in the STVG for different values of α parameter. The dashed gray line represents the trajectory of star in GR, while solid blue and red lines are responsible for $\alpha = 0.1$ and $\alpha = 0.4$. (Right) The initial position of star is a function the STVG parameter α.

.

approximated as $\delta \simeq 2$. Finally, the periastron precession of the S2 star reads

$$\delta\phi \simeq \delta\phi_{\rm GR}\left(1 + \frac{17\alpha}{6} + 2\alpha^2\right) \ , \tag{1.70}$$

which has a huge difference from what the authors obtained. It is also interesting to consider the periastron of the S2 star around the SMBH neglecting interact with the fifth force i.e. $\kappa = 0$. In this case the S2 star follows the geodesics line and the effect of STVG on star arises from pure background geometry. The periastron precession of the S2 star in STVG can be determined as $\delta\Phi \simeq \delta\Phi_{\rm GR}(1+\alpha)(1+5\alpha/6)$ which has extra $1+\alpha$ factor to that is obtained by authors.

In order to better understand the effects of the STVG we produce the trajectory of the S2 star around the SMBH and probe how the STVG parameter affects on the trajectory of the star. Figure 1.7 draws the trajectory of the S2 star around SMBH in the STVG theory for different values of the parameter α which is produced by a contour plot of $r/a = (\cos\phi, \sin\phi)(1-e^2)/u$, here u is obtained from equation (1.65) when $\delta = 2$. As one see that the periastron of the S2 star is very sensitive

to the parameter α and it might decreases approximately 7.5 times due to the STVG. It should be also noted that the initial position of the S2 star is different from that is predicted in GR. Recently the authors obtained new constraint for the STVG parameter using kinematic data of the S2-star by extending their previous studies and it is bounded as $\alpha \leq 0.662$ on the scales of the Galactic Centre at the 99.7% confidence level [51]. In their calculations the authors used the expression (1.67), which means $\delta\phi \leq 1.552\delta\phi_{\rm GR}$, however using the equation (1.70) periastron precission is estimated as $\delta\phi \leq 3.752\delta\phi_{\rm GR}$.

1.5 Conclusion

We have examined the geodesic motion in the Schwarzschild-MOG spacetime in STVG. Firstly, we have analyzed photon motion around the Schwarzschild-MOG black hole and derived analytical expressions for the photon sphere and critical impact parameter, which are crucial for understanding the black hole shadow. Our results showed that both the photon sphere and the size of the black hole shadow increase due to the presence of MOG. Furthermore, we applied these results to the observational data of M87* and Sgr A* observed by the Event Horizon Telescope (EHT) collaboration. Our analysis demonstrated that the shadow radius increases with the scalar parameter α, approaching a constant asymptotic value for large α. Importantly, the predicted shadow sizes are consistent with the EHT measurements for both black holes within the 1σ confidence level. This agreement provides meaningful constraints on the parameter $\alpha \leq 0.21$, highlighting its relevance in modeling compact objects beyond standard general relativity. Overall, the study shows that the scalar field parameter n plays a key role in modifying photon trajectories and black hole shadow profiles, and that current EHT observations can serve as an effective probe for testing STVG.

We have studied the circular motion of massive particles in the Schwarzschild-MOG spacetime, specifically examining the innermost stable circular orbit (ISCO). We found that the characteristic radii of these orbits are larger compared to those in the Schwarzschild spacetime. Through numerical calculations, we demonstrate that the innermost stable circular orbit (ISCO) of the massive particle is subject to the influence of an external force stemming from STVG. Furthermore, we determined the maximum energy efficiency of test particles around the Schwarzschild-MOG black hole, which can reach up to approximately 8.14%, indicating a relatively large efficiency compared to the Schwarzschild case. This external force

induces an increase in the particle's position. To visually illustrate this effect, we present graphical representations showcasing the dependence of the ISCO position on the STVG parameter denoted as α. These significant findings offer valuable insights into the impact of external forces on the motion of massive particles, enhancing our understanding of their behavior near black holes within the framework of STVG theory.

We have investigated the influence of the Scalar–Tensor–Vector Gravity (STVG) parameter α on the orbital motion of the S2 star around the supermassive black hole (SMBH) at the Galactic Centre. By constructing the trajectory of the S2 star within the STVG framework, we demonstrated that the periastron position is highly sensitive to variations in α. Our analysis reveals that an increase in the STVG parameter can lead to a noticeable decrease—up to approximately 7.5 times—in the periastron shift compared to the prediction of General Relativity (GR). Furthermore, the initial orbital position of the S2 star is found to deviate from that obtained in GR, highlighting the potential detectability of STVG effects through precise astrometric measurements. Recent observational analyzes have placed an upper bound on the STVG parameter as $\alpha \leq 0.662$ at the 99.7% confidence level using the kinematic data of the S2 star [51]. While earlier studies estimated the periastron precession as $\delta\phi \leq 1.552, \delta\phi_{\rm GR}$ using a dynamical mass limit approach, our results based on equation (1.70) suggest a stronger constraint, yielding $\delta\phi \leq 3.752, \delta\phi_{\rm GR}$. These findings indicate that precise monitoring of stellar orbits near the Galactic Centre can serve as a powerful test for modified gravity models such as STVG, offering an important avenue for probing deviations from GR in the strong-field regime.

Chapter II

Penrose process in the vicinity Kerr-MOG black hole

Imagination is more important than knowledge.

Albert Einstein

2.1 Introduction

Black holes, as described by Einstein's general theory of relativity, are among the most fascinating and extreme objects in the universe, characterized by their immense gravitational fields and event horizons from which nothing, not even light, can escape. The discovery of the Kerr solution in 1963, which describes rotating black holes, introduced a new dimension to black hole physics by revealing the ergosphere a region outside the event horizon where spacetime is dragged along by the black hole's rotation. This frame-dragging effect, a consequence of the black hole's angular momentum, enables unique physical processes, one of the most remarkable being the Penrose process, proposed by Roger Penrose in 1969 [52]. The Penrose process is a mechanism of energy extraction from a rotating black hole. The basic idea behind the Penrose process is that if a particle falls into a rotating black hole and splits into two fragments due to tidal forces in the region

so-called ergosphere, some of its mass can be captured by the black hole, while the rest can be flung outwards with a higher energy than the original object had. This happens because the black hole's rotation imparts energy to the debris as it is flung outward, in a process known as frame dragging [52]. The Penrose process has important implications for astrophysics, as it can help explain the origin of high-energy particles observed in various astrophysical phenomena, such as active galactic nuclei and gamma-ray bursts. The maximum amount of energy gain for a single particle around the extreme Kerr black hole is 20.7%, while larger efficiencies are possible for a charged particle around magnetized and charged rotating black holes [53–55]. The Penrose process is not an efficient means of extracting energy from a black hole, but it demonstrates how black holes can generate enormous amounts of energy from their strong gravitational fields. It is also a key concept in the study of black holes and their properties in the framework of MOG theory. In the present section, we are interested in investigating of dynamical motion of test particle around rotating black hole in STVG. We explicitly show the effect of the STVG in the ISCO position for massive particle. We also test STVG in gravitational analogue of the synchrotron radiation of massive particle and the Penrose process.

The theoretical foundation of the Penrose process lies in the Kerr spacetime's conserved quantities—energy and angular momentum—and the existence of negative-energy orbits within the ergosphere. Unlike non-rotating Schwarzschild black holes, where all infalling particles increase the black hole's mass, the Kerr geometry allows for energy extraction due to the coupling between the black hole's spin and the particle's motion. This phenomenon is closely related to other relativistic effects, such as superradiance, where waves can extract energy from a rotating black hole, amplifying their intensity. The Penrose process has inspired

a range of generalizations and astrophysical applications. Modified or continuous versions, such as the Blandford–Znajek mechanism [56], describe electromagnetic extraction of energy from magnetized rotating black holes and are widely invoked to explain relativistic jets in active galactic nuclei and quasars. Furthermore, extensions of the Penrose process have been explored in alternative gravity theories, charged and de Sitter spacetimes, and in the context of high-energy particle collisions near black hole horizons.

The Penrose process has profound implications for black hole thermodynamics and astrophysics. It provides insights into the second law of black hole mechanics, which states that the surface area of a black hole's event horizon cannot decrease, analogous to entropy in classical thermodynamics. By reducing the black hole's angular momentum, the Penrose process respects this law while allowing energy extraction, offering a window into the interplay between gravity, rotation, and thermodynamics. Astrophysically, it is considered a candidate mechanism for the immense energy outputs observed in quasars and other high-energy phenomena, where rotating supermassive black holes may drive relativistic outflows.

It is well-known that recent astronomical observations verify that the outflows as the form of winds and jets come out from active galactic nuclei (AGN) with the high energies being of order $E \approx 10^{42} - 10^{47}$ erg/s [57–59]. These outflows have so far been observed through X-ray, γ-ray and Very Long Baseline Interferometry (VLBI) observations. With this in view, test particle/charged particle motion would be related to these particle outflows from AGN. Therefore, one needs to explore a mechanism to propose an explanation for the above mentioned observations. In this respect, Banados, Silk, and West (BSW) [60] has been investigated that a Kerr black hole can serve as a particle accelerator. It has since been developed as the BSW mechanism. This means that when two particles collide near the

horizon of an extremal Kerr black hole, the center-of-mass energy (CME) can grow infinitely if the black hole has maximal rotation. If one of the colliding particles has a critical angular momentum, the CME increases even further for an extremal black hole. An extensive analysis has since been investigated in a large variety of situations [**?**, 60–77] generalizing the BSW mechanism to various gravity models and addressing the energy extraction from black holes and accretion disks and jets in AGNs. These generalizations have opened up new avenues in astrophysical applications, such as the understanding of phenomena like gamma-ray bursts and AGNs in the Galaxy.

In Ref. [61] it is discussed some practical limitations for the Kerr black hole to act as a particle accelerator and pointed out that the infinite CME for colliding particles can only be achieved when the black hole is exactly extremal and only on the horizon of the black hole. In [62] it is showed that the BSW mechanism near the Cauchy horizon can result in an infinite CME for colliding particles. The BSW mechanism has been extended to different black hole cases such as the Reissner-Nordstrom background and the Kerr-Newman black hole [65], the rotating black hole in Horava-Lifshitz gravity [78], Einstein-Maxwell-Dilaton black holes [79] and Kerr-(anti-)de Sitter black holes [80]. These extensions have demonstrated that the CME can become infinitely large near the horizon. The BSW mechanism has also been analyzed in regular black holes such as the Hayward's black hole metric [81].

Also there is extensive analysis on the constraints of the MOG parameter, e.g. it is shown by observational constraints on the Universe models that it would be small and thus the rate of change of gravitational constant is really small [82], it was also estimated to be $\alpha > 1$ by using observational data of millisecond pulsars [83]. It is well-known that there are various effects that allow for large CME as a

result of colliding particles or prevent particles from colliding with arbitrary high energy and confine the ability of serving as an accelerator for black holes. With this in view, it becomes increasingly important to study the impact of the MOG parameter on the energetic processes occurring in the close vicinity of black hole. In the present paper, we are aimed to discuss the collision of two massive particles falling from rest at infinity in the background of Kerr-MOG black holes. This problem is already studied in Ref. [33] however, the effect of the vector field is missed by author that might fail to get more information. We also discuss the novel effect due to in MOG theory in the Penrose process and BSW mechanism.

2.2 Axially-symmetric black hole solution

As previously noted, the spherically symmetric black hole solution in MOG is represented by the Schwarzschild–MOG spacetime, which closely resembles the Reissner–Nordström solution. When the black hole's rotation is taken into account, the corresponding solution becomes the Kerr–MOG spacetime, analogous to the Kerr–Newman geometry. In the Boyer-Lindquist coordinates, the spacetime around rotating black hole in the STVG is described by the Kerr-MOG metric [21]:

$$ds^2 = -\frac{\Delta}{\Sigma}\left(dt - a\sin^2\theta d\phi\right)^2 + \Sigma\left(\frac{dr^2}{\Delta} + d\theta^2\right) + \frac{\sin^2\theta}{\Sigma}\left[(r^2+a^2)d\phi - adt\right]^2 \ , \tag{2.1}$$

where $\Delta = r^2 - 2(1+\alpha)G_N M r + \alpha(1+\alpha)G_N^2 M^2 + a^2$ and $\Sigma = r^2 + a^2\cos^2\theta$. Here a is specific angular momentum (spin) of the black hole along mass of black hole M and parameter α in STVG theory. Notice that the associated vector potential, Φ_μ, to the spacetime (2.1) which characterize the fifth interaction between test body with external vector field and this interaction is described by the Coulomb-like potential in the static spacetime. While in the rotating spacetime the vector

potential can be extended as

$$\Phi_\mu = \frac{\sqrt{\alpha}Mr}{\Sigma}\left(-1, 0, 0, a\sin^2\theta\right) \ . \tag{2.2}$$

That means a rotating black hole posses magneto dipole-type potential due to rotation.

The horizon of the rotating black hole in STVG is located at

$$x_+ = 1 + \alpha + \sqrt{1 + \alpha - a_*^2} \ ,$$

while the ergosphere of the black hole is determined as

$$x_{\rm erg} = 1 + \alpha + \sqrt{1 + \alpha - a_*^2\cos^2\theta} \ ,$$

where $x = r/M$ is a dimensionless radial coordinate and $a_* = a/M$ is a dimensionless spin parameter. The irreducible mass of the black hole in STVG is determined as $M_{\rm irr} = Mx_+/2$. According to the expression (1.21) the STVG parameter is always positive, i.e. $\alpha \geq 0$. From the existence of the black hole horizon one can find the limit the black hole's spin parameter as $|a_*| \leq \sqrt{1+\alpha}$ which means in the STVG theory the black hole can rotate faster than Kerr black hole. The dependence of the maximal spin of the black hole from STVG parameter α is illustrated in Fig. 2.1. It is known that the maximal spin of Kerr black hole is $a_{*\rm max} = 1$ while in the STVG theory it equal to $a_{*\rm max} = \sqrt{1+\alpha}$. Figure 2.2 draws the ergosphere of the Kerr-MOG black hole for different values of the STVG parameter α. As one can see that from this result that when the α parameter gets a large the gravitational force dominates rotational force, therefore the region of the ergosphere gets smaller.

Now we consider massive particle motion around black hole in the STVG theory. In this theory massive particles do not follow the geodesic line in unlike other gravity theories. Therefore equation of motion for massive particle is governed by

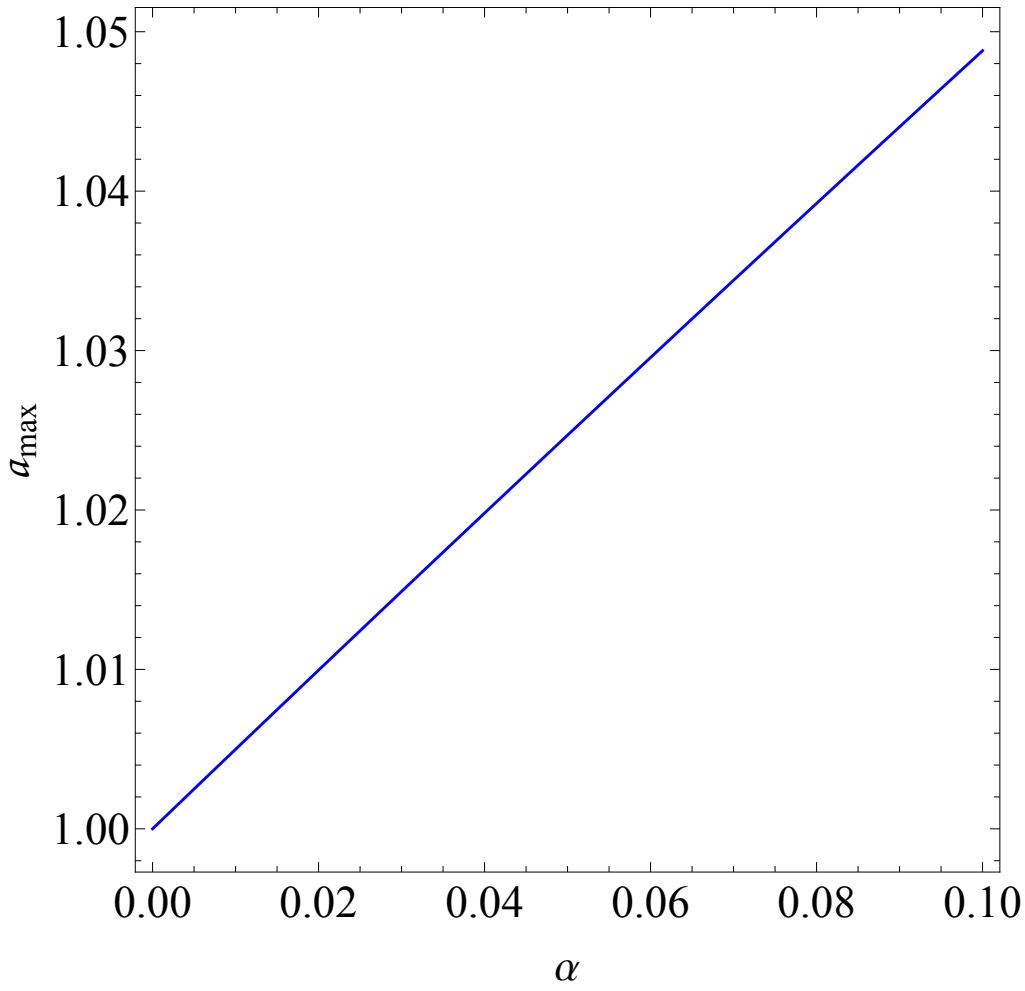


Figure 2.1: Dependence of the maximal spin of the black hole from the STVG parameter α which is given by the equation $a_{\max} = \sqrt{1+\alpha}$.

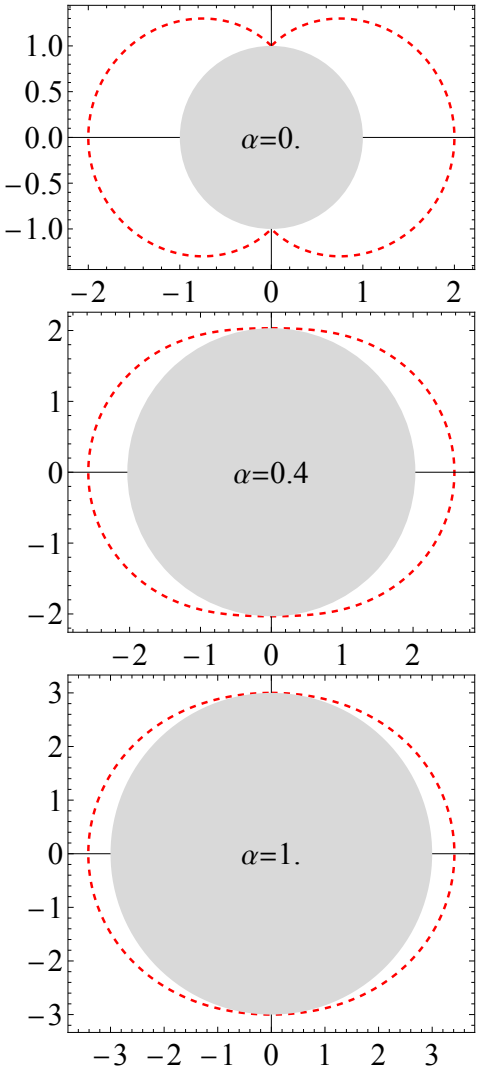


Figure 2.2: The ergoshere of the black hole for the different values of the STVG parameter α for $a_* = 1$.

the following equation [22]:

$$\ddot{x}^{\mu}+\Gamma^{\mu}_{\nu\lambda}\dot{x}^{\nu}\dot{x}^{\lambda}=\frac{q}{m}B^{\mu}{}_{\nu}\dot{x}^{\nu}\ , \qquad \dot{x}^{\mu}=\frac{dx^{\mu}}{ds}\ , \tag{2.3}$$

where m is the mass of test particle, $q=\kappa m=\sqrt{\alpha}m$ is the coupling constant of the interaction between the particle and the fifth force in STVG theory, $\dot{x}^{\mu}$ is the four-velocity of test particle normalized as $g_{\mu\nu}\dot{x}^{\mu}\dot{x}^{\nu}=-1$. An anti-symmetric tensor is defined as $B_{\mu\nu}=\partial_{\mu}\Phi_{\nu}-\partial_{\nu}\Phi_{\mu}$. The conserved quantities of motion, namely, the energy E, and the angular momentum L, of test particle are satisfied the following relations:

$$g_{tt}\dot{t}+g_{t\phi}\dot{\phi}=-\frac{E+q\Phi_t}{m}\ , \qquad g_{\phi\phi}\dot{\phi}+g_{t\phi}\dot{t}=\frac{L-q\Phi_{\phi}}{m}\ , \tag{2.4}$$

which allows to derive the following expressions:

$$\dot{t}=-\frac{1}{g_{tt}g_{\phi\phi}-g_{t\phi}^{2}}\left[\left(\frac{L-q\Phi_{\phi}}{m}\right)g_{t\phi}+\left(\frac{E+q\Phi_t}{m}\right)g_{\phi\phi}\right]\ , \tag{2.5}$$

$$\dot{\phi}=\frac{1}{g_{tt}g_{\phi\phi}-g_{t\phi}^{2}}\left[\left(\frac{L-q\Phi_{\phi}}{m}\right)g_{tt}+\left(\frac{E+q\Phi_t}{m}\right)g_{t\phi}\right]\ . \tag{2.6}$$

Using the normalization of the four-velocity and taking into account above expressions, one can have the following equation:

$$\begin{aligned}&\left(E+q\Phi_t\right)^{2}-2\omega\left(E+q\Phi_t\right)\left(L-q\Phi_{\phi}\right)\\&+\frac{g_{tt}}{g_{\phi\phi}}\left(L-q\Phi_{\phi}\right)^{2}+m^{2}\left(g_{rr}\dot{r}^{2}+g_{\theta\theta}\dot{\theta}^{2}+1\right)\psi=0\ .\end{aligned} \tag{2.7}$$

where $\omega=-g_{t\phi}/g_{\phi\phi}>0$ and $\psi=g_{tt}-g_{t\phi}^{2}/g_{\phi\phi}<0$. Considering motion of massive particle in circular orbit with the following conditions $\dot{r}=0$ and $\dot{\theta}=0$, one can find that in STVG, massive particle motion is bounded by the following effective potential [53]:

$$V=-q\Phi_t+\omega\left(L-q\Phi_{\phi}\right)+\sqrt{-\psi\left[m^{2}+\frac{\left(L-q\Phi_{\phi}\right)^{2}}{g_{\phi\phi}}\right]}\ , \tag{2.8}$$

satisfying the following condition $E = V$. It is well-known that the effective potential is a useful tool for understanding the motion of test particles around black holes, and the position of the innermost stable circular orbit (ISCO) can be determined by finding the minimum value of the effective potential. The ISCO position of massive particle around a black hole is the smallest possible orbit where a test particle can maintain a stable circular orbit without being drawn into the black hole or flung away into space. The ISCO is a significant location for astrophysical observations, as it can affect the emission of radiation and matter falling onto the black hole. The study of the ISCO can also provide insight into the properties of black holes and tests of general relativity including alternative theories of gravity. The ISCO position depends on the mass and spin of the black hole, as well as the STVG parameter in the present research work. Next thing what we discuss is finding the radius of the ISCO of massive particle around the black hole in STVG and to test how it depends on the α parameter. For simplicity, we consider motion of massive particle in the equatorial plane that means the effective potential depends only on the radial coordinate, i.e. $V = V(r)$. Using the standard method, the ISCO position can be found from the following conditions: $V(r) = E$, $V'(r) = 0$ and $V''(r) \leq 0$. Obtaining the analytical expression for the ISCO position, therefore, careful numerical analyzes showed that the ISCO position gets larger due the effect of STVG. Figure 2.3 shows the dependence of the ISCO position of massive particles orbiting around the Schwarzschild-MOG and extreme Kerr-MOG black holes from the α parameter. Notice that the ISCO position is located in the region between two curves in Fig. 2.3 for arbitrary values of the spin parameter with range of $0 < a_* < \sqrt{1+\alpha}$.

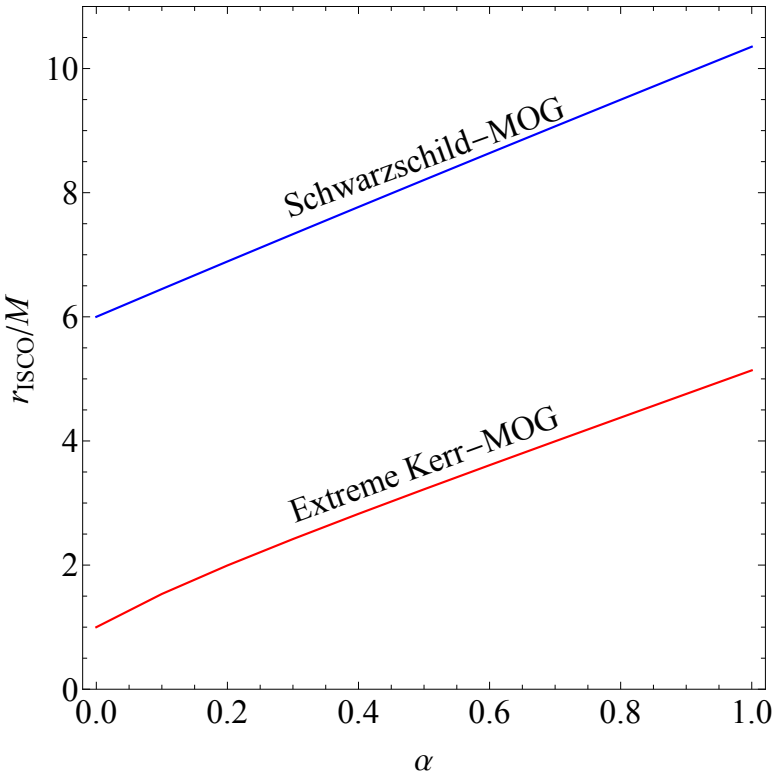


Figure 2.3: Dependence of the ISCO position for massive particle from the STVG parameter α for static and extreme black holes.

2.3 Penrose process

The Penrose process involves taking advantage of the strong gravitational field and rotation of a black hole to extract energy from it. In this process, a particle or a photon falls into the black hole's ergosphere, which is the region just outside the event horizon where spacetime is dragged along with the black hole's rotation. According to the Penrose process the particle falling onto the black hole separates into two parts in the ergosphere, with one part falling into the black hole and the other part escaping outwards. The part that escapes carries away some of the black hole's rotational energy, resulting in a net loss of energy for the black hole [52]. This extracted energy can then be used to power various astrophysical phenomena. The Penrose process is an important concept in theoretical astrophysics and is used to explain some of the most energetic phenomena in the universe.

In the present paper, we are aimed to test STVG theory with the Penrose process. The energy efficiency of the particle is depends of the mass, spin parameter and the STVG parameter. Assume that massive particle (1) of parameters $(m_1, E_1, L_1, \dot{r}_1, \dot{\theta}_1, \dot{\phi}_1)$ falls onto black hole from infinity and decays into two fragments (2) and (3) with parameters of $(m_2, E_2, L_2, \dot{r}_2, \dot{\theta}_2, \dot{\phi}_2)$ and $(m_3, E_3, L_3, \dot{r}_3, \dot{\theta}_3, \dot{\phi}_3)$ in the ergosphere of the rotating black hole, where m_i, E_i, L_i, $\dot{r}_i$ and $\dot{\theta}_i$ are, respectively, the mass, energy, angular momentum, radial, vertical and azimuthal velocities. The conservation laws for this process can be written

as

$$m_1 \geq m_2 + m_3 \ , \tag{2.9}$$

$$E_1 = E_2 + E_3 \ , \tag{2.10}$$

$$L_1 = L_2 + L_3 \ , \tag{2.11}$$

$$m_1\dot{r}_1 = m_2\dot{r}_2 + m_3\dot{r}_3 \ , \tag{2.12}$$

$$0 = m_2\dot{\theta}_2 + m_3\dot{\theta}_3 \ , \tag{2.13}$$

$$m_1\dot{\phi}_1 = m_2\dot{\phi}_2 + m_3\dot{\phi}_3 \ . \tag{2.14}$$

Again we consider circular motion of a massive particle with four-velocity of $\dot{x}^\mu = \dot{t}(1, v, 0, \Omega)$. Using the normalization of the four-velocity, the angular velocity of particle (1) is determined as [84]

$$\Omega_1 = \frac{-(u^2 + g_{tt})g_{t\phi} + u\sqrt{(-\psi)(u^2 + g_{tt})g_{\phi\phi}}}{u^2 g_{\phi\phi} + g_{t\phi}^2} \ , \tag{2.15}$$

where $u = (E_1 + q_1\Phi_t)/m_1$, while the angular velocity of the splitted fragments denote $\Omega_2 = \Omega_+$ and $\Omega_3 = \Omega_-$, where $\Omega_\pm$ are defined as

$$\Omega_\pm = -\frac{g_{t\phi}}{g_{\phi\phi}} \pm \sqrt{\left(\frac{g_{t\phi}}{g_{\phi\phi}}\right)^2 - \frac{g_{tt}}{g_{\phi\phi}}} \ . \tag{2.16}$$

From the inequality for particles mass in (2.9), relation between coupling constants can be obtained as $q_1 \geq q_2 + q_3$. Using equation (2.14) and after simple algebraic manipulations, the relation between energies of in falling and escaping particles can be found as

$$(E_3 + q_3\Phi_t)\frac{\Omega_3 - \Omega_2}{g_{tt} + \Omega_3 g_{t\phi}} \geq (E_1 + q_1\Phi_t)\frac{\Omega_1 - \Omega_2}{g_{tt} + \Omega_1 g_{t\phi}} \ . \tag{2.17}$$

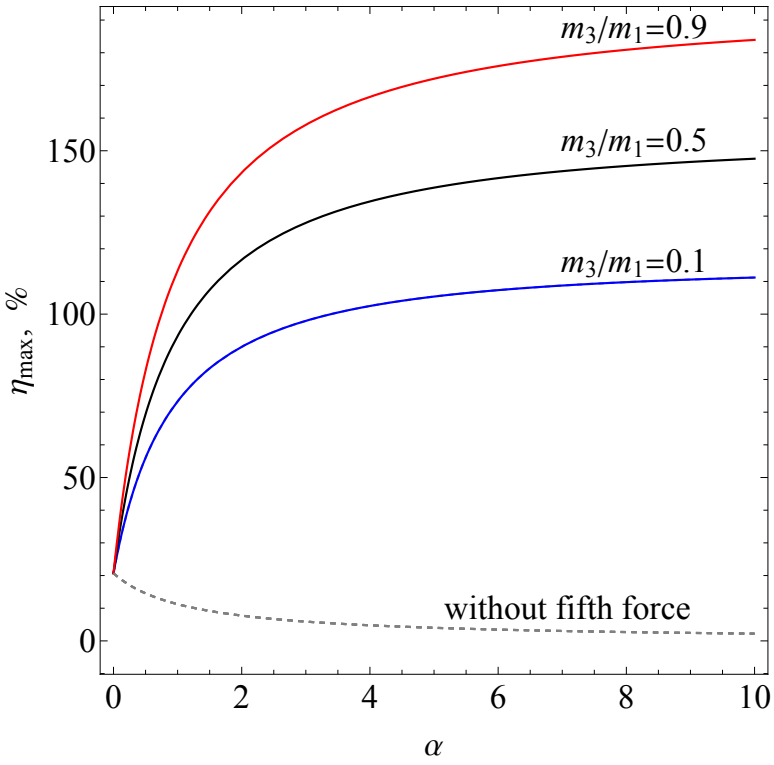


Figure 2.4: Dependence of the maximal energy efficiency of the black hole from the STVG parameter α.

The energy efficiency is determined as $\eta = E_3/E_1 - 1$, while in STVG theory is

$$\begin{aligned}\eta &\geq \left(1+\frac{q_1\Phi_t}{E_1}\right)\frac{\Omega_1-\Omega_2\,g_{tt}+\Omega_3 g_{t\phi}}{\Omega_3-\Omega_2\,g_{tt}+\Omega_1 g_{t\phi}} - \frac{q_3\Phi_t}{E_1} - 1 \\ &= \frac{1}{2}\left(\sqrt{1+\frac{g_{tt}}{u^2}}-1\right)\left(1+\frac{q_1}{E_1}\Phi_t\right) - \frac{q_1+q_3}{E_1}\Phi_t\,. \end{aligned} \tag{2.18}$$

To make qualitative analyses of the energy efficiency in STVG, one can estimate the energy of falling particle as $E_1 \simeq m_1$ and the expression (4.52) for the extreme rotating black hole (i.e. $x_+ = 1+\alpha$) reads

$$\eta_{\max} \geq \frac{1}{2(1+\alpha)}\left[\sqrt{2+\alpha}-1+2\alpha\left(1+\frac{m_3}{m_1}\right)\right]\,. \tag{2.19}$$

For large value of the STVG parameter, i.e. $\alpha \to \infty$, the energy efficiency is $\eta_{\max} \geq 1 + m_3/m_1$, which is greater than 100% because of mass ratio of escaping and falling particles, while in the case of the extreme Kerr black black hole, $\eta_{\max} = (\sqrt{2}-1)/2 \simeq 0.207$, which is around $\sim 21\%$. Figure 2.4 shows that

maximal efficiency of energy extraction from the Kerr-MOG black hole reaches up to $\sim 200\%$ for particular value of mass ratio of escaping and falling which is quite huge. However, in the research paper [53], it has been demonstrated that a magnetized Kerr black hole is considered one of the most promising candidates for accelerating high-energy particles. The study reports that the efficiency of energy extraction from a magnetized Kerr black hole can exceed 100% due to the induced electrostatic potential resulting from rotation and magnetic field effects. Likewise, in the framework of STVG theory, the external fifth-potential plays a crucial role in generating high-energy particles and potentially surpassing the 100% efficiency limit in energy extraction from a Kerr-MOG black hole.

We see that under some circumstances the efficiency of energy extraction via Penrose process can be very large, exceeding $> 100\%$. This might open the possibilities to obtain additional constraints on MOG parameter α which might be a good topic for further research. In the paper [13], the authors have suggested that MOG may have implications for the radio emission properties of pulsars. The upper limit for the parameter α in MOG using observational data from specific millisecond pulsars has been estimated. For the millisecond pulsar J2145-0750, the estimated upper limit for α is ~ 1.6011. Similarly, for the millisecond pulsars J0024-7204D and J0024-7204H, the estimated upper limits for α are ~ 3.06528 and ~ 0.9747, respectively. However these values of MOG parameter are quite huge for the black hole. In Ref. [38], the constraint on MOG parameter α has been obtained considering the motion of the S2-star around the supermassive black hole at the center of the Milky Way described Schwarzschild-MOG spacetime and by comparing the predicted orbital motion of the S2-star based on the with the available astrometric data, including measurements of positions, radial velocities, and orbital precession consisting of 145 position measurements, 44 radial velocity

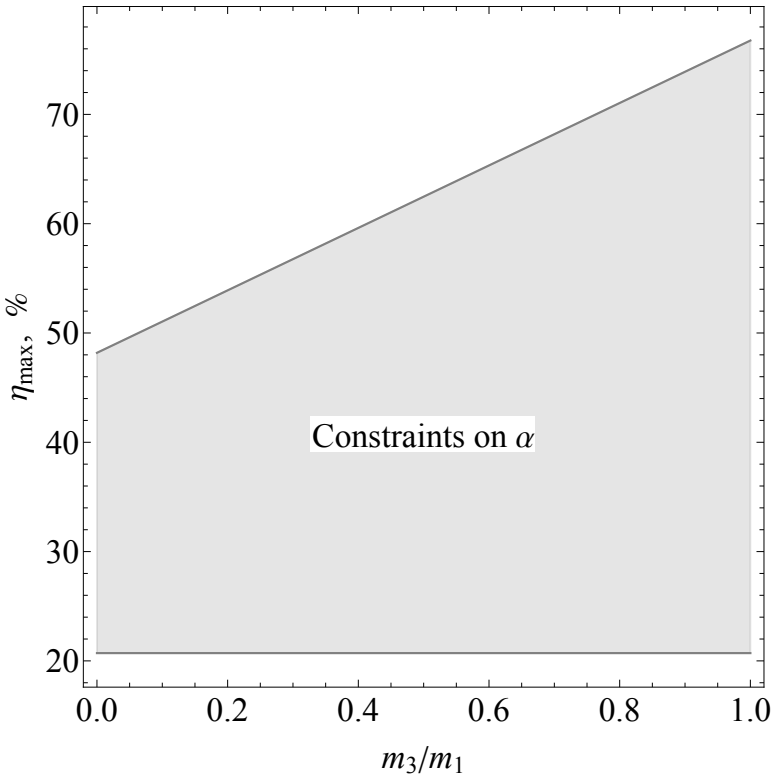


Figure 2.5: Dependence of the maximal energy efficiency of the black hole from mass ratio of escaping and falling particles at $\alpha \lesssim 0.41$.

measurements. Using a Monte Carlo Markov Chain (MCMC) algorithm, it has been found that the constrained to be $\alpha \lesssim 0.41$ at the 99.7% confidence level. Using this upper value for MOG parameter dependence of the maximum efficiency of energy extraction via Penrose process from mass ratio of escaping and falling particle is illustrated in Fig. 2.5 and in this case, the maximum energy efficiency reaches up to $\sim 78\%$ at $\alpha \lesssim 0.41$.

2.4 Collision of two massive particles near Kerr-MOG black hole

One can also discuss the very similar mechanism around rotating black hole in the STVG which is known as the Banados-Silk-West (BSW) process which inverse

process to the Penrose one. This process is a theoretical mechanism for the creation of a black hole in the collision of two high-energy particles [85]. The BSW process is significant because it provides a new way to study the properties of black holes and the nature of gravity. It also has implications for the study of high-energy physics and the behavior of particles at extremely high energies.

The BSW process involves the collision of two high-energy massive particles. In this process, the size of the resulting black hole depends on the energy of the colliding particles, which can be related to their mass and velocity through the principles of special relativity. The exact equations and calculations involved in the BSW process are complex and beyond the scope of a simple answer, but they involve the principles of general relativity, quantum mechanics, and particle physics.

The equation of motion in the background of the Kerr-MOG spacetime can be derived as

$$\Sigma^2\dot{r}^2 = \left[(r^2+a^2)\mathcal{E} - a\mathcal{L} - \alpha Mr\right]^2 - \Delta\left(\mathcal{K} + r^2\right) \ , \tag{2.20}$$

$$\Sigma^2\dot{\theta}^2 = \mathcal{K} - \left(\frac{\mathcal{L}}{\sin\theta} - a\mathcal{E}\sin\theta\right)^2 - a^2\cos^2\theta \ , \tag{2.21}$$

$$\Sigma\dot{\phi} = \frac{a}{\Delta}[(r^2+a^2)\mathcal{E} - a\mathcal{L} - \alpha Mr] + \frac{\mathcal{L} - a\mathcal{E}\sin^2\theta}{\sin^2\theta} \ , \tag{2.22}$$

$$\Sigma\dot{t} = \frac{r^2+a^2}{\Delta}[(r^2+a^2)\mathcal{E} - a\mathcal{L} - \alpha Mr] + a(\mathcal{L} - a\mathcal{E}\sin^2\theta) \ , \tag{2.23}$$

where $\mathcal{K}$ is the Carter constant of motion. For simplicity, we consider circular motion of massive particle in the equatorial plane of the Kerr-MOG black hole i.e. $\theta = \pi/2$, in this case the Carter constant takes a form $\mathcal{K} = (\mathcal{L} - a\mathcal{E})^2 = M^2\ell^2$.

Then radial motion of test particle takes a form:

$$\dot{r}^2 = \left(\mathcal{E} - \frac{\alpha M}{r} - \frac{\ell a_* M^2}{r^2}\right)^2 - \left(1 - \frac{2(1+\alpha)M}{r} + \frac{[\alpha(1+\alpha)+a_*^2]M^2}{r^2}\right)\left(1 + \frac{\ell^2 M^2}{r^2}\right) . \tag{2.24}$$

Now we discuss the collision of two massive neutral particles near the Kerr-MOG black holes and examine how MOG parameter affects to this process. According to Ref. [85] the energy of centre-mass (ECM) of two particle reads $E^2_{\rm c.m.} = -g^{\mu\nu}(p_{1\mu}+p_{2\mu})(p_{1\nu}+p_{2\nu})$, where $p_{1\mu}$ and $p_{2\mu}$ are the four-momentum of particles, respectively. The ECM of two neutral particle near Kerr-MOG black hole reads

$$E^2_{\rm c.m.} = -g^{\mu\nu}(p_{1\mu}+p_{2\mu})(p_{1\nu}+p_{2\nu}) \tag{2.25}$$

$$= m_1^2 + m_2^2 - 2m_1 m_2 g_{\mu\nu} U_1^\mu U_2^\nu \tag{2.26}$$

$$= 2m_1 m_2 \left(1 + \frac{(m_1-m_2)^2}{2m_1 m_2} - g_{\mu\nu} U_1^\mu U_2^\nu\right) , \tag{2.27}$$

with $p_{i\mu} = P_{i\mu} - q_i\phi_\mu$ and $U_{i\mu} = u_{i\mu} - (q_i/m_i)\phi_\mu$ being the four-velocities of massive particles with $i = (1,2)$ in the presence of the external vector potential. Using equation of motion (4.46)-(4.49), the ECM in the background of the Kerr-MOG spacetime takes a form [86]:

$$\frac{E^2_{\rm c.m.}}{2m_1 m_2} = 1 + \frac{(m_1-m_2)^2}{2m_1 m_2} - \frac{T_1(\theta)T_2(\theta) + \sqrt{\mathcal{K}_1 - T_1^2(\theta) - a^2\cos^2\theta}\sqrt{\mathcal{K}_2 - T_2^2(\theta) - a^2\cos^2\theta}}{\Sigma} + \frac{R_1(r)R_2(r) - \sqrt{R_1^2(r) - \Delta(r^2+\mathcal{K}_1)}\sqrt{R_2^2(r) - \Delta(r^2+\mathcal{K}_2)}}{\Sigma\Delta} , \tag{2.28}$$

where $T_i(\theta) = \mathcal{L}_i \csc\theta - a\mathcal{E}_i \sin\theta$, and $R_i(r) = (r^2+a^2)\mathcal{E}_i - a\mathcal{L}_i - \alpha G_N M r$. As one can see that ECM of two particles divergences at two points, one is at the horizon of black hole because of the condition $\Delta = 0$, while other one is located at the polar region of the black hole (i.e., $\theta = 0, \pi$) because of $\csc\theta$. Therefore to

avoid this problem the last term of equation (2.29) can be modified as

$$\frac{E^2_{\rm c.m.}}{2m_1m_2} = 1 + \frac{(m_1-m_2)^2}{2m_1m_2} - \frac{T_1(\theta)T_2(\theta) + \sqrt{\mathcal{K}_1 - T_1^2(\theta) - a^2\cos^2\theta}\sqrt{\mathcal{K}_2 - T_2^2(\theta) - a^2\cos^2\theta}}{\Sigma} + \frac{R_1^2(r)(r^2+\mathcal{K}_2) + R_2^2(r)(r^2+\mathcal{K}_1) + (r^2+\mathcal{K}_1)(r^2+\mathcal{K}_2)\Delta}{\Sigma\left[R_1(r)R_2(r) + \sqrt{R_1^2(r) - \Delta(r^2+\mathcal{K}_1)}\sqrt{R_2^2(r) - \Delta(r^2+\mathcal{K}_2)}\right]} . \quad (2.29)$$

and there are no more problem with the last term however, there are still problem at the polar region $\theta = 0$ and $\theta = \pi$. Therefore in our future calculations, we consider particular value of the angle θ.

Assume two particles collide in the equatorial plane $\theta = \pi/2$ of the Kerr-MOG black hole. In this case the Carter constant takes a form $\mathcal{K}_i = (\mathcal{L}_i - a\mathcal{E}_i)^2 = M^2\ell_i^2$. From equation (2.29), ECM of particles at the black hole's horizon takes a form:

$$\frac{E^2_{\rm c.m.}(r_+)}{2m_1m_2} = 1 + \frac{(m_1-m_2)^2}{2m_1m_2} - \frac{\ell_1\ell_2M^2}{r_+^2} + \frac{r_+^2\mathcal{E}_1 - a\ell_1M - \alpha Mr_+}{2(r_+^2\mathcal{E}_2 - a\ell_2M - \alpha Mr_+)}\left(1 + \frac{\ell_2^2M^2}{r_+^2}\right) + \frac{r_+^2\mathcal{E}_2 - a\ell_2M - \alpha Mr_+}{2(r_+^2\mathcal{E}_1 - a\ell_1M - \alpha Mr_+)}\left(1 + \frac{\ell_1^2M^2}{r_+^2}\right) , \quad (2.30)$$

in the case when $\mathcal{L}_i = a\mathcal{E}_i$ or $\ell_i = 0$, one can get

$$\frac{E^2_{\rm c.m.}(r_+)}{2m_1m_2} = 1 + \frac{(m_1-m_2)^2}{2m_1m_2} + \frac{r_+\mathcal{E}_1 - \alpha M}{2[r_+\mathcal{E}_2 - \alpha M]} + \frac{r_+\mathcal{E}_2 - \alpha M}{2[r_+\mathcal{E}_1 - \alpha M]} , \quad (2.31)$$

which has singularities when of particle's energy is equal to $\mathcal{E}_{1,2} = \alpha M/r_+$.

Collision in the equatorial plane of near Schwarzschild-MOG black hole

For simplicity, one can consider collision of two particle near the Schwarzschild-MOG spacetime (i.e., $a = 0$), and ECM is determined as

$$\frac{E^2_{\rm c.m.}(r_+)}{2m_1m_2} = 1 + \frac{(m_1-m_2)^2}{2m_1m_2} - \frac{\ell_1\ell_2M^2}{r_+^2} + \frac{r_+\mathcal{E}_1 - \alpha M}{2[r_+\mathcal{E}_2 - \alpha M]}\left(1 + \frac{\ell_2^2M^2}{r_+^2}\right) + \frac{r_+\mathcal{E}_2 - \alpha M}{2[r_+\mathcal{E}_1 - \alpha M]}\left(1 + \frac{\ell_1^2M^2}{r_+^2}\right) . \quad (2.32)$$

It is also interesting to consider particles approaching from infinity, in this case, specific energies of particle will be $\mathcal{E}_1 = \mathcal{E}_2 = 1$, then

$$\frac{E^2_{\text{c.m.}}(r_+)}{2m_1m_2} = 2 + \frac{(m_1 - m_2)^2}{2m_1m_2} + \frac{(\ell_2 - \ell_1)^2 M^2}{r_+^2} \ , \tag{2.33}$$

while for equal mass particles $m_1 = m_2 = m$, one obtains $E^2_{\text{c.m.}} = 4m^2 + 2(\ell_2 - \ell_1)^2 M^2/r_+^2$ which coincides with result in [85].

Collision in the equatorial plane of extreme Kerr black hole

Now we consider collision of two massive particles near extremal Kerr-MOG black hole. From expression for the horizon of Kerr-MOG black hole one can immediately find that maximum spin of black holes is $a_{\text{max}} = M\sqrt{1+\alpha}$ that means $r_+ = M(1+\alpha)$, then ECM of particles approaching from infinity with specific energies of $\mathcal{E}_1 = \mathcal{E}_2 = 1$ yields

$$\begin{aligned}\frac{E^2_{\text{c.m.}}(r_+)}{2m_1m_2} &= 1 + \frac{(m_1 - m_2)^2}{2m_1m_2} + \frac{\ell_1 - 2\sqrt{1+\alpha}}{\ell_2 - 2\sqrt{1+\alpha}} + \frac{\ell_2 - 2\sqrt{1+\alpha}}{\ell_1 - 2\sqrt{1+\alpha}} \\ &\quad - \frac{\alpha(\ell_2 - \ell_1)^2}{2(1+\alpha)(\ell_1 - 2\sqrt{1+\alpha})(\ell_2 - 2\sqrt{1+\alpha})} \ .\end{aligned} \tag{2.34}$$

The last term of the expression (2.34) is responsible for the effect arises due to the external vector potential. In particular case when $\ell_1 = \ell_2$ and $m_1 = m_2 = m$, ECM in expression (2.34) takes a form $E^2_{\text{cm}} = 2m^2$. Indeed, form the expression (2.34), one can see that in absence of MOG parameter i.e. $\alpha = 0$, the expression for ECM reduces to result obtained for the extreme Kerr spacetime in Ref. [85]. As a result one can conclude that ECM of two particle near Kerr-MOG black hole is divergent when angular momentum of one of particle is to be $\ell = 2\sqrt{1+\alpha}$, which is the key requirement to reach the arbitrarily large energy [85]. The point to be noted here is that the ECM starts growing as black hole spin a increases as a consequence of the BSW mechanism considered here. However, the maximum

largest energy grows till the spin parameter reaches its maximal value, thus resulting in being arbitrarily large in the maximal spin parameter, i.e., $a \to a_{max}$. This is a surprising aspect of the BSW mechanism. Thus, for finite CME only finite values of the angular momentum are allowed in particular, for the same values of angular momentum and mass of particles one obtain $E^2_{\text{c.m.}} = 2m^2$. The behavior of the CME as a function of α in the presence of the external vector field is depicted in Fig. 2.6. The collision occurring near the horizon of the Kerr-MOG black hole can produce high energy as compared to Kerr black holes and increases with the increase of the parameter α. We see that the CME strongly depends on the MOG parameter α. A high energy can be achieved with the maximum spin. It is noted that a maximum CME can be produced in the presence of a vector field as compared to its absence. The CME has decreasing behavior with the increase of radial distance r and becomes almost constant away from the event horizon of BH. The CME for colliding particles does not diverge in the absence/presence of a external vector field.

In the STVG, it can be represented as

$$\frac{E^2_{\text{cm}}}{2m_0^2} = 1 - \frac{a^2}{r^2} + \frac{T^2 - (2+\alpha)aMr(l_1+l_2) + (a^2-\Delta)l_1 l_2}{\Delta r^2} - \sqrt{\left[\frac{(T-al_1)^2}{r^2\Delta} - \frac{(l_1-a)^2}{r^2} - 1\right]\left[\frac{(T-al_2)^2}{r^2\Delta} - \frac{(l_2-a)^2}{r^2} - 1\right]}, \tag{2.35}$$

where $T = r^2 + a^2 - \alpha Mr$. This expression divergences at the horizon because of $\Delta = 0$, however, our analyses showed that numerator of the expression also divergences. Therefore near the horizon the expression (2.35) reduces to

$$\frac{E^2_{\text{cm}}}{2m_0^2} = \frac{l_1 - 2\sqrt{1+\alpha}}{l_2 - 2\sqrt{1+\alpha}} + \frac{l_2 - 2\sqrt{1+\alpha}}{l_1 - 2\sqrt{1+\alpha}} - \frac{\alpha(l_2-l_1)^2}{2(1+\alpha)(l_1 - 2\sqrt{1+\alpha})(l_2 - 2\sqrt{1+\alpha})}, \tag{2.36}$$

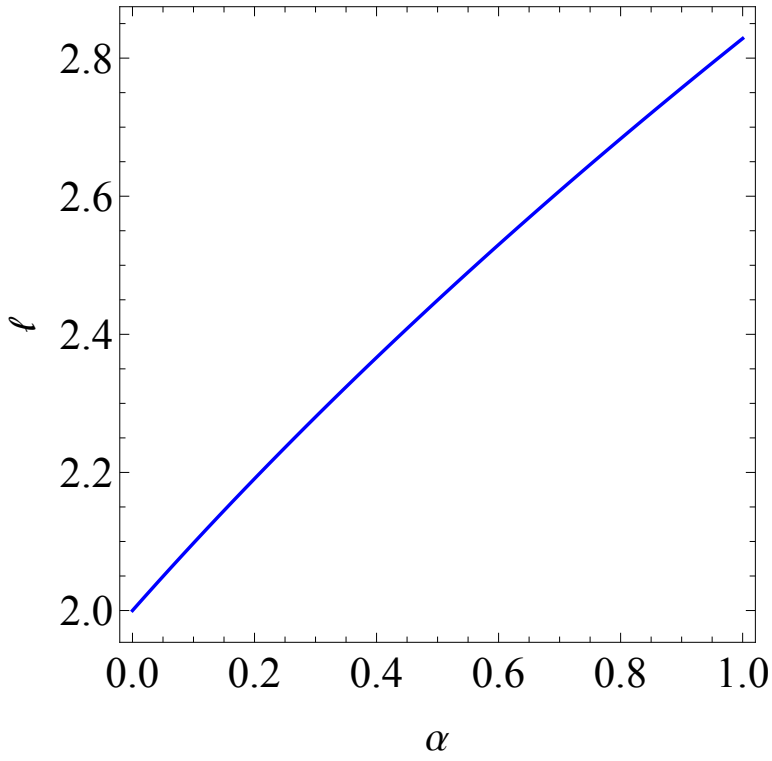


Figure 2.6: Dependence of the critical value of the angular momentum of particles from the MOG parameter α.

for the equal values of the angular momentum $l_1 = l_2$, the energy of the centre mass of the system will be $E_{\rm cm} = 2m_0$. The radial dependence of the energy of the centre mass showed that it tends to infinity, that means the Kerr-MOG black hole might be a source of the high-energy particles.

2.5 Conclusions

We have first tested particle motion around Kerr-MOG black hole and find the ISCO position for massive particle orbiting a rotating black hole in STVG. Our study delves into the behavior of massive particles in the vicinity of black holes within the framework of STVG, revealing intriguing deviations from the conventional Lorentz-like equation of motion. Specifically, we focus on the circular motion of massive test particles near the Kerr-MOG black hole, which is a solution derived

within the STVG theory. To simplify our analysis, we consider the motion to be confined to the equatorial plane, allowing us to derive the effective potential that governs the particle's orbit around the Kerr-MOG black hole.

We have studied energy extraction from the Kerr-MOG black hole via the Penrose process in the context of the STVG (Scalar-Tensor-Vector Gravity), particularly, with respect to the efficiency of energy transfer from black holes. The derived relations between particle energies, coupling constants, and the influence of the external scalar potential show that under certain conditions, the efficiency of energy extraction can exceed 100%. This is in stark contrast to the classical case of the extreme Kerr black hole, where the efficiency is around 21%. Specifically, for high values of the STVG parameter α, the maximum energy efficiency can surpass 100%, suggesting that mass ratios between escaping and falling particles can lead to unexpectedly large energy yields. The significant efficiency enhancements observed in the Kerr-MOG (Kerr with Modified Gravity) black holes, reaching up to 200%, highlight the potential of STVG theory to generate high-energy particles, further reinforcing the idea that the external fifth-potential plays a crucial role in these processes. This aligns with previous studies in the context of magnetized black holes, where rotation and magnetic fields also lead to efficiency values exceeding 100%, as seen in the work on magnetized Kerr black holes. These results open avenues for further research into the constraints on the MOG parameter α. Notably, observational data from pulsars and the orbital motion of stars around supermassive black holes could provide valuable insights into the possible values for α, offering constraints that could help refine our understanding of modified gravity theories. With a constrained value of $\alpha \lesssim 0.41$, the maximum energy efficiency from the Penrose process is found to reach about 78%, demonstrating that even within the confines of observational limits, energy extraction from Kerr-MOG

black holes remains highly efficient.

We extended the concept that massive particles experience four-acceleration due to external vector fields, subsequently incorporating the radiation reaction term into the equation of motion. Based on this insight, we delved into the gravitational analogue of radiation reaction experienced by a massive particle orbiting a Schwarzschild-MOG black hole. By employing the Landau trick, we simplified the equation of motion by discarding high-order terms concerning damping time. Furthermore, we investigated the gravitational counterpart of radiation reaction occurring when a stellar black hole orbits a supermassive black hole. This exceptionally high intensity value suggests that such systems may serve as potent sources of gravitational waves. Indeed, the detection of gravitational waves stemming from binary black hole mergers by the LIGO and Virgo collaborations has ushered in a fresh perspective on the study of black holes and their surrounding environments within the framework of STVG. The potential observation of gravitational waves originating from other black hole systems, particularly those involving orbiting massive particles, holds the promise of yielding deeper insights into the fundamental physics governing black holes and their intricate interactions with their surroundings. Moreover, we extensively investigate the BSW mechanism in the context of the Kerr-MOG black hole and propose a remarkable augmentation in the CME of two particles undergoing collision. This observation suggests that the Scalar-Tensor-Vector Gravity (STVG) theory could potentially impact high-energy collisions. These remarkable revelations open up captivating avenues for forthcoming investigations in this domain. Also we would like to point out that our approach helps to understand qualitatively the process under study to make useful astrophysical predictions since the spin parameter can have values $a > 1$ in the Kerr-MOG black hole case.

Recent studies have demonstrated that high CME is possible with maximum spin in both Kerr-MOG and Kerr spacetimes. Consequently, it has been discovered that the CME of a colliding pair of particles near an extremal Kerr-MOG black hole can reach extraordinary magnitudes, taking on arbitrary values. Specifically, when the angular momentum of one of the particles is $\ell = 2\sqrt{1+\alpha}$, where $\alpha > 0$, it has been observed that a higher critical angular momentum is required in the Kerr-MOG spacetime compared to the Kerr spacetime in order to achieve infinite CME. Finite CME, denoted as $E^2_{\text{c.m.}} = 2m^2$, can be obtained when the colliding particles have identical mass and angular momentum. These results align with previous findings in the Schwarzschild and Kerr spacetimes [85]. Furthermore, it has been demonstrated that the maximum CME of a colliding pair of particles depends on the disparity in the specific energy values of the individual particles. Conversely, it remains independent of the vector field, and the effect of STVG emerges solely from the spacetime geometry. Recently, it has been shown that CME of colliding pair of particles might be extremely high in the polar region of the Kerr black hole [86]. Fascinatingly, our own analysis showed that this phenomenon holds true even within the Kerr-MOG spacetime.

Chapter III

Gravitational synchrotron radiation and radiation reaction

I think I can safely say that nobody understands quantum mechanics.

Richard Feynman

3.1 Introduction

Radiation reaction refers to the phenomenon in physics where a charged particle experiences a deceleration or acceleration due to the emission of electromagnetic radiation (photons) as it moves through space. This phenomenon is a consequence of the particle's interaction with its own electromagnetic fields according to classical electrodynamics and when a charged particle accelerates or decelerates, it produces changing electric and magnetic fields, which in turn generate electromagnetic radiation. This radiation carries away energy and momentum from the particle, causing it to lose kinetic energy and slow down. The particle's motion is affected by its own emitted radiation, leading to a self-interaction that can influence its trajectory [87–89].

The concept of radiation reaction is important in various areas of physics, including radiation theory, high-energy particle physics and astrophysics. For instance, the effect of the radiation reaction force in the trajectory of charged particle around the magnetized Schwarzschild spacetime has been investigated in [90–92]. On the other hand, it is also interesting to consider the gravitational radiation reaction in a curved spacetime and in Refs. [56, 93–95], radiative gravitational field and gravitational radiation reaction has been extensively studied in the framework of general relativity.

In our preceding research [96], we have suggested new approach that explain gravitational analogue of synchrotron radiation from massive particle orbiting a black hole in Scalar-Tensor-Vector Gravity (STVG) theory which is a modification of General Relativity (GR) that incorporates an additional scalar and vector fields [8,22]. According to this theory the geodesic equation is not valid for massive particle and its four-acceleration is not equal to zero. It means massive particles generate gravitational radiation.

In later works MOG field equations were directly obtained from the least action principle and solutions of those equations were compared to cosmological and astrophysical observations [9]. The theory was successfully applied for explanation of galaxy rotation curves [10], cluster dynamics [11], gravitational lensing [12, 15, 24–28], black hole shadow [21, 23], quasi-periodic oscillations [36, 41, 42] and quasi-normal modes [97–99]. Some other studies on galaxy clusters and acceleration data include [31, 31, 32]. There is a wide range of works on particle motion around compact gravitational objects in MOG focusing on different aspects, namely stable orbits [33–35] and energy extraction [36]. The motion of S2 star orbiting around Sagittarius A* SMBH has been studied in [37–40].

The need for modified theories of gravity in astrophysics stems from the perplexing astrophysical phenomena that elude explanation within the confines of traditional general relativity established by Einstein. General relativity has been remarkably successful in describing gravitational interactions at a macroscopic scale [12]. However, at the vast reaches of the Universe, significant discrepancies arise, necessitating a reevaluation of our fundamental understanding of gravity. Dark matter and dark energy, proposed to account for unexplained gravitational behaviors, remain elusive. Modified theories, such as $f(R)$ gravity [100, 101] or Modified Gravity [8, 102], offer promising alternatives to bridge these gaps. By modifying the fundamental gravitational principles, these theories seek to elucidate galactic rotation curves, gravitational lensing, and the dynamics of large-scale structures in the universe. A deeper comprehension of gravity on cosmic scales is vital for accurately interpreting astrophysical phenomena and advancing our understanding of the fundamental forces shaping the Universe.

3.2 Gravitational synchrotron radiation

It is well established that accelerating charged particles emit synchrotron radiation, which is a form of electromagnetic radiation that is emitted when a charged particle is accelerated in a curved path in the presence of a magnetic field. The intensity of synchrotron radiation emitted by the charged particle is proportional to the square of the acceleration $I \sim w_\mu w^\mu$ and the frequency of the emitted radiation depends on the strength of the magnetic field. It is interesting to note that the synchrotron radiation emitted by relativistic charged particles around magnetized and charged black holes has been the subject of recent research. This is because black holes are known to have strong gravitational and electromagnetic fields that can affect the motion of charged particles and alter the characteristics of the emitted radiation. In the Refs. [50, 90, 91, 103], it is provided insights into the synchrotron radiation spectrum of relativistic charged particles around black holes, and their results have important implications for our understanding of the astrophysical phenomena associated with black holes.

Here we will discuss gravitational analogue of the synchrotron radiation from massive particle orbiting around black hole in STVG. As we mentioned before that in this theory, massive particle does not follow geodesics line due to the fifth force and from equation of motion in (2.3), the four-acceleration of massive particle is given as [104]

$$w^\mu = \frac{q}{m} B^\mu{}_\nu \dot{x}^\nu \ , \qquad w_\mu \dot{x}^\nu = 0 \ , \tag{3.1}$$

which is always perpendicular to the four-velocity of particle. Notice that equation (3.1) is gravitational analogue of the Lorentz equation, and charge of particle is replaced by the coupling constant q, while anti-symmetric tensor $B_{\mu\nu}$ stands instead of the Faraday tensor in Lorentz equation.

Our main assumption is that if massive particle orbits with non-zero value of the four-acceleration in the presence of the external force then it should emits radiation. We call this radiation as *gravitational synchrotron radiation*. Then the intensity of accelerating massive particle in STVG is determined as

$$I = -\frac{2q^2}{3} w_\mu w^\mu = \frac{2q^4}{3m^2} B_{\mu\lambda} B^{\mu\nu} \dot{x}^\lambda \dot{x}_\nu \ . \tag{3.2}$$

Considering circular motion of a massive particle with four-velocity of $\dot{x}^\mu = \dot{t}(1, v, 0, \Omega)$, where $v = dr/dt$ and $\Omega = d\phi/dt$ are radial and angular velocities of massive particle. Hereafter, performing simple algebra manipulations one can obtain the expression for the acceleration the following the form:

$$w_\mu = \frac{q}{m} \dot{t} (v B_{tr}, B_{rt} + \Omega B_{r\phi}, B_{\theta t} + \Omega B_{\theta\phi}, v B_{\phi r}) \ , \tag{3.3}$$

where non-zero components of the anti-symmetric tensor can be found as

$$B_{rt} = \frac{\sqrt{\alpha} M}{\Sigma^2} (r^2 - a^2 \cos^2\theta) \ , \qquad B_{r\phi} = -B_{rt} a \sin^2\theta \ , \tag{3.4}$$

$$B_{\theta t} = -\frac{\sqrt{\alpha} M r a^2 \sin 2\theta}{\Sigma^2} \ , \qquad B_{\theta\phi} = -B_{\theta t} \frac{r^2 + a^2}{a} \ , \tag{3.5}$$

and $\dot{t}$ can be found using normalization of the four-velocity $\dot{t}^{-1} = \sqrt{-g_{tt} - 2\Omega g_{t\phi} - \Omega^2 g_{\phi\phi} - v^2 g_{rr}}$.

The expression for the intensity of the radiating massive particle orbiting around Kerr-MOG black hole in equatorial plane reads

$$I = \frac{2\alpha^3 G^3 m^2 M^2}{3c^3 r^4} \dot{t}^2 \left[\frac{\Delta}{r^2} (1 - \Omega a)^2 - \frac{r^2}{\Delta} \frac{v^2}{c^2} \right] \ . \tag{3.6}$$

As one can see from above equation that massive particle emits gravitational radiation even in arbitrary stable orbit (i.e. $v = 0$) and in the case of a non-rotating black hole $\dot{t}^2$ can be canceled with expression in bracket. In Fig. 3.1 a schematically picture of gravitational radiating SBH in the vicinity of a SMBH is illustrated. As a result one can estimate the intensity of gravitational radiation

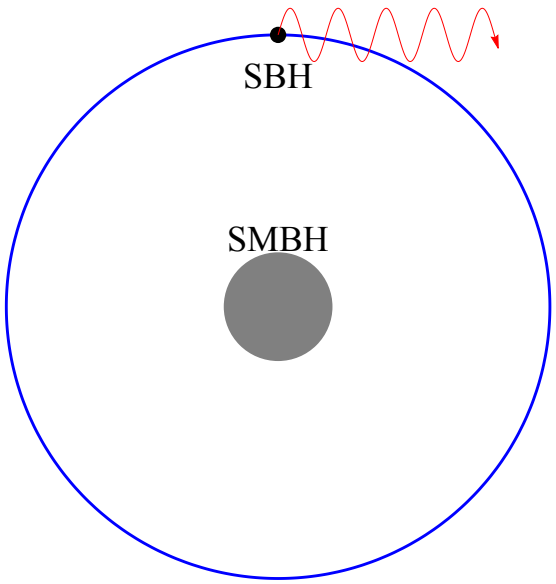


Figure 3.1: The schematical picture of radiated SBH around SMBH in STVG.

from the stellar black hole (SBH) orbiting around supermassive black hole (SMBH) as

$$I \sim 2.43 \times 10^{39} \alpha^3 \left(\frac{m}{10 M_\odot}\right)^2 \left(\frac{M}{10^9 M_\odot}\right)^{-2} \left(\frac{10GM}{c^2 r}\right)^4 \text{erg/s} \ , \tag{3.7}$$

which depends on the radial coordinate. It is also interesting to calculate the intensity at the ISCO position and determine how it depends on the α parameter. Figure 3.2 shows the dependence of the intensity on the α parameter. As one can see from the figure, in the absence of the STVG parameter, the intensity becomes zero because, in this case, the massive particle follows a geodesic line near the black hole and does not emit gravitational radiation. However, in the presence of the STVG (i.e., $\alpha \neq 0$), the intensity of the radiating particle becomes non-zero and increases with an increase in the α parameter.

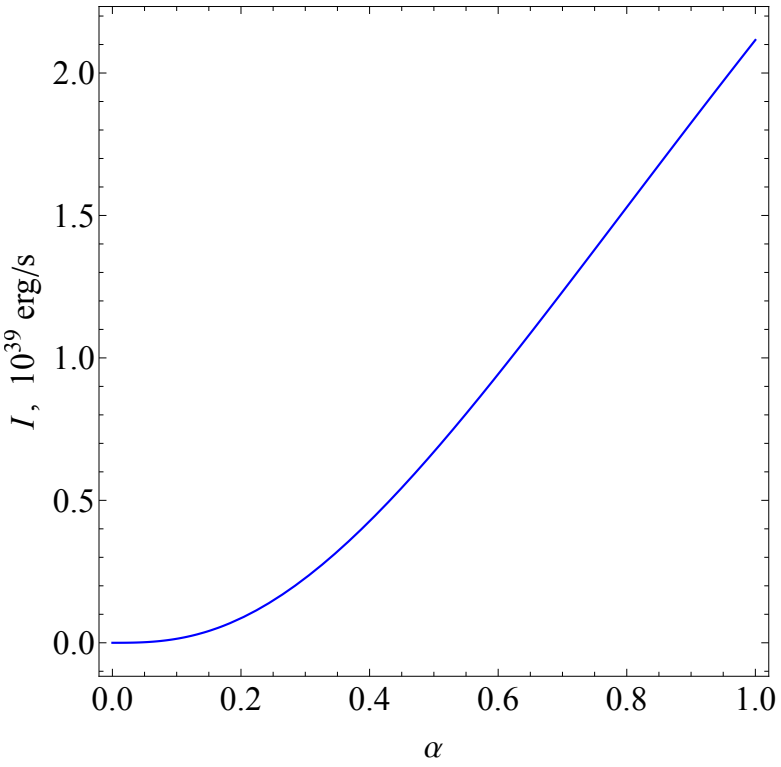


Figure 3.2: Dependence of the intensity of a radiating SBH at the ISCO position from the α parameter.

3.3 Gravitational radiation reaction

Now we examine the dynamics of massive particles within the framework of the STVG theory, which incorporates a radiation reaction term. While the Lorentz-Abraham-Dirac (LAD) equation is widely recognized as the equation governing radiation reaction for charged particles (See e.g. [90, 105]), our research focuses on the gravitational counterpart of this phenomenon. In this context, the equation of motion (1.25) can be modified as

$$\frac{Du^\mu}{ds} = \frac{\tilde{q}}{m} B^\mu{}_\nu u^\nu + \frac{1}{2}\tau_0 \left(R^\mu{}_\nu + u^\mu u_\lambda R^\lambda{}_\nu\right) u^\nu + \tau_0 \left(\frac{D^2 u^\mu}{ds^2} + u^\mu u_\lambda \frac{D^2 u^\lambda}{ds^2}\right) \ , \quad (3.8)$$

where $R_{\mu\nu}$ is the Ricci tensor, τ_0 is the damping time of gravitational radiation defined as $\tau_0 = 2\tilde{q}^2/(3m) << 1s$ and this parameter can play a role of expansion parameter. To have an idea one can estimate of damping time for electron and it

yields

$$\tau_0 = \frac{2\alpha G_N m_e}{3c^3}\left(\frac{m}{m_e}\right) \sim 10^{-66}\alpha\left(\frac{m}{m_e}\right)\text{s}\ , \tag{3.9}$$

while the stellar black hole (SBH) orbiting around supermassive black hole (SMBH) is

$$\tau_0 \simeq 3.3\times 10^{-4}\alpha\left(\frac{m}{10M_\odot}\right)\text{s}\ . \tag{3.10}$$

Given that the final term of equation (3.8) is significantly smaller when compared to the other terms, therefore one can employ the Landau trick to expand the equation in terms of the damping time τ_0. By differentiating equation (3.8) and neglecting the highest-order terms with respect to the damping time τ_0, we obtain:

$$\frac{D^2u^\mu}{ds^2} \simeq \frac{\tilde{q}}{m}\left(u^\alpha\nabla_\alpha B^\mu{}_\nu + \frac{\tilde{q}}{m}B^\mu{}_\alpha B^\alpha{}_\nu\right)u^\nu + \mathcal{O}\left(\tau_0\right)\ . \tag{3.11}$$

Substituting expression (3.11) into to (3.8) and after simple algebraic manipulations, equation of motion can be rewritten as

$$\frac{Du^\mu}{ds} = \frac{\tilde{q}}{m}B^\mu{}_\nu u^\nu + \frac{1}{2}\tau_0 h^{\mu\lambda}R_{\lambda\nu}u^\nu + \tau_0\frac{\tilde{q}}{m}\left(u^\alpha\nabla_\alpha B^\mu{}_\nu + \frac{\tilde{q}}{m}h^{\mu\lambda}B_{\lambda\alpha}B^\alpha{}_\nu\right)u^\nu\ , \tag{3.12}$$

where $h^{\mu\nu} = g^{\mu\nu} + u^\mu u^\nu$ and $h_{\mu\nu}u^\nu = 0$.

The main idea of the reducing equation (3.8) into form of (3.12) is that it is the third order system of differential equations for four coordinates. It turns out that one has to find twelve constants of motion which one of main issue in particle motion in curved spacetime. However, this problem can be avoided using the Landau trick and equation of motion reduces to the second order system of equations for four coordinates x^μ. The analytical form equations for each coordinates in (3.12) are too long therefore we will not report them in the Letter. However, careful numerical analyses for given initial conditions $(0, r_0, \theta_0, 0)$

and $\left\{-\mathcal{E}/f(r_0), 0, 0, \mathcal{L}/(r_0 \sin\theta_0)^2\right\}$, allows to find each coordinates as function of affine parameter, i.e., $x^\mu = x^\mu(s)$. Hereafter performing coordinate transformation $x = r\cos\phi\sin\theta$, $y = r\sin\phi\sin\theta$, and $z = r\cos\theta$ the trajectories of particle can be produced in Cartesian coordinates using parametric plots in $2D$ or $3D$.
In Fig 3.3, we present trajectory of massive particle including and without including radiation reaction term in STVG. In order to see the effect of radiation reaction term in circular motion we set damping time to $\tau_0 = 1$s. However, real value of the damping time τ_0 can be calculated by following formulae (3.9) for electron and (3.10) for stellar black hole. This means that damping time is much lower than 1s and particle rounds many times than shown in Fig 3.3 around black hole and eventually fall into black hole due to radiation reaction force. It is evident from Fig. 3.4 that for the larger values of MOG parameter α and damping time τ_0, a particle falls into black hole faster.

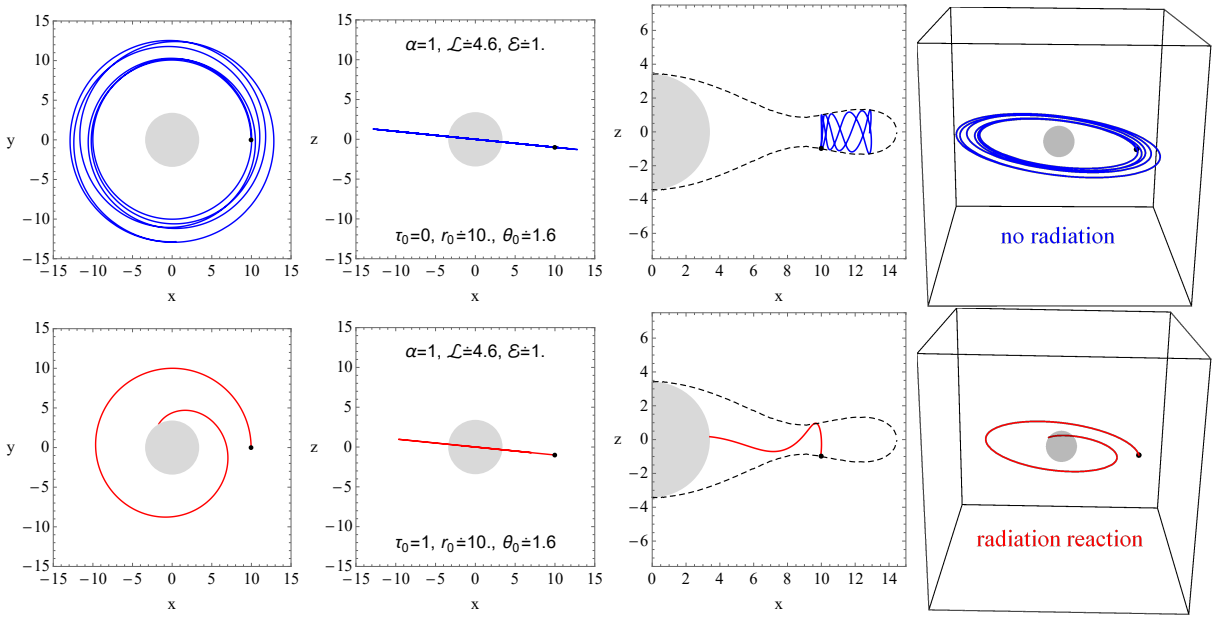


Figure 3.3: The trajectories of massive particle orbiting the Schwarschild-MOG black hole with (bottom panel) and without (top panel) including radiation reaction force, respectively. Initial conditions are chosen to be the same for each cases and shown in the second row. The initial position of particle is depicted by black dot in each plots. The first and second columns represent the trajectory of massive particle in $(x-y)$ and $(x-z)$ planes, respectively. The third column represents finite motion of test particle in the region given by dashed line (contour plot of the effective potential), while in the last column particle's trajectory is shown in $3D$.

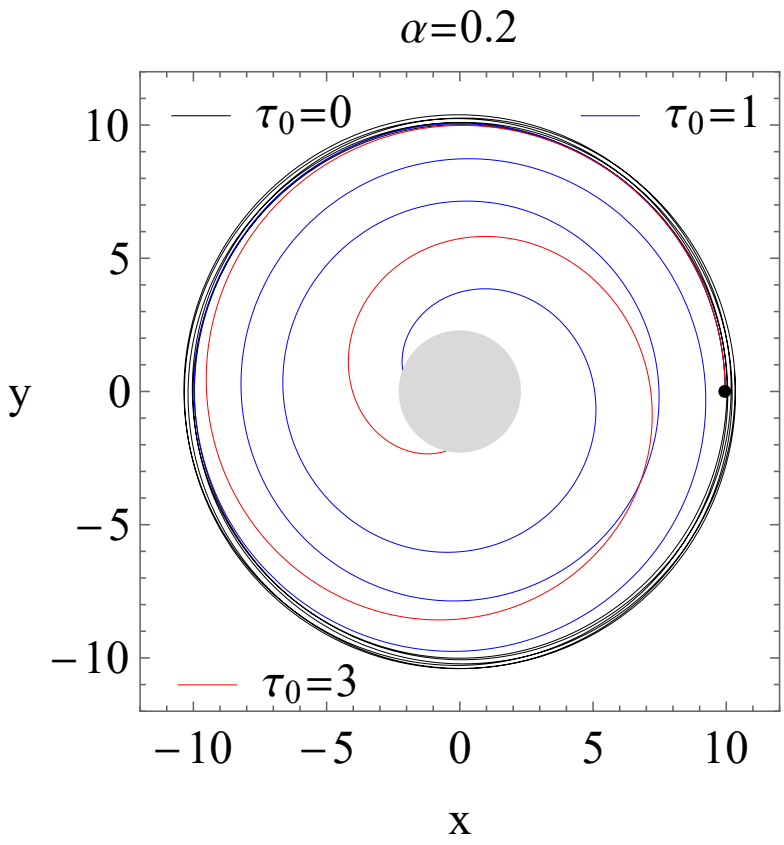


Figure 3.4: Plot is comparing the trajectories of a particle without radiation reaction force (black circular line) and with radiation reaction force for different τ parameter (blue and red). In each cases, initial positions are chosen to be the same and depicted by black dot.

3.4 Conclusion

It is well-established that the motion of massive particles around black holes in STVG does not follow a geodesic line. Building upon this fact, we have conducted a study of the circular motion of massive test particles in the vicinity of the Kerr-MOG black hole, which is one of the black hole solutions in STVG. To simplify our analysis, we have focused on circular motion in the equatorial plane and have derived the effective potential governing the motion of the massive particle in orbit around the Kerr-MOG black hole. Through numerical calculations, we have discovered that the position of the ISCO (innermost stable circular orbit) for the massive particle around the black hole increases due to an external force arising from STVG. We have also graphically demonstrated the dependence of the ISCO position on the STVG parameter α. Overall, our research sheds light on the behavior of massive particles orbiting around black holes in the context of STVG theory, providing new insights into the effects of external forces on the motion of these particles.

As we mentioned before, massive particles occurs four-acceleration due to the fifth force in STVG, and the equation of motion resembles the Lorentz equation for charged particles. Based on this fact, we have discussed the gravitational analogue of synchrotron radiation from a massive particle orbiting around a Kerr-MOG black hole due to the fifth force in STVG. Additionally, we have studied the gravitational radiation emitted by a massive particle falling radially onto a Kerr-MOG black hole with angular velocity. We are arguing that massive particle, such as black hole, orbiting around the SMBH, can emit intense radiation and generate gravitational waves that can be observed. This effect is known as "gravitational radiation reaction", and it is caused by the particle's motion in the strong gravitational field of the SMBH. The intensity of the radiation emitted by

the orbiting particle depends on various factors, such as its mass, velocity, and distance from the black hole. Based on our analysis, for a typical SMBH with a mass of $10^9 M_\odot$ and SBH of mass $10 M_\odot$ orbiting around it, the intensity of the radiation has been estimated to be $I \sim 2.43 \times 10^{39}$. This is a very large value and suggests that such systems could be strong sources of gravitational waves. Indeed, the observation of gravitational waves from binary black hole mergers by the LIGO and Virgo collaborations has opened up a new window into the study of black holes and their environments in the STVG. The detection of gravitational waves from other types of black hole systems, such as those with orbiting massive particles, would provide further insights into the physics of black holes and their interactions with their surroundings.

As previously discussed, massive particles exhibit non-geodesic behavior when navigating the vicinity of black holes within the framework of STVG. This peculiar behavior arises from the similarity between the equations of motion governed by the external vector field and the Lorentz-like equation. Taking into account this fact, this research endeavors to explore the circular motion of massive test particles in the equatorial plane around the Schwarzschild-MOG black hole. We have concentrated on circular orbits and derived the effective potential that dictates the motion of these massive particles orbiting the Schwarzschild-MOG black hole. Our numerical computations have unveiled a noteworthy revelation: the ISCO position for massive particles orbiting the black hole experiences a notable shift in position due to the presence of an external vector field within the STVG framework. Furthermore, we have visually depicted this ISCO's dependence on the MOG parameter α through graphical representations. These findings collectively contribute to a deeper understanding of the intricate dynamics governing massive particle motion in the context of STVG theory as well as on their trajectories.

Chapter IV

Black hole perturbations in STVG

Space-time grips mass, telling it how to move, and mass grips space-time, telling it how to curve

John Archibald Wheeler

4.1 Introduction

The direct detection of gravitational waves by the LIGO [106] and Virgo Collaboration has opened an entirely new observational window onto the strong-field regime of gravity. For the first time in the history of physics, we are able to probe the dynamical formation of black holes—not through electromagnetic radiation, but through spacetime itself. Each merger event provides a unique laboratory for testing the fundamental predictions of general relativity in previously inaccessible regimes, where nonlinear dynamics and strong curvature dominate.

Black holes, enigmatic objects predicted by Einstein's general theory of relativity, represent regions of spacetime where gravity is so intense that nothing, not even light, can escape beyond their event horizons. First theorized as solutions to the Einstein field equations—such as the spherically symmetric Schwarzschild metric in 1916 and the rotating Kerr metric in 1963—these entities have transitioned from mathematical curiosities to observable phenomena, confirmed through grav-

itational wave detections by LIGO and Virgo, and direct imaging by the Event Horizon Telescope. The study of black holes not only probes the extremes of gravity but also intersects with quantum mechanics, thermodynamics, and cosmology, making them central to modern physics. Since the recent detection of gravitational waves by LIGO [106], black hole quasinormal modes are no longer merely theoretical objects: their measurement is crucial to pin down the mass and angular momentum of the final black hole after a binary merger.

In the context of general relativity, exact solutions like the Schwarzschild and Kerr metrics describe isolated, stationary black holes. However, real astrophysical scenarios often involve perturbations—small deviations from these ideal configurations caused by external matter, gravitational waves, or infalling objects. Black hole perturbations theory provides a powerful framework for analyzing these deviations, approximating the spacetime metric as a background solution plus small corrections. This approach is essential for understanding dynamical processes, such as the emission of gravitational radiation during binary inspirals or the ringdown phase following mergers, where the black hole settles into a quiescent state through the emission of quasinormal modes.

When a black hole is subject to external perturbations, characteristic vibration modes appear. These modes decay in time due to gravitational radiation emission. That is the reason why they are called quasinormal modes. They are characterized by complex frequencies. The real part of these frequencies corresponds to the frequency of vibration, and the imaginary part corresponds to the rate at which each mode is damped as a result of the emission of radiation (See [107] for a review).

In some exceptional cases they can be computed exactly. Nevertheless, in most cases these calculations require approximations or numerical methods. We will fol-

low the first alternative and use the WKB approximation, widely used in Quantum Mechanics, to compute them. Here, we present one of the pioneering techniques in black hole quasinormal modes computation developed by Schutz and Will [108], that involves a first order WKB approximation. Next we show succinctly how one could push the computation to higher orders following this path. In the following we will not be interested in pursuing these ideas. We will present a recent method based on the idea of Blome et al. [109] to connect black hole quasinormal modes with bound state energies of anharmonic oscillators. This relation will allow us to use a technique due to Bender and Wu [110] to compute quasinormal modes, and will enable us to automate their calculation. Throughout this work we will consider only the Schwarzschild black hole. We have verified that the method proposed by Y. Hatsuda to compute the quasinormal modes works, since it reproduces the values present in the literature. Using this technique, the problem encountered when using the prior methods, namely that to increase an order in the WKB expansion has a very high computational cost, becomes obsolete. Now we can push the calculation to any desired order just by running a simple code using the Bender-Wu package [111]. In a certain way, the problem has been trivialized. An interesting question remains open. We have limited our verification of the method by Y. Hatsuda to the Schwarzschild black hole [112]. An interesting next step would be to extend this work to the more realistic case of a rotating black hole.

The foundations of black hole perturbations theory trace back to the late 1950s with the pioneering work of Regge and Wheeler [113], who studied odd-parity perturbations of the Schwarzschild spacetime using a gauge-invariant formalism. This was extended in 1970 by Zerilli [114] to even-parity perturbations, leading to decoupled wave equations that describe the propagation of gravitational dis-

turbances. A major advancement came in 1973 with Teukolsky's derivation of separable equations for perturbations in the Kerr spacetime, applicable to scalar, electromagnetic, and gravitational fields [115]. These developments enabled the computation of quasinormal modes—characteristic oscillation frequencies of perturbed black holes—first identified by Vishveshwara in 1970 [116] and numerically explored by Press [117] and others. Quasinormal modes dominate the ringdown signal in gravitational wave observations, offering a means to test the no-hair theorem and probe black hole properties.

A key extension of perturbations theory is the gravitational self-force formalism, which accounts for the backreaction of a small object's gravitational field on its own motion in a curved background. Originating from Dirac's 1938 treatment of self-interaction in electromagnetism, this concept was adapted to general relativity by DeWitt and Brehme in 1960 and formalized in the 1990s through the MiSaTaQuWa equation by Mino, Sasaki, Tanaka, Quinn, and Wald. In this framework, the small body is modeled as a point mass, and its trajectory deviates from a geodesic due to the self-force, which includes both conservative (time-symmetric) and dissipative (radiation-reaction) components. This is particularly relevant for extreme-mass-ratio inspirals (EMRIs), where a stellar-mass compact object orbits a supermassive black hole, producing gravitational waves detectable by space-based observatories like LISA.

perturbations theory employs various mathematical tools, including multipolar expansions, Fourier decompositions, and numerical methods to solve master equations like the Regge-Wheeler-Zerilli [113, 114] or Teukolsky [115] equations. For non-rotating (Schwarzschild) black holes, perturbations can be decomposed into scalar, vector, and tensor spherical harmonics, leading to wave-like equations that reveal the stability of the background metric against small fluctuations.

In rotating (Kerr) cases, the complexity increases due to frame-dragging effects, necessitating spheroidal harmonics and advanced techniques for mode summation. Recent computational toolkits, such as the Black Hole perturbations Toolkit (https://bhptoolkit.org/), facilitate these calculations by integrating open-source codes for waveform generation, quasinormal mode analysis, and self-force computations, accelerating research in gravitational wave astronomy.

The significance of black hole perturbations theory extends beyond theoretical insights. It underpins the modeling of gravitational waveforms for binary systems, enabling parameter estimation from detector data and tests of general relativity in strong-field regimes. For instance, in the post-merger ringdown, perturbations reveal information about the final black hole's mass and spin, while in EMRIs, self-force effects accumulate over thousands of orbits, requiring high-order expansions for accurate predictions. Moreover, perturbations methods interface with numerical relativity for intermediate regimes and post-Newtonian approximations for weak fields, forming a comprehensive toolkit for multi-messenger astrophysics.

The thermodynamical properties of black holes in MOG have been explored in [118], showing similarities with the Einstein–Maxwell solutions, but with the electric charge replaced by a mass-dependent parameter. The stability and evolution of black holes through their quasinormal modes have been investigated in several works [97–99], with some studies fitting these models to gravitational wave observations from neutron star mergers [119]. Scalar field dynamics in the vicinity of compact MOG objects have been explored in [120–122], and tests of cosmic censorship in this context were conducted in [123].

In this chapter, I mainly focus on the applications of perturbations theory to quasinormal modes in Schwarzschild-MOG black holes, building on these foundational concepts, the mathematical formalism for the Schwarzschild-MOG perturbations.

Before that we study thermodynamics of the black hole in STVG. Through this work, we aim to contribute to the understanding of black hole dynamics and their role in the universe.

4.2 Thermodynamic properties of black hole

Recent, detection of gravitational wave by LIGO/Virgo collaboration showed that there are possible observation evidences of the Hawking surface [124], which motivates to study thermodynamic properties of the black holes. Certainly, studying the thermodynamic properties of black holes in STVG and investigating the influence of the MOG parameter on these quantities is an intriguing endeavor. We begin by considering the first law of black hole thermodynamics in STVG, which can be expressed as:

$$dM = TdS + \Phi_t dQ \ , \tag{4.1}$$

where T and S denote the Hawking temperature and entropy of the black hole, respectively. Notably, the second term of equation (4.1) emerges due to the presence of STVG, and it has the potential to impact the thermodynamic properties of the black hole.

The Hawking temperature on the surface of the Schwarzschild-MOG black hole can be determined as follows:

$$T = \frac{1}{4\pi}\left(\frac{dg_{tt}}{dr}\right)\Bigg|_{r=r_+} = \frac{1}{2\pi G_N M\sqrt{1+\alpha}\left(1+\sqrt{1+\alpha}\right)^2} \ , \tag{4.2}$$

Remarkably, this expression aligns with the findings reported in Ref. [118].

Using the area law the entropy of the Schwarzschild-MOG black hole is determined as [118]

$$S_A = \frac{A}{4G} = \frac{\pi r_+^2}{4G_N(1+\alpha)} = \pi G_N M^2\left(1+\sqrt{1+\alpha}\right)^2 \ , \tag{4.3}$$

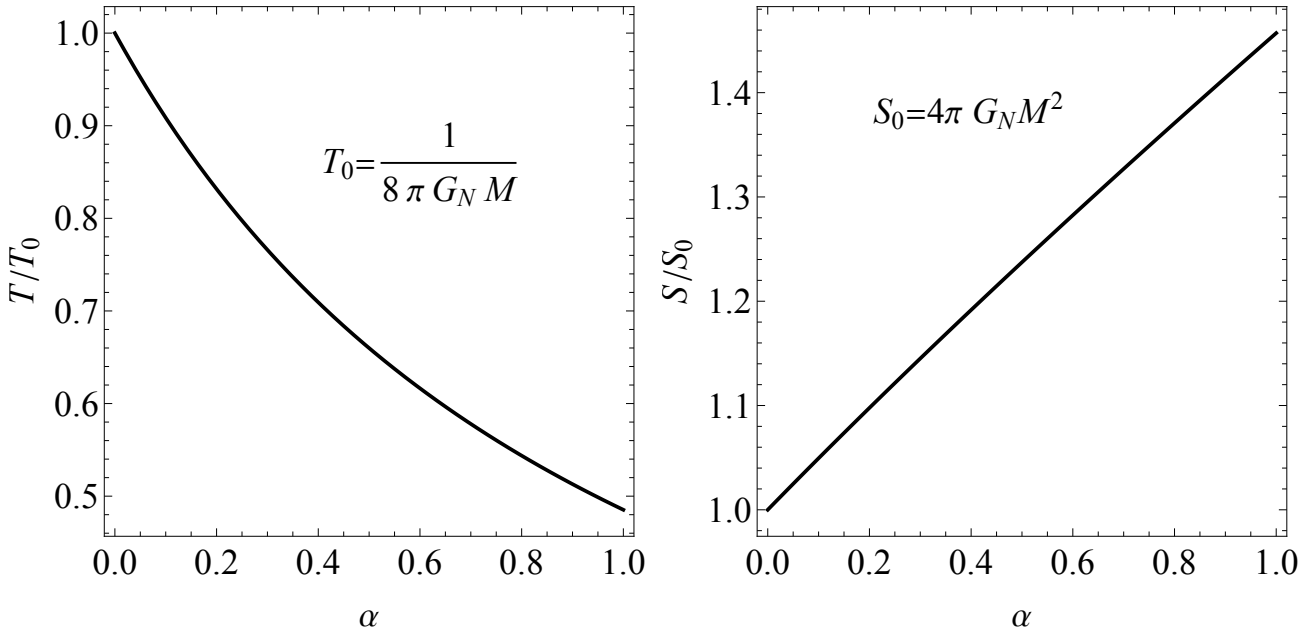


Figure 4.1: Dependence of the Hawking temperature (left panel) and entropy (right panel) of the Schwarzschild-MOG black hole form MOG parameter α.

on other hand, using equation (4.1), the entropy of the black hole can be calculated as

$$\begin{aligned} S_T &= \int \frac{dM}{T} - \int \frac{\Phi_t dQ}{T} = \int \frac{dM}{T}\left(1 - \frac{\alpha G_N M}{r_+}\right) \\ &= \int \frac{dM}{T}\frac{1}{\sqrt{1+\alpha}} = \pi G_N M^2 \left(1+\sqrt{1+\alpha}\right)^2 , \end{aligned} \tag{4.4}$$

which coincides with the result in (4.3) and the difference of entropy in (4.3) and (4.4) is zero, that means $S_A = S_T$. Here we can conclude that the entropy of the black hole determined via using area law and the first law of black hole thermodynamics give the same result.

It is evident from equation (4.2), the Hawking temperature of the black hole decreases due to the influence of MOG in the black hole's spacetime, as illustrated in Fig. 4.1.

Now, utilizing the expressions for the temperature and entropy, we can determine

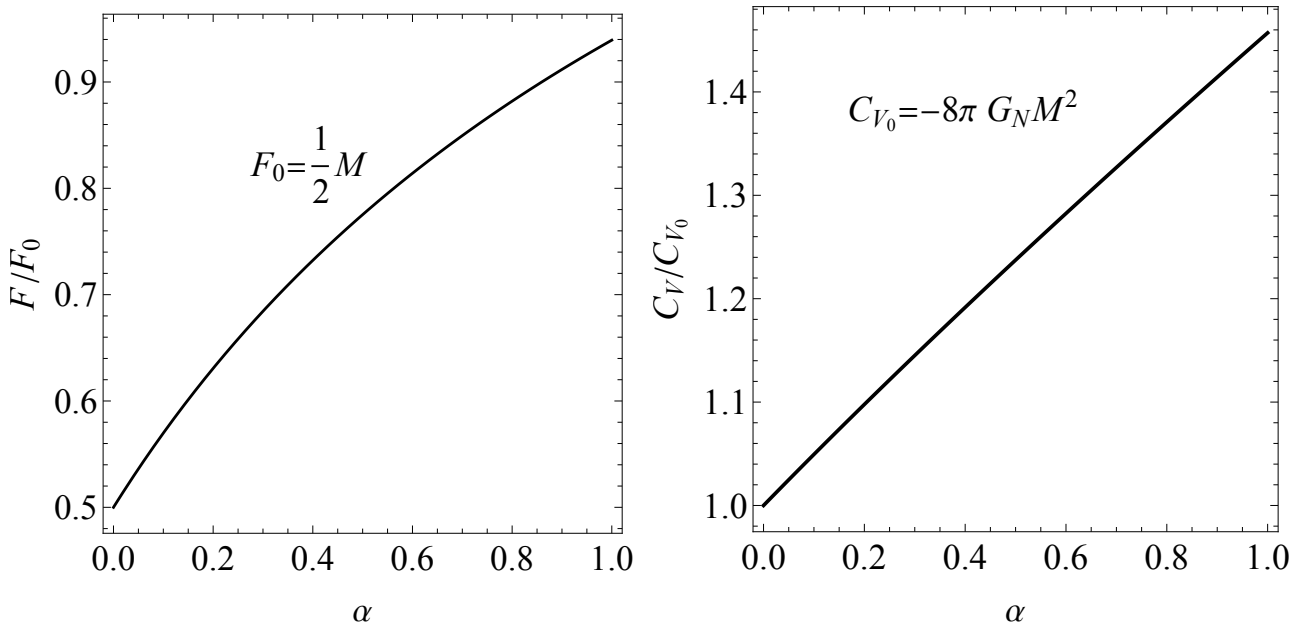


Figure 4.2: Dependence of the free energy (left panel) and heat capacity (right panel) of the Schwarzschild-MOG black hole from MOG parameter α.

the free energy of the Schwarzschild-MOG black hole as presented in [125]:

$$F = M - ST - Q\Phi_t = \frac{M}{2\sqrt{1+\alpha}} \ . \tag{4.5}$$

Now we focus on calculating the heat capacity of the Schwarzschild-MOG black hole. From the thermodynamics course the isochoric heat capacity is given as $C_V = T(\partial S/\partial T)$, which depends on the entropy of the black hole. Using this expression heat capacity of the Schwarzschild-MOG black hole can be determined as

$$C_V = T\frac{\partial S}{\partial M}\left(\frac{\partial T}{\partial M}\right)^{-1} = -2\pi G_N M^2\left(1+\sqrt{1+\alpha}\right)^2 \ . \tag{4.6}$$

In Figure 4.2, we provide a comparison of the entropy and free energy values of the black hole based on the MOG parameter. The solid lines represent the actual entropy and free energy of the black hole, calculated using equations (4.3) or (4.4) and (4.5), which presumably correspond to a new approach. Based on the available information, the statement concludes that the entropy and free energy exhibit a

unique behavior. This potentially implies that the new formulation provides a consistent and unified description of these quantities for black holes. However, given the limited context and details provided, it is challenging to provide a more comprehensive interpretation without further clarification on the specific content of the paper and the equations involved.

Another important feature of the black hole is it's lifetime. The rate of energy loss from the Schwarzschild-MOG black hole can be approximated with the Stephan-Boltzmann radiation law as [126]

$$\frac{dM}{dt} = -\sigma A T^4 + \frac{Q}{r_+}\frac{dQ}{dt} = -\sigma A T^4 + \frac{\alpha G_N M}{r_+}\frac{dM}{dt} \ , \tag{4.7}$$

where σ is the Stephan-Boltzmann constant and the second term arises due to the external potential in STVG. Hereafter isolating dt and dM in equation (4.7) and integrating from M to 0, the life time of the Schwarzschild-MOG black hole can be expressed as

$$\tau = \frac{4\pi}{3\sigma} G_N^2 M^3 \sqrt{1+\alpha}\left(1+\sqrt{1+\alpha}\right)^6 \ , \tag{4.8}$$

In Fig. 4.3 dependence of the lifetime of the black hole from MOG parameter is illustrated.

The outer and inner horizons of Kerr-MOG black hole are located at $r_\pm = G_N M\left(1+\alpha \pm \sqrt{1+\alpha-a_*^2}\right)$, where $a_* = a/(G_N M)$, and Hawking temperature of Kerr-MOG black hole takes a form:

$$T = \frac{1}{4\pi G_N M(1+\alpha)} \frac{\sqrt{1+\alpha-a_*^2}}{1+\frac{\alpha}{2}+\sqrt{1+\alpha-a_*^2}} \ , \tag{4.9}$$

which vanishes in the case of the extreme Kerr-MOG black hole when $a_* = \sqrt{1+\alpha}$, while in the case when $a_* = 0$ the expression (4.9) reduces to (4.2). Using the area law the entropy of Kerr-MOG black hole reads

$$S = \frac{A}{4G} = 2\pi G_N M^2\left(1+\frac{\alpha}{2}+\sqrt{1+\alpha-a_*^2}\right) \ , \tag{4.10}$$

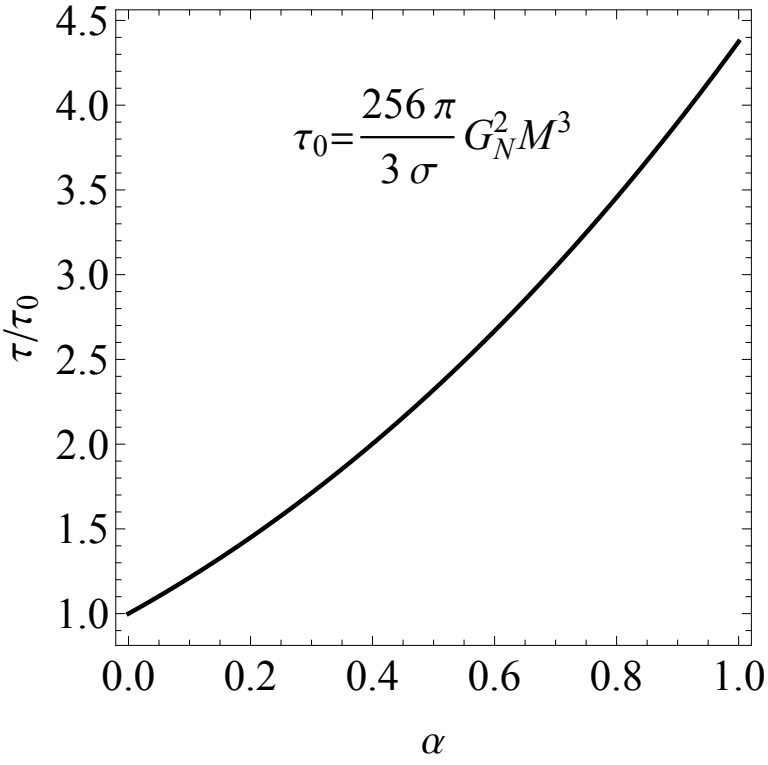


Figure 4.3: Dependence of the heat capacity (left panel) and lifetime (right panel) of the Schwarzschild-MOG black hole from MOG parameter α.

which also can be derived from the first law of black hole thermodynamics $dM = TdS + \Omega dJ + \Phi_t dQ$. Once the Hawking temperature and entropy of black hole are derived, the expression for other thermodynamic quantities, namely, heat capacity, free energy as well as lifetime of the Kerr-MOG black hole can immediately be derived. However, one has to include the effect of black hole rotation in each thermodynamics quantities in proper way which is not mentioned in [118].

4.3 Black hole perturbations

Black hole perturbations theory is a powerful method for studying how black holes respond to small disturbances in their surrounding spacetime or fields. Instead of solving the full nonlinear Einstein equations, one expands the metric and matter fields around a known exact solution—typically the Schwarzschild/Kerr or alternative metric—and keeps only linear (or sometimes second-order) terms. This yields a set of linear differential equations that capture how different types of fluctuations evolve and decay.

perturbations are important for understanding gravitational-wave emission, stability of black holes, scattering phenomena, and quasi-normal modes. In general, the perturbations can be classified according to how they transform on the 2-sphere S^2. This classification naturally separates perturbations into scalar, vector, and tensor types.

1. Scalar perturbations

Scalar perturbations are fluctuations that behave as scalars under rotations on the sphere. Physically, they may arise from: a test scalar field (Klein–Gordon field), density inhomogeneities, scalar degrees of freedom in modified gravity theories.

For a minimally coupled scalar field Φ on a black hole background, the perturbations equation takes the form $\Box\Phi = 0$, which can be separated into spherical

harmonics and radial modes. Scalar perturbations are often the simplest to study and provide a clean framework for understanding black hole quasi-normal modes.

2. Vector (Electromagnetic) perturbations

Vector perturbations transform as vectors on the sphere and include electromagnetic fluctuations or axial (odd-parity) perturbations of the metric. For a Maxwell field A_μ on a black hole background, the linearized Maxwell equations $\nabla_\mu F^{\mu\nu} = 0$ yield a master function that satisfies a Schrödinger-like equation similar to the scalar case. In Schwarzschild spacetime, vector perturbations correspond to Regge–Wheeler odd-parity gravitational perturbations, as well as true electromagnetic waves. These modes are important for studying: (i) electromagnetic scattering by black holes, (ii) stability of black holes under EM fluctuations, (iii) coupled Einstein–Maxwell systems (Reissner–Nordström).

3. Tensor (Gravitational) perturbations

Tensor perturbations represent true gravitational-wave fluctuations of the metric. They can be divided into two parity sectors:

- even-parity (polar) perturbations, governed by the Zerilli equation,
- odd-parity (axial) perturbations, governed by the Regge–Wheeler equation.

The metric perturbations is expanded as: $g_{\mu\nu} = g^{(0)}_{\mu\nu} + h_{\mu\nu}$, and one linearizes the Einstein equations in $h_{\mu\nu}$. After separating variables using tensor spherical harmonics, the perturbations reduce to master equations:

$$\frac{d^2\Psi_{\rm RW}}{dr_*^2} + \left[\omega^2 - V_{\rm RW}(r)\right]\Psi_{\rm RW} = 0 \ , \tag{4.11}$$

$$\frac{d^2\Psi_{\rm Z}}{dr_*^2} + \left[\omega^2 - V_{\rm Z}(r)\right]\Psi_{\rm Z} = 0 \ . \tag{4.12}$$

Tensor perturbations encode gravitational radiation and determine the quasi-normal mode spectrum that is observed in gravitational-wave detectors such as

LIGO/Virgo/KAGRA. Black hole perturbations theory thus decomposes all possible disturbances into these three classes, each governed by a wave equation with a characteristic potential. Their evolution determines stability, scattering behavior, and the quasi-normal mode spectrum of black holes.

Type	**Origin**	**Master Equation**	**Physical Meaning**
Scalar	Scalar modes	Regge–Wheeler (RW)–type	Scalar waves scattered by BH
Vector	Electromagnetic wave	Maxwell / RW equation	EM waves, axial perturbations
Tensor	Metric perturbations	RW and Zerilli equations	Gravitational radiation

Table 4.1: Classification of black hole perturbations.

4.4 Scalar perturbations

One of the simplest models for the black hole perturbations is described by the scalar (field) perturbations. In order to describe the scalar perturbations, we use the Klein-Gordon in the fixed curved spacetime:

$$\nabla_\mu \nabla^\mu \Phi = \frac{1}{\sqrt{-g}} \partial_\mu \left(g^{\mu\nu} \sqrt{-g} \partial_\nu \Phi \right) = 0 \ , \tag{4.13}$$

where ∇_μ is the covariant derivative, Φ is a scalar field. In the Schwarzschild-MOG spacetime, equations (4.13) can be rewritten as

$$-\frac{1}{f}\partial_t^2 \Phi + \frac{1}{r^2}\partial_r (r^2 f \partial_r \Phi) + \frac{1}{r^2}\nabla_\Omega^2 \Phi = 0 \ , \tag{4.14}$$

where ∇_Ω^2 is the angular part of the Laplacian operator defined as

$$\nabla_\Omega^2 = \frac{1}{\sin\theta}\frac{\partial}{\partial\theta}\left(\sin\theta \frac{\partial}{\partial\theta}\right) + \frac{1}{\sin^2\theta}\frac{\partial^2}{\partial\phi^2} \ . \tag{4.15}$$

It is evident that equations (4.14) can be separated into radial and angular parts, if the wave function is chosen as harmonically time dependent form as follows

$$\Phi(x) = e^{-i\omega t}\frac{R_\ell(r)}{r} Y_\ell^m(\theta, \phi) \ , \tag{4.16}$$

where ω is the frequency of quasinormal modes for scalar and electromagnetic perturbations, $R_\ell(r)$ is the radial profile function for the scalar perturbations, $Y_\ell^m(\theta,\phi)$ is the spherical harmonics satisfied the following equation: $\nabla_\Omega^2 Y_\ell^m(\theta,\phi) = -\ell(\ell+1)Y_\ell^m(\theta,\phi)$ and normalized as follows:

$$\int d\Omega Y_\ell^{m*}(\theta,\phi) Y_{\ell'}^{m'}(\theta,\phi) = \delta_{\ell\ell'}\delta_{mm'} \ . \tag{4.17}$$

By inserting the separation ansatz (4.16) into Eq. (4.14), we arrive at the following stationary Schr"odinger-type equation for the radial function:

$$\left[\frac{d^2}{dr_*^2} + \omega^2 - V(r)\right] R_\ell(r) = 0 \ , \tag{4.18}$$

where r_* denotes the tortoise coordinate associated with the Schwarzschild-MOG spacetime, defined as

$$r_* = \int \frac{dr}{f} = r + \frac{r_+^2}{r_+ - r_-}\ln(r - r_+) - \frac{r_-^2}{r_+ - r_-}\ln(r - r_-) \ . \tag{4.19}$$

The function $V(r)$ represents the effective potential governing the dynamics of the scalar perturbations and is given by

$$V(r) = f(r)\left[\frac{\ell(\ell+1)}{r^2} + \frac{1}{r}\frac{df}{dr}\right] \ . \tag{4.20}$$

One can verify that the effective potential (4.34) vanishes both at spatial infinity, $V(r \to \infty) \to 0$, and at the event horizon of the black hole, $V(r \to r_+) \to 0$. Consequently, the radial equation (4.18) admits purely scattering solutions with plane-wave asymptotics near the horizon and at infinity. In particular, the absence of a confining potential well implies that no quasi-bound states are supported by the scalar field in the Schwarzschild-MOG background. The location of the peak of the effective potential, which plays a crucial role in wave scattering and quasinormal mode analysis, can be determined from the condition $V'(r) = 0$. In Fig. **??**, we illustrate the radial dependence of the effective potential for scalar perturbations,

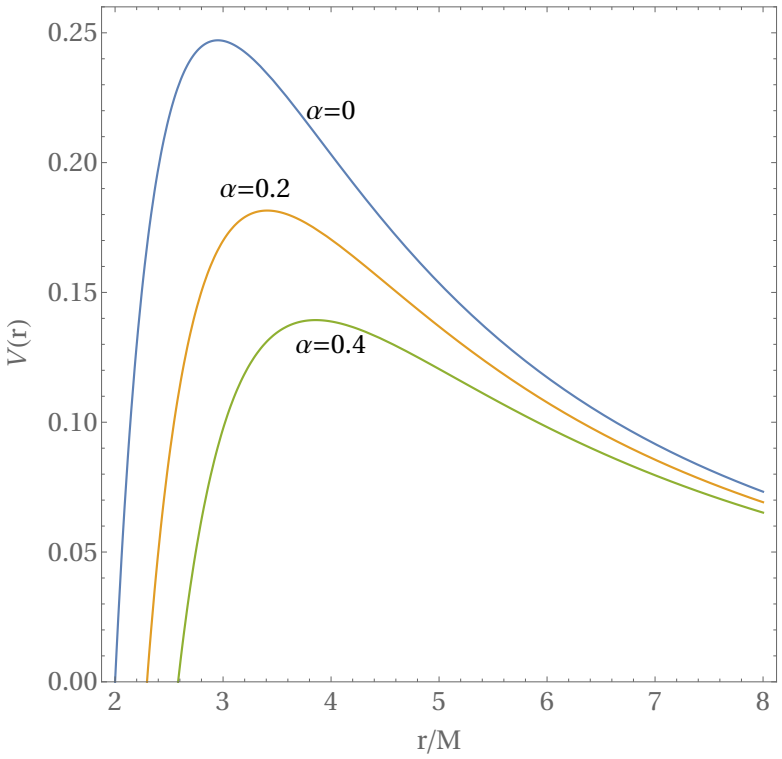


Figure 4.4: Radial profiles of the effective potential for scalar perturbations corresponding to different values of the MOG parameter α at the fixed multipole number $\ell = 2$.

showing a single potential barrier whose height and position depend on the angular momentum number ℓ. The vanishing of the effective potential at both the event horizon and spatial infinity, together with its single-barrier structure, indicates that scalar perturbations of the Schwarzschild-MOG black hole are dynamically stable. The system does not support quasi-bound states, and the wave dynamics is governed entirely by scattering off the effective potential barrier. These features closely resemble those of scalar perturbations in the standard Schwarzschild spacetime, suggesting that, at the linear level, the Schwarzschild-MOG black hole remains stable under scalar field perturbations.

4.5 Electromagnetic perturbations

Another simple black hole perturbations is described the electromagnetic perturbations. The electromagnetic perturbations are described by small fluctuations of the vector potential of the electromagnetic field A_μ propagating on a fixed background metric $g_{\mu\nu}$. In order to describe this particular perturbations, we use the Maxwell equations in the fixed curved spacetime:

$$\nabla_\mu F^{\mu\nu} = \frac{1}{\sqrt{-g}}\partial_\mu\left(\sqrt{-g}F^{\mu\nu}\right) = 0 \ , \tag{4.21}$$

where backreaction on the geometry is neglected. Here $F_{\mu\nu} = \partial_\mu A_\nu - \partial_\nu A_\mu$ is the antisymmetric Faraday tensor. For simplicity, we consider the Maxwell equations in the Schwarzschild-MOG spacetime, which can be explicitly written as

$$\frac{1}{r^2}\partial_r\left(r^2F^{rt}\right) + \frac{1}{\sin\theta}\partial_\theta\left(\sin\theta F^{\theta t}\right) + \partial_\phi F^{\phi t} = 0 \ , \tag{4.22}$$

$$\frac{1}{\sin\theta}\partial_\theta\left(\sin\theta F^{\theta r}\right) + \partial_\phi F^{\phi r} + \partial_t F^{tr} = 0 \ , \tag{4.23}$$

$$\frac{1}{r^2}\left(r^2\partial_r F^{r\theta}\right) + \partial_\phi F^{\phi\theta} + \partial_t F^{t\theta} = 0 \ , \tag{4.24}$$

$$\frac{1}{r^2}\partial_r\left(r^2F^{r\phi}\right) + \frac{1}{\sin\theta}\partial_\theta\left(\sin\theta F^{\theta\phi}\right) + \partial_t F^{t\phi} = 0 \ , \tag{4.25}$$

where components of the anti-symmetric tensor can be expressed in the form:

$$F^{tr} = \partial_r A_t - \partial_t A_r = -F^{rt} \ , \tag{4.26}$$

$$F^{t\theta} = \frac{1}{fr^2}\left(\partial_\theta A_t - \partial_t A_\theta\right) = -F^{\theta t} \ , \tag{4.27}$$

$$F^{t\phi} = \frac{1}{fr^2\sin^2\theta}\left(\partial_\phi A_t - \partial_t A_\phi\right) = -F^{\phi t} \ , \tag{4.28}$$

$$F^{r\theta} = \frac{f}{r^2}\left(\partial_r A_\theta - \partial_\theta A_r\right) = -F^{\theta r} \ , \tag{4.29}$$

$$F^{r\phi} = \frac{f}{r^2\sin^2\theta}\left(\partial_r A_\phi - \partial_\phi A_r\right) = -F^{\phi r} \ , \tag{4.30}$$

$$F^{\theta\phi} = \frac{1}{r^4\sin^2\theta}\left(\partial_\theta A_\phi - \partial_\phi A_\theta\right) = -F^{\phi\theta} \ . \tag{4.31}$$

It is evident that equations (4.22)-(4.25) can be separated into radial and angular parts, if the wave function is chosen as harmonically time dependent form as follows

$$A_\mu(x) = e^{-i\omega t}\left[-f\partial_r R^E_\ell(r), \frac{i\omega}{f}R^E_\ell(r), \frac{R^B_\ell(r)}{\sin\theta}\partial_\phi, -R^B_\ell(r)\sin\theta\partial_\theta\right] Y^m_\ell(\theta,\phi) \ , \tag{4.32}$$

where ω is the frequency of quasinormal modes for the electromagnetic perturbations, $R^E_\ell(r)$ and $R^B_\ell(r)$ are, respectively, radial profile functions for the electromagnetic (electric and magnetic cases) perturbations. By inserting expression (4.32) into equations (4.22)-(4.25), we obtain the following stationary Schrödinger-type equations:

$$\left[\frac{d^2}{dr^2_*} + \omega^2 - V(r)\right]\psi = 0 \ , \tag{4.33}$$

where $\psi = \{R^E_\ell, R^E_\ell\}$ denotes the radial functions for the electromagnetic perturbations, $V(r)$ is the effective potential in the given perturbations defined as

$$V(r) = f\frac{\ell(\ell+1)}{r^2} \ . \tag{4.34}$$

Notice that similar to the case of the scalar perturbations, the effective potential (4.34) goes to zero both at large distances, i.e. $V_s(r\to\infty)\to 0$, and at the black-hole horizon $V_s(r\to r_+)\to 0$. The stationary point of the potential is found from condition $V'(r)=0$. For the given metric function $f(r) = 1-2M(1+\alpha)/r+M^2\alpha(1+\alpha)/r^2$, the overall factor $\ell(\ell+1)$ does not affect the location of stationary points. After simple analyses, the stationary point of potential is computed as

$$r_0 = \frac{M}{2}\left[3(1+\alpha)+\sqrt{(1+\alpha)(9+\alpha)}\right] \ , \tag{4.35}$$

which is the same as the photonsphere position. Substituting $r=r_0$ into $V(r)$ allows to find the maximum value of the potential:

$$V_0 = V(r_0) = f(r_0)\frac{\ell(\ell+1)}{r_0^2} \ .$$

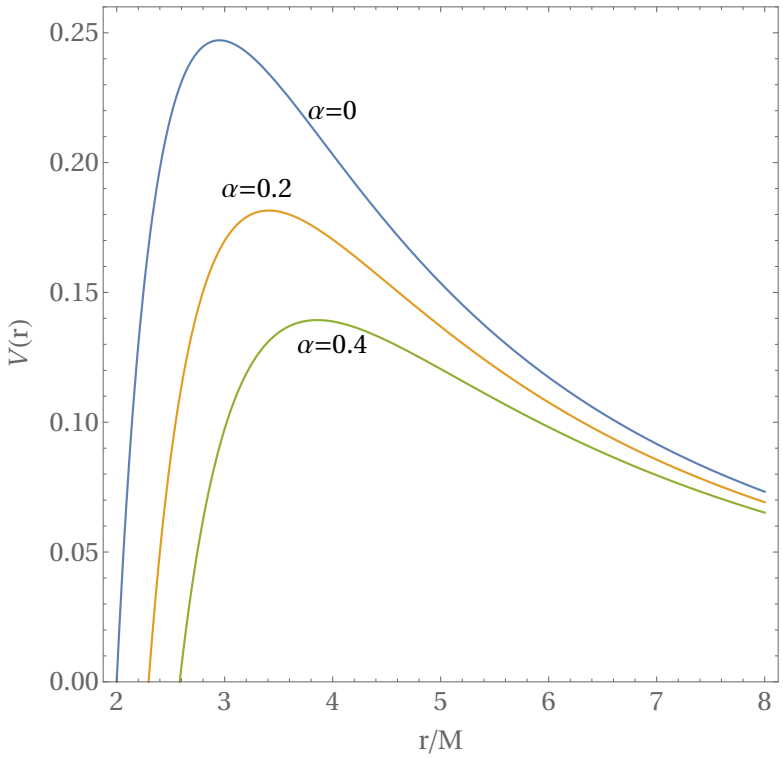


Figure 4.5: Radial profiles of the effective potential for scalar perturbations corresponding to different values of the MOG parameter α at the fixed multipole number $\ell = 2$.

This expression is exact and compact; an explicit expanded form is lengthy but straightforward, therefore, we did not included it in the thesis. For $\alpha = 0$, one finds $r_0 = 3M$, which reproduces the standard result for electromagnetic perturbations in the Schwarzschild spacetime.

In Fig. 4.5, we show radial dependence of the potential for the electromagnetic perturbations. One can see that the effective potential vanishes at large distances $r \to \infty$ as well as near horizon of the black hole.

4.6 Gravitational perturbations

Gravitational perturbations theory deals with small deviations from an exact background spacetime and provides a powerful framework for studying the dynamics of black holes in realistic astrophysical situations. In this approach, the space-

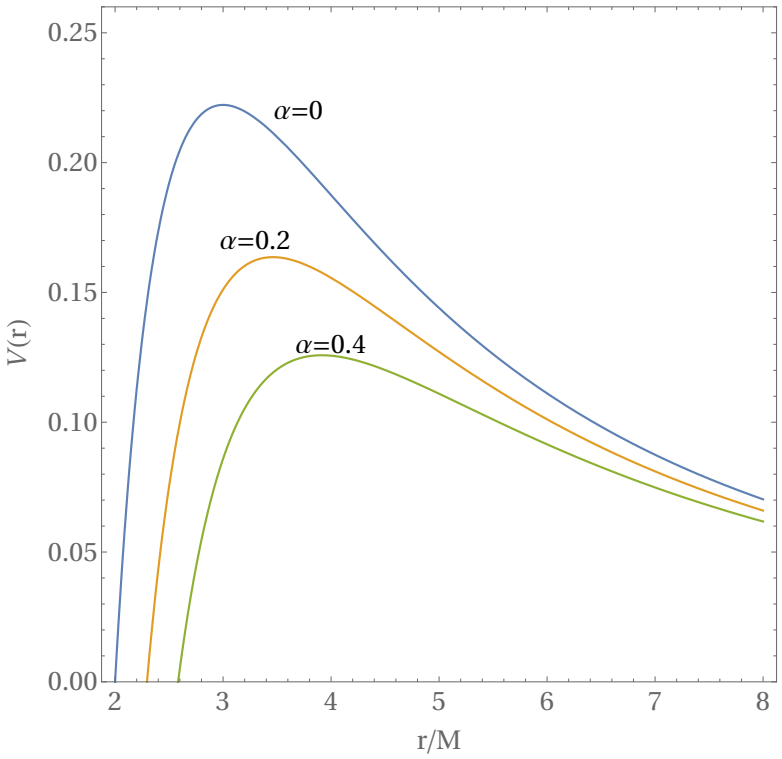


Figure 4.6: Radial profiles of the effective potential for electromagnetic perturbations corresponding to different values of the MOG parameter α at the fixed multipole number $\ell = 2$.

time metric is decomposed as $g_{\mu\nu} = \bar{g}_{\mu\nu} + h_{\mu\nu}$, where $\bar{g}_{\mu\nu}$ represents a known background solution of Einstein's equations, such as the Schwarzschild or Kerr metric describing a black hole, and $h_{\mu\nu}$ denotes a small perturbations satisfying $|h_{\mu\nu}| \ll 1$. Linearizing Einstein's equations with respect to $h_{\mu\nu}$ yields a set of tractable equations that capture the essential physics of weak disturbances while avoiding the full complexity of the nonlinear theory.

This formalism is particularly well suited for analyzing small disturbances of black hole spacetimes, such as those produced by infalling particles, weak gravitational waves, or compact objects in extreme mass-ratio systems. By exploiting the symmetries of the background spacetime, the perturbations equations can often be separated into radial and angular parts using methods such as the Regge–Wheeler and Zerilli formalisms for non-rotating black holes, or the Teukolsky formalism for

rotating ones. These perturbations fully account for GR effects in strong fields, unlike weak-field approximations.

According to Ref. [113] the metric perturbations is indicated with $h_{\mu\nu}$, along background metric metric $g_{\mu\nu}$ which is solution of the Einstein field equation

$$G_{\mu\nu}(g) = 8\pi G T_{\mu\nu}(\Phi) \ , \tag{4.36}$$

where $G_{\mu\nu}$ is the Einstein tensor dependence on the metric tensor and $T_{\mu\nu}$ is the energy momentum tensor of the vector field. Notice that the explicit form of the energy-momentum tensor depends on type of the matter field. The Einstein field equation can be rewritten in terms of the metric perturbations:

$$G_{\mu\nu}(g+h) = 8\pi T_{\mu\nu}(\Phi + \delta\Phi) \ , \tag{4.37}$$

and can be expended in the power of metric perturbations as follows

$$G_{\mu\nu}(g) - \frac{1}{2}H_{\mu\nu}(h) + ... = 8\pi G \left[T_{\mu\nu}(\Phi) + S_{\mu\nu}(\delta\Phi) + ...\right] \tag{4.38}$$

$$H_{\mu\nu} = -16\pi G S_{\mu\nu}(\delta q) \ , \tag{4.39}$$

where $H_{\mu\nu}$ and $S_{\mu\nu}$ are, respectively, Einstein and energy momentum tensor for perturbed tensor and vector fields defined as

$$H_{\mu\nu} = \nabla^2 h_{\mu\nu} + \nabla_\mu \nabla_\nu h^\lambda_\lambda + \nabla({}_\mu \nabla^\gamma h_\nu)_\lambda + g_{\mu\nu}(\nabla\lambda\nabla^\gamma h_{\lambda\gamma} - \nabla^2 h^\lambda_\lambda) + R_\mu{}^\lambda{}_\nu{}^\gamma h_{\lambda\gamma} \ ,$$
$$S_{\mu\nu} = 2(B_{\mu\alpha}\delta B^\alpha_\nu - \frac{1}{4}g_{\mu\nu}B_{\alpha\beta}\delta B_{\alpha\beta}) \ ,$$

where $\delta B_{\mu\nu} = \partial_\mu \delta\Phi_\nu - \partial_\nu \delta\Phi_\mu$. Notice that perturbed vector field is satisfied the Maxwell-like equation: $\nabla_\mu \delta B^{\mu\nu} = 0$.

We must emphasize that according to Regge and Wheeler the gravitational perturbations can be decomposed as $h_{\mu\nu} = h^+_{\mu\nu} + h^-_{\mu\nu}$, where $h^+_{\mu\nu}$ and $h^-_{\mu\nu}$ are polar

and axial perturbations. The axial gravitational "Odd" perturbations is [113]

$$h^{-}_{\mu\nu} = \begin{bmatrix} 0 & 0 & -h_0 \csc\theta\partial_\phi & h_0 \sin\theta\partial_\theta \\ 0 & 0 & -h_1 \csc\theta\partial_\phi & h_1 \sin\theta\partial_\theta \\ * & * & h_2 \csc\theta(\partial^2_{\theta\phi} - \cot\theta\partial_\phi) & \frac{1}{2}h_2(\csc\theta\partial^2_\phi + \cos\theta\partial_\theta - \sin\theta\partial^2_\theta) \\ * & * & * & -h_2 \sin\theta(\partial^2_{\theta\phi} - \cot\theta\partial_\phi) \end{bmatrix} Y^m_\ell \ , \tag{4.40}$$

while the polar gravitational "Even" perturbations reads

$$h^{+}_{\mu\nu} = \begin{bmatrix} fH_0 & H_1 & h_0\partial_\theta & h_0\partial_\phi \\ * & \frac{1}{f}H_2 & h_1\partial_\theta & h_1\partial_\phi \\ * & * & r^2\left(K + G\partial^2_\theta\right) & r^2 G(\partial^2_{\theta\phi} - \cot\theta\partial_\phi) \\ * & * & * & r^2\left[K\sin^2\theta + G(\partial^2_\phi + \sin\theta\cos\theta\partial_\theta)\right] \end{bmatrix} Y^m_\ell \ , \tag{4.41}$$

where $h_0(t,r)$, $h_2(t,r)$ and $h_2(t,r)$ are profile functions in axial perturbations, while $H_0(t,r)$, $H_1(t,r)$, $H_2(t,r)$, $K(t,r)$ and $G(t,r)$ are profile functions in polar perturbations.

4.6.1 Axial gravitational perturbations and Regge-Wheeler equation

After applying a gauge transformation in axial perturbations we can consider perturbations the simple spherically symmetric case and remove the second angular derivative in equation (4.40). Using the following gauge $h_2 = 0$, the axial gravitational perturbations to metric function with $\ell \neq 0$ and $m = 0$ can be expressed as

$$h^{-}_{\mu\nu} = \begin{pmatrix} 0 & 0 & 0 & h_0(r) \\ 0 & 0 & 0 & h_1(r) \\ 0 & 0 & 0 & 0 \\ * & * & 0 & 0 \end{pmatrix} \sin\theta \frac{dP_\ell(\cos\theta)}{d\theta} e^{-i\omega t} \ , \tag{4.42}$$

where $h_0(r)$ and $h_1(r)$ are unknown radial functions, $P_\ell(\cos\theta)$ is the Legendre polynomial satisfied the following relation:

$$\frac{1}{\sin\theta}\frac{d}{d\theta}\left(\sin\theta \frac{dP_\ell(\cos\theta)}{d\theta}\right) = -\ell(\ell+1)P_\ell(\cos\theta) \ , \tag{4.43}$$

and normalized as

$$\int_0^\pi P_\ell(\cos\theta) P_{\ell'}(\cos\theta)\sin\theta d\theta = \frac{2}{2\ell+1}\delta_{\ell\ell'} \ . \tag{4.44}$$

Similarly, the axial vector perturbations can be expressed as

$$\delta\Phi_\mu = (0,0,0,1)F(r)\sin\theta \frac{dP_\ell(\cos\theta)}{d\theta} e^{-i\omega t} \ , \tag{4.45}$$

where $F(r)$ is the radial vector perturbations.

Inserting equations (4.42) and (4.45) into Einstein field equations and Maxwell equations, radial equations for functions $h_0(r)$, $h_1(r)$ and $F(r)$ can be derived as

$$h_0'' = \left(\frac{\ell^2+\ell-2}{r^2 f} + \frac{2}{r^2}\right) h_0 - i\omega\left(h_1' + \frac{2}{r}h_1\right) - \frac{4\tilde{Q}}{r^2}F' \ , \tag{4.46}$$

$$h_0' = \frac{2}{r}h_0 + \left[\frac{f\left(\ell^2+\ell-2\right)}{r^2\omega^2} - 1\right] i\omega h_1 - \frac{4\tilde{Q}}{r^2}F \ , \tag{4.47}$$

$$i\omega h_0 + f\left(f h_1\right)' = 0 \ , \tag{4.48}$$

$$\frac{d^2F}{dr_*^2} + \left(\omega^2 - f\frac{\ell(\ell+1)}{r^2}\right)F + \frac{f\tilde{Q}}{r^2}\left(h_0' - \frac{2h_0}{r} + i\omega h_1\right) \ . \tag{4.49}$$

Before proceeding further, new function can be introduced as

$$h_1(r) = \frac{r}{f}\psi_g(r) \ , \quad \text{and} \quad F(r) = \psi_e(r) \ . \tag{4.50}$$

After eliminating h_0 from equations (4.47)-(4.49), the Regge-Wheeler equation for $\psi_g(r)$ and $\psi_e(r)$ can be derived as:

$$\frac{d^2\psi_g}{dr_*^2} + \left[\omega^2 - V_g(r)\right]\psi_g(r) = \frac{4i\omega qf}{r^3}\psi_v(r) \ , \tag{4.51}$$

$$\frac{d^2\psi_v}{dr_*^2} + \left[\omega^2 - V_v(r)\right]\psi_v(r) = \frac{i\left(\ell^2+\ell-2\right)qf}{r^3\omega}\psi_g(r) \ , \tag{4.52}$$

where $V_g(r)$ and $V_e(r)$ are the potential defined as

$$V_g(r) = f\left(\frac{\ell(\ell+1)}{r^2} - \frac{6M}{r^3} + \frac{4\tilde{Q}^2}{r^4}\right) \ ,$$

$$V_e(r) = f\left(\frac{\ell(\ell+1)}{r^2} + \frac{4\tilde{Q}^2}{r^4}\right) \ ,$$

However, equations (4.51) and (4.52) are coupled and it is difficult to solve equations. In order to decouple these equation we consider linear combinations of profile functions for tensor and vector perturbations. Introducing the vector

$$\Psi = \begin{pmatrix}\psi_g \\ \psi_v\end{pmatrix} , \tag{4.53}$$

the system can be written as

$$\frac{d^2\Psi}{dr_*^2} + \left(\omega^2 I - V\right)\Psi = 0, \tag{4.54}$$

where the potential matrix is

$$V = \begin{pmatrix}V_g & C_1 \\ C_2 & V_v\end{pmatrix} , \tag{4.55}$$

with

$$C_1 = -\frac{4i\omega qf}{r^3}, \qquad C_2 = -\frac{i(\ell^2+\ell-2)qf}{r^3\omega}. \tag{4.56}$$

To decouple the system, we introduce new master variables as linear combinations of the original perturbations,

$$Z_\pm = a_\pm\psi_g + b_\pm\psi_v, \tag{4.57}$$

where the constants $(a_\pm, b_\pm)$ are chosen such that they diagonalize the potential matrix. This leads to the eigenvalue problem

$$\det \begin{pmatrix} V_g - \lambda & C_1 \\ C_2 & V_v - \lambda \end{pmatrix} = 0. \tag{4.58}$$

Solving for λ yields

$$\lambda_\pm = \frac{V_g + V_v}{2} \pm \frac{1}{2}\sqrt{(V_g - V_v)^2 + 4C_1C_2}. \tag{4.59}$$

The perturbations are now governed by two independent Schr/"odinger-type equations

$$\frac{d^2 Z_\pm}{dr_*^2} + \left[\omega^2 - V_\pm(r)\right] Z_\pm = 0 \ , \tag{4.60}$$

where the potentials simplify to

$$V_\pm = f\left(\frac{\ell(\ell+1)}{r^2} - \frac{3M}{r^3} + \frac{4\tilde{Q}^2}{r^4}\right) \pm \frac{2f}{r^3}\sqrt{9M^2 - 4(\ell^2+\ell-2)\tilde{Q}^2 f}. \tag{4.61}$$

It is evident that (4.60) are fully decoupled equations for vector and tensor perturbations. These expressions clearly demonstrate that the equations for Z_+ and Z_- are completely decoupled, corresponding respectively to the vector and tensor sectors of the perturbations. In the absence of the MOG parameter $\alpha = 0$ (or $\tilde{Q} = 0$), the potential in (4.61) reduces the following form:

$$V_+ = f\left(\frac{\ell(\ell+1)}{r^2}\right) \ , \qquad V_- = f\left(\frac{\ell(\ell+1)}{r^2} - \frac{6M}{r^3}\right) \ . \tag{4.62}$$

which correspond to vector and tensor perturbation in the Schwarzschild spacetime [113]. Therefore, one can conclude that potential V_+ corresponds to vector and V_+ corresponds to tensor perturbations. As a result, the analysis of their behavior can be carried out independently, greatly simplifying the study of the system's stability and quasinormal mode spectrum.

4.7 Method and Results

We present our main result on Quasi-Normal Modes (QMN) of the Schwarzschild-MOG black hole. We apply The Wentzel–Kramers–Brillouin (WKB) method is a semi-analytical technique widely used to compute the quasinormal mode (QNM) frequencies of black holes. QNMs correspond to solutions of the perturbation equations that satisfy purely outgoing boundary conditions at infinity and purely ingoing boundary conditions at the horizon. In the WKB approach, the wave equation for perturbations is typically cast in a Schrödinger-like form:

$$\left[\frac{d^2}{dr_*^2} + \omega^2 - V_s(r)\right]\psi_s = 0 \ , \tag{4.63}$$

where ψ_s denotes the radial functions for scalar and electromagnetic perturbations, $V_s(r)$ is the effective potential in the given perturbations defined as

$$V_s(r) = f\left[\frac{\ell(\ell+1)}{r^2} + \frac{1-s^2}{r}\frac{df}{dr}\right] \ . \tag{4.64}$$

Here s denotes the spin of the particle: $(s = 0)$ corresponds to scalar perturbations, while $(s = 1)$ corresponds to electromagnetic perturbations. It is straightforward to verify that the effective potential (4.34) goes to zero both at large distances, i.e. $V_s(r \to \infty) \to 0$, and at the black-hole horizon $V_s(r \to r_+) \to 0$.

$$\frac{i(\omega^2 - V_0)}{\sqrt{-2V_0''}} - \sum_{j=2}^{N}\Lambda_j = n + \frac{1}{2}, \quad n = 0, 1, 2, \ldots$$

Here, V_0 is the maximum of the potential, V_0'' its second derivative at the peak, n the overtone number, and Λ_j are higher-order WKB correction terms. The WKB method is particularly effective for low-lying modes $(n < \ell)$ and has been extended to higher-order approximations (up to 6th or 7th order in Ref. [127]) to improve accuracy. Its semi-analytical nature makes it a convenient tool for exploring QNM spectra across various black hole spacetimes.

In this study, we investigated the quasi-normal modes (QNMs) of the Schwarzschild-MOG (Modified Gravity) black hole, focusing on both scalar and electromagnetic perturbations. The frequency of QNMs is a crucial aspect in understanding the stability and oscillatory behavior of black holes when perturbed. We obtained the QNM frequencies for various values of the MOG parameter α, as detailed in Tables 4.2 and 4.3. Table 4.2 presents the quasi-normal frequencies for the massless scalar perturbations, while Table 4.3 shows the corresponding results for the electromagnetic perturbations. For both types of perturbations, we observe a consistent trend: as the MOG parameter α increases, the real part of the frequency decreases, while the imaginary part also decreases, indicating that the oscillations become slower and more heavily damped. In the absence of the MOG parameter ($\alpha = 0$), the results reduce to those for the Schwarzschild black hole, providing a baseline for comparison. As α increases from 0 to 1, the frequencies of both scalar and electromagnetic perturbations decrease monotonically. This suggests that the presence of the MOG parameter enhances the gravitational effects, leading to longer damping times and slower oscillation frequencies, as compared to the Schwarzschild black hole. The results presented in these tables highlight how the inclusion of the MOG parameter modifies the black hole's response to external perturbations, affecting both its stability and the time scales over which it returns to equilibrium.

Using the time-domain integration method, one can numerically evolve the non-stationary Schrödinger-like equation to study the dynamics of perturbations in black hole spacetimes. In Figs.4.7 the time evolution profiles of scalar, electromagnetic, gravitational (tensor), and vector perturbations are presented. It is evident that the scalar and electromagnetic perturbations decay at nearly the same rate, although their oscillation frequencies differ, indicating that these per-

α	$\omega\ (\ell = 2)$	$\omega\ (\ell = 3)$	$\omega\ (\ell = 4)$
0.	$0.506317 - 0.0961232i$	$0.691728 - 0.0961481i$	$0.880197 - 0.0961713i$
0.2	$0.433660 - 0.0807996i$	$0.592954 - 0.0808258i$	$0.754779 - 0.0808460i$
0.4	$0.379726 - 0.0696219i$	$0.519562 - 0.0696467i$	$0.661552 - 0.0696639i$
0.6	$0.338011 - 0.0611098i$	$0.462752 - 0.0611321i$	$0.589363 - 0.0611467i$
0.8	$0.304735 - 0.0544140i$	$0.417402 - 0.0544334i$	$0.531717 - 0.0544456i$
1.	$0.277542 - 0.0490113i$	$0.380319 - 0.0490279i$	$0.484568 - 0.049038i$

Table 4.2: Quasi-normal modes of the massless scalar perturbations in the Schwarzschild-MOG spacetime for $n = 0$.

α	$\omega\ (\ell = 2)$	$\omega\ (\ell = 3)$	$\omega\ (\ell = 4)$
0.	$0.480754 - 0.0943536i$	$0.673438 - 0.0952575i$	$0.865960 - 0.0956364i$
0.2	$0.412178 - 0.0793758i$	$0.577579 - 0.0801080i$	$0.742810 - 0.0804145i$
0.4	$0.361213 - 0.0684375i$	$0.506310 - 0.0690487i$	$0.651235 - 0.0693041i$
0.6	$0.321755 - 0.0600997i$	$0.451114 - 0.0606215i$	$0.580301 - 0.0608392i$
0.8	$0.290252 - 0.0535355i$	$0.407032 - 0.0539888i$	$0.523644 - 0.0541777i$
1.	$0.264488 - 0.0482354i$	$0.370972 - 0.0486347i$	$0.477291 - 0.048801i$

Table 4.3: Quasi-normal modes of the electromagnetic perturbations in the Schwarzschild-MOG spacetime for $n = 0$.

α	$\omega\ (\ell = 2)$	$\omega\ (\ell = 3)$	$\omega\ (\ell = 4)$
0.	$0.398850 - 0.0882854i$	$0.616561 - 0.0923181i$	$0.822303 - 0.0939294i$
0.2	$0.351606 - 0.0750712i$	$0.535440 - 0.0780357i$	$0.710420 - 0.0792072i$
0.4	$0.314453 - 0.0652472i$	$0.473723 - 0.0675159i$	$0.626160 - 0.0684089i$
0.6	$0.284483 - 0.0576534i$	$0.425099 - 0.0594465i$	$0.560266 - 0.0601515i$
0.8	$0.259796 - 0.0516084i$	$0.385746 - 0.0530628i$	$0.507239 - 0.0536349i$
1.	$0.239104 - 0.0466838i$	$0.353210 - 0.0478886i$	$0.463594 - 0.048363i$

Table 4.4: Quasi-normal modes of the gravitational perturbations in the Schwarzschild-MOG spacetime for $n = 0$.

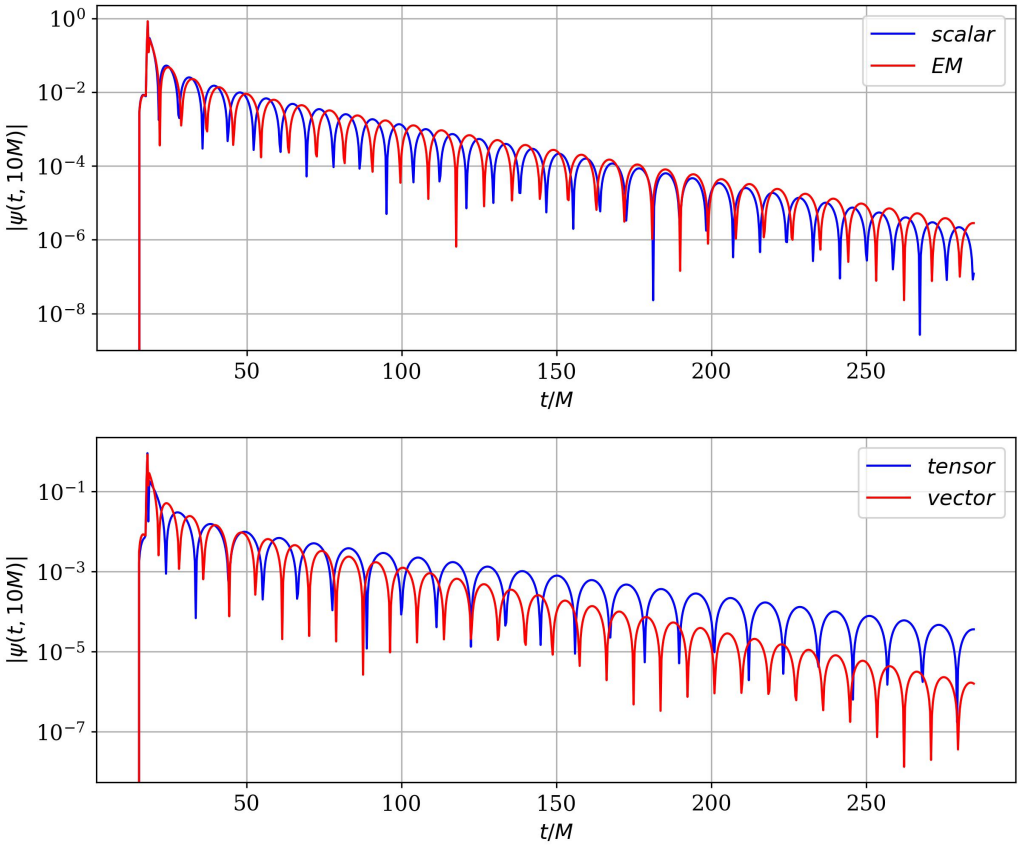


Figure 4.7: Semilogoty time-domain profiles of the scalar and electromagnetic perturbations (on top), vector and tenzor perturbations (on bottom) at $\alpha = 0.5$ and $\ell = 2$.

turbations are similarly influenced by the spacetime geometry but exhibit distinct characteristic modes. On the other hand, it is shown that vector perturbations decay more rapidly than tensor perturbations, suggesting that vector modes are less stable and dissipate faster in the given background. These results highlight the varying damping behaviors and oscillation characteristics of different types of perturbations, providing insight into the stability and energy dissipation mechanisms around black holes.

4.8 Conclusion

We have studied the thermodynamic properties of the Schwarzschild-MOG black hole in STVG and investigated thermodynamic observational quantities of the black hole. The exploration of thermodynamic properties of black holes within the framework of STVG and the investigation of the MOG parameter's influence on these properties represent a captivating and intellectually stimulating pursuit. The formulation of the first law of black hole thermodynamics in STVG, as expressed by equation (4.1). This additional term, arising from the presence of STVG, introduces a distinctive element that has the potential to significantly impact the thermodynamic characteristics of black holes within this modified theoretical framework. The thermodynamic analysis of the Schwarzschild-MOG black hole reveals significant deviations from classical general relativity due to the influence of the MOG parameter α. The Hawking temperature decreases with increasing α, while the entropy is consistently greater than in the standard Schwarzschild case—confirming consistency between the area law and first law of thermodynamics. Additionally, the negative isochoric heat capacity, with a larger absolute value than in general relativity, suggests enhanced instability and invites further scrutiny of black hole thermodynamics within the STVG framework. These findings offer deeper insights into the impact of modified gravity on black hole physics.

One of the significant aspect of the black holes, their lifetime in STVG, has been studied. The investigation utilizes the Stephan-Boltzmann radiation law to approximate the rate of energy loss, incorporating contributions from the external potential in STVG. The derived expression for the lifetime of the Schwarzschild-MOG black hole demonstrates a dependence on the MOG parameter. Notably, the calculated lifetime, considering both modified gravity and the influence of the vector field, exceeds that of the Schwarzschild black hole. This finding is in con-

trast to previous results presented in the literature, where the contribution from the vector field was overlooked. The significance of this study lies in recognizing that the black hole's lifetime is longer in the context of STVG, showcasing the impact of modified gravity and the vector field on the overall dynamics of black holes. Overall, these results contribute to a deeper understanding of black hole behavior within the realm of modified gravity theories.

The study of quasi-normal modes (QNMs) of the Schwarzschild-MOG black hole under scalar and electromagnetic perturbations has yielded insightful results. It has been shown how the MOG parameter α affects the frequencies of QNMs. For both scalar and electromagnetic perturbations, an increase in the value of α leads to a decrease in both the real and imaginary parts of the frequencies, indicating a shift towards longer decay times and lower oscillation frequencies.

This trend demonstrates the significant influence of the MOG parameter on the dynamical response of the Schwarzschild-MOG black hole, with higher values of α generally resulting in more damped modes. These findings provide a deeper understanding of the stability and vibrational characteristics of black holes in the Modified Gravity framework, contributing to the broader field of black hole physics and gravitational perturbations theory. Future work could explore the impact of higher modes or the inclusion of other types of perturbations to further refine our understanding of these black holes' dynamical properties.

Main results and conclusions

Below we present the main results of the dissertation.

1. We have examined the geodesic motion in the Schwarzschild-MOG spacetime in STVG. Firstly, we have analyzed photon motion around the Schwarzschild-MOG black hole and derived analytical expressions for the photon sphere and critical impact parameter, which are crucial for understanding the black hole shadow. Our results showed that both the photon sphere and the size of the black hole shadow increase due to the presence of MOG. Furthermore, we applied these results to the observational data of M87* and Sgr A* observed by the Event Horizon Telescope (EHT) collaboration. Our analysis demonstrated that the shadow radius increases with the scalar parameter α, approaching a constant asymptotic value for large α. Importantly, the predicted shadow sizes are consistent with the EHT measurements for both black holes within the 1σ confidence level. This agreement provides meaningful constraints on the parameter $\alpha \leq 0.21$, highlighting its relevance in modeling compact objects beyond standard general relativity. Overall, the study shows that the scalar field parameter n plays a key role in modifying photon trajectories and black hole shadow profiles, and that current EHT observations can serve as an effective probe for testing STVG.

2. We have studied the circular motion of massive particles in the Schwarzschild-MOG spacetime, specifically examining the innermost stable circular orbit

(ISCO). We found that the characteristic radii of these orbits are larger compared to those in the Schwarzschild spacetime. Through numerical calculations, we demonstrate that the innermost stable circular orbit (ISCO) of the massive particle is subject to the influence of an external force stemming from STVG. Furthermore, we determined the maximum energy efficiency of test particles around the Schwarzschild-MOG black hole, which can reach up to approximately 8.14%, indicating a relatively large efficiency compared to the Schwarzschild case. This external force induces an increase in the particle's position. To visually illustrate this effect, we present graphical representations showcasing the dependence of the ISCO position on the STVG parameter denoted as α. These significant findings offer valuable insights into the impact of external forces on the motion of massive particles, enhancing our understanding of their behavior near black holes within the framework of STVG theory.

3. We have investigated the influence of the Scalar–Tensor–Vector Gravity (STVG) parameter α on the orbital motion of the S2 star around the supermassive black hole (SMBH) at the Galactic Centre. By constructing the trajectory of the S2 star within the STVG framework, we demonstrated that the periastron position is highly sensitive to variations in α. Our analysis reveals that an increase in the STVG parameter can lead to a noticeable decrease—up to approximately 7.5 times—in the periastron shift compared to the prediction of General Relativity (GR). Furthermore, the initial orbital position of the S2 star is found to deviate from that obtained in GR, highlighting the potential detectability of STVG effects through precise astrometric measurements. Recent observational analyzes have placed an upper bound on the STVG parameter as $\alpha \leq 0.662$ at the 99.7% confidence level

using the kinematic data of the S2 star [51]. While earlier studies estimated the periastron precession as $\delta\phi \leq 1.552, \delta\phi_{\rm GR}$ using a dynamical mass limit approach, our results based on equation (1.70) suggest a stronger constraint, yielding $\delta\phi \leq 3.752, \delta\phi_{\rm GR}$. These findings indicate that precise monitoring of stellar orbits near the Galactic Centre can serve as a powerful test for modified gravity models such as STVG, offering an important avenue for probing deviations from GR in the strong-field regime.

4. We have first tested particle motion around Kerr-MOG black hole and find the ISCO position for massive particle orbiting a rotating black hole in STVG. Our study delves into the behavior of massive particles in the vicinity of black holes within the framework of STVG, revealing intriguing deviations from the conventional Lorentz-like equation of motion. Specifically, we focus on the circular motion of massive test particles near the Kerr-MOG black hole, which is a solution derived within the STVG theory. To simplify our analysis, we consider the motion to be confined to the equatorial plane, allowing us to derive the effective potential that governs the particle's orbit around the Kerr-MOG black hole.

5. We have studied energy extraction from the Kerr-MOG black hole via the Penrose process in the context of the STVG (Scalar-Tensor-Vector Gravity), particularly, with respect to the efficiency of energy transfer from black holes. The derived relations between particle energies, coupling constants, and the influence of the external scalar potential show that under certain conditions, the efficiency of energy extraction can exceed 100%. This is in stark contrast to the classical case of the extreme Kerr black hole, where the efficiency is around 21%. Specifically, for high values of the STVG parameter α, the maximum energy efficiency can surpass 100%, suggesting that mass ratios

between escaping and falling particles can lead to unexpectedly large energy yields. The significant efficiency enhancements observed in the Kerr-MOG (Kerr with Modified Gravity) black holes, reaching up to 200%, highlight the potential of STVG theory to generate high-energy particles, further reinforcing the idea that the external fifth-potential plays a crucial role in these processes. This aligns with previous studies in the context of magnetized black holes, where rotation and magnetic fields also lead to efficiency values exceeding 100%, as seen in the work on magnetized Kerr black holes. These results open avenues for further research into the constraints on the MOG parameter α. Notably, observational data from pulsars and the orbital motion of stars around supermassive black holes could provide valuable insights into the possible values for α, offering constraints that could help refine our understanding of modified gravity theories. With a constrained value of $\alpha \lesssim 0.41$, the maximum energy efficiency from the Penrose process is found to reach about 78%, demonstrating that even within the confines of observational limits, energy extraction from Kerr-MOG black holes remains highly efficient.

6. We extended the concept that massive particles experience four-acceleration due to external vector fields, subsequently incorporating the radiation reaction term into the equation of motion. Based on this insight, we delved into the gravitational analogue of radiation reaction experienced by a massive particle orbiting a Schwarzschild-MOG black hole. By employing the Landau trick, we simplified the equation of motion by discarding high-order terms concerning damping time. Furthermore, we investigated the gravitational counterpart of radiation reaction occurring when a stellar black hole orbits a supermassive black hole. This exceptionally high intensity value suggests that

such systems may serve as potent sources of gravitational waves. Indeed, the detection of gravitational waves stemming from binary black hole mergers by the LIGO and Virgo collaborations has ushered in a fresh perspective on the study of black holes and their surrounding environments within the framework of STVG. The potential observation of gravitational waves originating from other black hole systems, particularly those involving orbiting massive particles, holds the promise of yielding deeper insights into the fundamental physics governing black holes and their intricate interactions with their surroundings. Moreover, we extensively investigate the BSW mechanism in the context of the Kerr-MOG black hole and propose a remarkable augmentation in the CME of two particles undergoing collision. This observation suggests that the Scalar-Tensor-Vector Gravity (STVG) theory could potentially impact high-energy collisions. These remarkable revelations open up captivating avenues for forthcoming investigations in this domain. Also we would like to point out that our approach helps to understand qualitatively the process under study to make useful astrophysical predictions since the spin parameter can have values $a > 1$ in the Kerr-MOG black hole case.

7. Recent studies have demonstrated that high CME is possible with maximum spin in both Kerr-MOG and Kerr spacetimes. Consequently, it has been discovered that the CME of a colliding pair of particles near an extremal Kerr-MOG black hole can reach extraordinary magnitudes, taking on arbitrary values. Specifically, when the angular momentum of one of the particles is $\ell = 2\sqrt{1+\alpha}$, where $\alpha > 0$, it has been observed that a higher critical angular momentum is required in the Kerr-MOG spacetime compared to the Kerr spacetime in order to achieve infinite CME. Finite CME, denoted as $E^2_{\text{c.m.}} = 2m^2$, can be obtained when the colliding particles have identical

mass and angular momentum. These results align with previous findings in the Schwarzschild and Kerr spacetimes [85]. Furthermore, it has been demonstrated that the maximum CME of a colliding pair of particles depends on the disparity in the specific energy values of the individual particles. Conversely, it remains independent of the vector field, and the effect of STVG emerges solely from the spacetime geometry. Recently, it has been shown that CME of colliding pair of particles might be extremely high in the polar region of the Kerr black hole [86]. Fascinatingly, our own analysis showed that this phenomenon holds true even within the Kerr-MOG spacetime.

8. It is well-established that the motion of massive particles around black holes in STVG does not follow a geodesic line. Building upon this fact, we have conducted a study of the circular motion of massive test particles in the vicinity of the Kerr-MOG black hole, which is one of the black hole solutions in STVG. To simplify our analysis, we have focused on circular motion in the equatorial plane and have derived the effective potential governing the motion of the massive particle in orbit around the Kerr-MOG black hole. Through numerical calculations, we have discovered that the position of the ISCO (innermost stable circular orbit) for the massive particle around the black hole increases due to an external force arising from STVG. We have also graphically demonstrated the dependence of the ISCO position on the STVG parameter α. Overall, our research sheds light on the behavior of massive particles orbiting around black holes in the context of STVG theory, providing new insights into the effects of external forces on the motion of these particles.

9. As we mentioned before, massive particles occurs four-acceleration due to the fifth force in STVG, and the equation of motion resembles the Lorentz

equation for charged particles. Based on this fact, we have discussed the gravitational analogue of synchrotron radiation from a massive particle orbiting around a Kerr-MOG black hole due to the fifth force in STVG. Additionally, we have studied the gravitational radiation emitted by a massive particle falling radially onto a Kerr-MOG black hole with angular velocity. We are arguing that massive particle, such as black hole, orbiting around the SMBH, can emit intense radiation and generate gravitational waves that can be observed. This effect is known as "gravitational radiation reaction", and it is caused by the particle's motion in the strong gravitational field of the SMBH. The intensity of the radiation emitted by the orbiting particle depends on various factors, such as its mass, velocity, and distance from the black hole. Based on our analysis, for a typical SMBH with a mass of $10^9 M_\odot$ and SBH of mass $10 M_\odot$ orbiting around it, the intensity of the radiation has been estimated to be $I \sim 2.43 \times 10^{39}$. This is a very large value and suggests that such systems could be strong sources of gravitational waves. Indeed, the observation of gravitational waves from binary black hole mergers by the LIGO and Virgo collaborations has opened up a new window into the study of black holes and their environments in the STVG. The detection of gravitational waves from other types of black hole systems, such as those with orbiting massive particles, would provide further insights into the physics of black holes and their interactions with their surroundings.

10. As previously discussed, massive particles exhibit non-geodesic behavior when navigating the vicinity of black holes within the framework of STVG. This peculiar behavior arises from the similarity between the equations of motion governed by the external vector field and the Lorentz-like equation. Taking into account this fact, this research endeavors to explore the circular motion of

massive test particles in the equatorial plane around the Schwarzschild-MOG black hole. We have concentrated on circular orbits and derived the effective potential that dictates the motion of these massive particles orbiting the Schwarzschild-MOG black hole. Our numerical computations have unveiled a noteworthy revelation: the ISCO position for massive particles orbiting the black hole experiences a notable shift in position due to the presence of an external vector field within the STVG framework. Furthermore, we have visually depicted this ISCO's dependence on the MOG parameter α through graphical representations. These findings collectively contribute to a deeper understanding of the intricate dynamics governing massive particle motion in the context of STVG theory as well as on their trajectories.

11. We have studied the thermodynamic properties of the Schwarzschild-MOG black hole in STVG and investigated thermodynamic observational quantities of the black hole. The exploration of thermodynamic properties of black holes within the framework of STVG and the investigation of the MOG parameter's influence on these properties represent a captivating and intellectually stimulating pursuit. The formulation of the first law of black hole thermodynamics in STVG, as expressed by equation (4.1). This additional term, arising from the presence of STVG, introduces a distinctive element that has the potential to significantly impact the thermodynamic characteristics of black holes within this modified theoretical framework. The thermodynamic analysis of the Schwarzschild-MOG black hole reveals significant deviations from classical general relativity due to the influence of the MOG parameter α. The Hawking temperature decreases with increasing α, while the entropy is consistently greater than in the standard Schwarzschild case—confirming consistency between the area law and first law of thermodynamics. Addition-

ally, the negative isochoric heat capacity, with a larger absolute value than in general relativity, suggests enhanced instability and invites further scrutiny of black hole thermodynamics within the STVG framework. These findings offer deeper insights into the impact of modified gravity on black hole physics.

12. One of the significant aspect of the black holes, their lifetime in STVG, has been studied. The investigation utilizes the Stephan-Boltzmann radiation law to approximate the rate of energy loss, incorporating contributions from the external potential in STVG. The derived expression for the lifetime of the Schwarzschild-MOG black hole demonstrates a dependence on the MOG parameter. Notably, the calculated lifetime, considering both modified gravity and the influence of the vector field, exceeds that of the Schwarzschild black hole. This finding is in contrast to previous results presented in the literature, where the contribution from the vector field was overlooked. The significance of this study lies in recognizing that the black hole's lifetime is longer in the context of STVG, showcasing the impact of modified gravity and the vector field on the overall dynamics of black holes. Overall, these results contribute to a deeper understanding of black hole behavior within the realm of modified gravity theories.

13. The study of quasi-normal modes (QNMs) of the Schwarzschild-MOG black hole under scalar and electromagnetic perturbations has yielded insightful results. The data, presented in Tables 4.2 and 4.3, reveals how the MOG parameter α affects the frequencies of QNMs. For both scalar and electromagnetic perturbations, an increase in the value of α leads to a decrease in both the real and imaginary parts of the frequencies, indicating a shift towards longer decay times and lower oscillation frequencies. This trend demonstrates the significant influence of the MOG parameter on the dynam-

ical response of the Schwarzschild-MOG black hole, with higher values of α generally resulting in more damped modes. It turns out that, within STVG, waves associated with vector perturbations decay more rapidly than those corresponding to tensor perturbations.

Bibliography

[1] R. V. Pound and J. L. Snider, "Effect of Gravity on Nuclear Resonance," *Phys. Rev. Lett.*, vol. 13, no. 18, pp. 539–540, Nov. 1964.

[2] A. Einstein, "Lens-Like Action of a Star by the Deviation of Light in the Gravitational Field," *Science*, vol. 84, no. 2188, pp. 506–507, Dec. 1936.

[3] G. M. Clemence, "The Relativity Effect in Planetary Motions," *Reviews of Modern Physics*, vol. 19, no. 4, pp. 361–364, Oct. 1947.

[4] C. Brans and R. H. Dicke, "Mach's principle and a relativistic theory of gravitation," *Phys. Rev.*, vol. 124, pp. 925–935, 1961.

[5] S. Kozyrev, "Exact vacuum solutions of Jordan, Brans-Dicke field equations," 12 2005.

[6] R. E. Morganstern, "Brans-Dicke Cosmologies in Arbitrary Units: Solutions in Flat Friedmann Universes," *Phys. Rev. D*, vol. 4, pp. 278–282, 1971.

[7] R. E. Morganstern, "Exact solutions to brans-dicke cosmologies in flat friedmann universes," *Phys. Rev. D*, vol. 4, pp. 946–954, 1971.

[8] J. W. Moffat, "Scalar tensor vector gravity theory," *JCAP*, vol. 2006, no. 3, p. 004, Mar. 2006.

[9] J. W. Moffat, "Time delay predictions in a modified gravity theory," *Classical and Quantum Gravity*, vol. 23, no. 23, pp. 6767–6771, Dec. 2006.

[10] J. W. Moffat and V. T. Toth, "Testing Modified Gravity with Globular Cluster Velocity Dispersions," *ApJ*, vol. 680, no. 2, pp. 1158–1161, Jun. 2008.

[11] J. R. Brownstein and J. W. Moffat, "The Bullet Cluster 1E0657-558 evidence shows modified gravity in the absence of dark matter," *MNRAS*, vol. 382, no. 1, pp. 29–47, Nov. 2007.

[12] J. W. Moffat, "a Modified Gravity and its Consequences for the Solar System, Astrophysics and Cosmology," *International Journal of Modern Physics D*, vol. 16, pp. 2075–2090, Jan. 2007.

[13] J. Rayimbaev and P. Tadjimuratov, "Can modified gravity silence radio-loud pulsars?" *Phys. Red. D*, vol. 102, no. 2, p. 024019, Jul. 2020.

[14] J. W. Moffat and V. T. Toth, "Modified Gravity and the origin of inertia," *MNRAS*, vol. 395, no. 1, pp. L25–L28, May 2009.

[15] J. W. Moffat and V. T. Toth, "The bending of light and lensing in modified gravity," *MNRAS*, vol. 397, no. 4, pp. 1885–1892, Aug. 2009.

[16] J. Moffat and V. Toth, "Cosmological Observations in a Modified Theory of Gravity (MOG)," *Galaxies*, vol. 1, no. 1, pp. 65–82, Jun. 2013.

[17] J. W. Moffat and V. T. Toth, "The cosmological background and the "external field" in modified gravity (MOG)," *European Physical Journal C*, vol. 81, no. 9, p. 836, Sep. 2021.

[18] J. W. Moffat and V. Toth, "Scalar-Tensor-Vector Modified Gravity in Light of the Planck 2018 Data," *Universe*, vol. 7, no. 10, p. 358, Sep. 2021.

[19] J. W. Moffat and S. Rahvar, "The MOG weak field approximation and observational test of galaxy rotation curves," *MNRAS*, vol. 436, no. 2, pp. 1439–1451, Dec. 2013.

[20] J. W. Moffat and S. Rahvar, "The MOG weak field approximation - II. Observational test of Chandra X-ray clusters," *MNRAS*, vol. 441, no. 4, pp. 3724–3732, Jul. 2014.

[21] J. W. Moffat, "Black holes in modified gravity (MOG)," *European Physical Journal C*, vol. 75, p. 175, Apr. 2015.

[22] J. W. Moffat, "Black holes in modified gravity (MOG)," *European Physical Journal C*, vol. 75, p. 175, Apr. 2015.

[23] J. W. Moffat and V. T. Toth, "Masses and shadows of the black holes Sagittarius A* and M87* in modified gravity," *Phys. Rev. D*, vol. 101, no. 2, p. 024014, Jan. 2020.

[24] S. Rahvar and J. W. Moffat, "Propagation of electromagnetic waves in MOG: gravitational lensing," *MNRAS*, vol. 482, no. 4, pp. 4514–4518, Feb. 2019.

[25] J. Moffat, S. Rahvar, and V. Toth, "Applying MOG to Lensing: Einstein Rings, Abell 520 and the Bullet Cluster," *Galaxies*, vol. 6, no. 2, p. 43, Apr. 2018.

[26] A. Övgün, İ. Sakallı, and J. Saavedra, "Weak gravitational lensing by Kerr-MOG black hole and Gauss-Bonnet theorem," *Annals of Physics*, vol. 411, p. 167978, Dec. 2019.

[27] G. Y. Tuleganova, R. N. Izmailov, R. K. Karimov, A. A. Potapov, and K. K. Nandi, "Times of arrival (TOA) of signals in the Kerr-MOG black hole," *General Relativity and Gravitation*, vol. 52, no. 4, p. 31, Apr. 2020.

[28] R. N. Izmailov, R. K. Karimov, E. R. Zhdanov, and K. K. Nandi, "Modified gravity black hole lensing observables in weak and strong field of gravity," *MNRAS*, vol. 483, no. 3, pp. 3754–3761, Mar. 2019.

[29] J. W. Moffat, "LIGO GW150914 and GW151226 gravitational wave detection and generalized gravitation theory (MOG)," *Physics Letters B*, vol. 763, pp. 427–433, Dec. 2016.

[30] J. W. Moffat and M. H. Zhoolideh Haghighi, "Modified gravity (MOG) and the Abell 1689 cluster acceleration data," *European Physical Journal Plus*, vol. 132, no. 10, p. 417, Oct. 2017.

[31] J. W. Moffat and V. T. Toth, "NGC 1052-DF2 and modified gravity (MOG) without dark matter," *MNRAS*, vol. 482, no. 1, pp. L1–L3, Jan. 2019.

[32] M. A. Green and J. W. Moffat, "Modified Gravity (MOG) fits to observed radial acceleration of SPARC galaxies," *Physics of the Dark Universe*, vol. 25, p. 100323, Sep. 2019.

[33] M. Sharif and M. Shahzadi, "Particle dynamics near Kerr-MOG black hole," *European Physical Journal C*, vol. 77, no. 6, p. 363, Jun. 2017.

[34] H.-C. Lee and Y.-J. Han, "Innermost stable circular orbit of Kerr-MOG black hole," *European Physical Journal C*, vol. 77, no. 10, p. 655, Oct. 2017.

[35] D. Pérez, F. G. L. Armengol, and G. E. Romero, "Accretion disks around black holes in scalar-tensor-vector gravity," *Phys. Rev. D*, vol. 95, no. 10, p. 104047, May 2017.

[36] P. Pradhan, "Study of energy extraction and epicyclic frequencies in Kerr-MOG (modified gravity) black hole," *European Physical Journal C*, vol. 79, no. 5, p. 401, May 2019.

[37] R. Della Monica, I. de Martino, and M. de Laurentis, "Constraining MOdified Gravity with the S2 Star," *Universe*, vol. 8, no. 2, p. 137, Feb. 2022.

[38] R. Della Monica, I. de Martino, and M. de Laurentis, "Orbital precession of the S2 star in Scalar-Tensor-Vector Gravity," *MNRAS*, vol. 510, no. 4, pp. 4757–4766, Mar. 2022.

[39] B. V. Turimov, "Comment on "Orbital precession of the S2 star in scalar-tensor-vector gravity"," *MNRAS*, vol. 516, no. 1, pp. 434–436, Oct. 2022.

[40] R. Della Monica, I. de Martino, and M. de Laurentis, "Response to: Comment on 'Orbital precession of the S2 star in scalar-tensor-vector gravity'," *MNRAS*, vol. 521, no. 1, pp. 474–477, May 2023.

[41] M. Kološ, M. Shahzadi, and Z. Stuchlík, "Quasi-periodic oscillations around Kerr-MOG black holes," *European Physical Journal C*, vol. 80, no. 2, p. 133, Feb. 2020.

[42] J. Rayimbaev, P. Tadjimuratov, A. Abdujabbarov, B. Ahmedov, and M. Khudoyberdieva, "Dynamics of Test Particles and Twin Peaks QPOs around Regular Black Holes in Modified Gravity," *Galaxies*, vol. 9, no. 4, p. 75, Oct. 2021.

[43] G. S. Bisnovatyi-Kogan and O. Y. Tsupko, "Gravitational lensing in a non-uniform plasma," *Mon. Not. R. Astron. Soc*, vol. 404, pp. 1790–1800, Jun. 2010.

[44] B. Turimov, B. Ahmedov, A. Abdujabbarov, and C. Bambi, "Gravitational lensing by a magnetized compact object in the presence of plasma," *International Journal of Modern Physics D*, vol. 28, no. 16, pp. 2 040 013–187, Jan. 2019.

[45] B. Ahmedov, B. Turimov, Z. Stuchlík, and A. Tursunov, "Optical properties of magnetized black hole in plasma," in *International Journal of Modern Physics Conference Series*, ser. International Journal of Modern Physics Conference Series, vol. 49, Jan. 2019, p. 1960018.

[46] P. Schneider, J. Ehlers, and E. E. Falco, *Gravitational Lenses*, 1992.

[47] K. S. Thorne, "Disk-Accretion onto a Black Hole. II. Evolution of the Hole," *Astrophys. Jour.*, vol. 191, pp. 507–520, Jul. 1974.

[48] T. J. Lemmon and A. R. Mondragon, "Alternative derivation of the relativistic contribution to perihelic precession," *American Journal of Physics*, vol. 77, no. 10, pp. 890–893, Oct. 2009.

[49] R. Della Monica, I. de Martino, and M. de Laurentis, "Orbital precession of the S2 star in Scalar-Tensor-Vector Gravity," *MNRAS*, vol. 510, no. 4, pp. 4757–4766, Mar. 2022.

[50] B. Turimov, M. Boboqambarova, B. Ahmedov, and Z. Stuchlík, "Distinguishable feature of electric and magnetic charged black hole," *European Physical Journal Plus*, vol. 137, no. 2, p. 222, Feb. 2022.

[51] R. Della Monica, I. de Martino, and M. de Laurentis, "Constraining MOdified Gravity with the S2 Star," *Universe*, vol. 8, no. 2, p. 137, Feb. 2022.

[52] R. Penrose and R. M. Floyd, "Extraction of Rotational Energy from a Black Hole," *Nature Physical Science*, vol. 229, no. 6, pp. 177–179, Feb. 1971.

[53] N. Dadhich, A. Tursunov, B. Ahmedov, and Z. Stuchlík, "The distinguishing signature of magnetic Penrose process," *MNRAS*, vol. 478, no. 1, pp. L89–L94, Jul. 2018.

[54] M. Bhat, S. Dhurandhar, and N. Dadhich, "Energetics of the Kerr-Newman black hole by the Penrose process," *Journal of Astrophysics and Astronomy*, vol. 6, pp. 85–100, Jun. 1985.

[55] Z. Stuchlík, M. Kološ, and A. Tursunov, "Penrose Process: Its Variants and Astrophysical Applications," *Universe*, vol. 7, no. 11, p. 416, Oct. 2021.

[56] L. Blanchet and T. Damour, "Radiative gravitational fields in general relativity. I. General structure of the field outside the source." *Proceedings of the Royal Society of London Series A*, vol. 320, no. 1555, pp. 379–430, Jan. 1986.

[57] R. P. Fender, T. M. Belloni, and E. Gallo, "Towards a unified model for black hole X-ray binary jets," *Mon. Not. R. Astron. Soc.*, vol. 355, no. 4, pp. 1105–1118, Dec. 2004.

[58] K. Auchettl, J. Guillochon, and E. Ramirez-Ruiz, "New Physical Insights about Tidal Disruption Events from a Comprehensive Observational Inventory at X-Ray Wavelengths," *Astrophys. J.*, vol. 838, no. 2, p. 149, Apr. 2017.

[59] The IceCube Collaboration and et al., "Multimessenger observations of a flaring blazar coincident with high-energy neutrino IceCube-170922A," *Science*, vol. 361, no. 6398, p. eaat1378, Jul. 2018.

[60] M. Bañados, J. Silk, and S. M. West, "Kerr Black Holes as Particle Accelerators to Arbitrarily High Energy," *Phys. Rev. Lett.*, vol. 103, no. 11, p. 111102, Sep. 2009.

[61] T. Jacobson and T. P. Sotiriou, "Spinning Black Holes as Particle Accelerators," *Phys. Rev. Lett.*, vol. 104, no. 2, p. 021101, Jan. 2010.

[62] K. Lake, "Particle Accelerators inside Spinning Black Holes," *Phys. Rev. Lett.*, vol. 104, no. 21, p. 211102, May 2010.

[63] M. Kimura, K.-i. Nakao, and H. Tagoshi, "Acceleration of colliding shells around a black hole: Validity of the test particle approximation in the Banados-Silk-West process," *Phys. Rev. D*, vol. 83, p. 044013, 2011.

[64] O. B. Zaslavskii, "Acceleration of particles as a universal property of rotating black holes," *Phys. Rev. D*, vol. 82, no. 8, p. 083004, Oct. 2010.

[65] O. B. Zaslavskii, "Acceleration of particles by nonrotating charged black holes?" *Soviet Journal of Experimental and Theoretical Physics Letters*, vol. 92, no. 9, pp. 571–574, Nov. 2010.

[66] F. Atamurotov, B. Ahmedov, and S. Shaymatov, "Formation of black holes through BSW effect and black hole-black hole collisions," *Astrophys. Space Sci.*, vol. 347, pp. 277–281, Oct. 2013.

[67] O. B. Zaslavskii, "Acceleration of particles by black holes: Kinematic explanation," *Phys. Rev. D*, vol. 84, no. 2, p. 024007, Jul. 2011.

[68] O. B. Zaslavskii, "Acceleration of particles by black holes—a general explanation," *Classical and Quantum Gravity*, vol. 28, no. 10, p. 105010, May 2011.

[69] A. A. Grib and Y. V. Pavlov, "On particle collisions in the gravitational field of the Kerr black hole," *Astroparticle Physics*, vol. 34, no. 7, pp. 581–586, Feb. 2011.

[70] A. A. Grib and Y. V. Pavlov, "On particle collisions near rotating black holes," *Gravitation and Cosmology*, vol. 17, no. 1, pp. 42–46, Jan. 2011.

[71] M. Patil and P. S. Joshi, "Naked singularities as particle accelerators," *Phys. Rev. D*, vol. 82, no. 10, p. 104049, Nov. 2010.

[72] M. Patil, P. S. Joshi, and D. Malafarina, "Naked singularities as particle accelerators. II." *Phys. Rev. D*, vol. 83, no. 6, p. 064007, Mar. 2011.

[73] M. Patil and P. S. Joshi, "High energy particle collisions in superspinning Kerr geometry," *Phys. Rev. D*, vol. 84, no. 10, p. 104001, Nov. 2011.

[74] M. Patil and P. Joshi, "Kerr naked singularities as particle accelerators," *Classical and Quantum Gravity*, vol. 28, no. 23, p. 235012, Dec. 2011.

[75] T. Harada and M. Kimura, "Collision of two general geodesic particles around a Kerr black hole," *Phys. Rev. D*, vol. 83, no. 8, p. 084041, Apr. 2011.

[76] T. Harada and M. Kimura, "Collision of an object in the transition from adiabatic inspiral to plunge around a Kerr black hole," *Phys. Rev. D*, vol. 84, no. 12, p. 124032, Dec. 2011.

[77] S. Shaymatov, B. Narzilloev, A. Abdujabbarov, and C. Bambi, "Charged particle motion around a magnetized Reissner-Nordström black hole," *Phys. Rev. D*, vol. 103, no. 12, p. 124066, Jun. 2021.

[78] A. Abdujabbarov, B. Ahmedov, and B. Ahmedov, "Energy extraction and particle acceleration around a rotating black hole in Hořava-Lifshitz gravity," *Phys. Rev. D*, vol. 84, no. 4, p. 044044, Aug. 2011.

[79] P.-J. Mao, R. Li, L.-Y. Jia, and J.-R. Ren, "Acceleration of particles in Einstein-Maxwell-dilaton black holes," *Chinese Physics C*, vol. 41, no. 6, p. 065101, Jun. 2017.

[80] Y. Li, J. Yang, Y.-L. Li, S.-W. Wei, and Y.-X. Liu, "Particle acceleration in Kerr-(anti-)de Sitter black hole backgrounds," *Classical and Quantum Gravity*, vol. 28, no. 22, p. 225006, Nov. 2011.

[81] M. Amir and S. G. Ghosh, "Rotating Hayward's regular black hole as particle accelerator," *Journal of High Energy Physics*, vol. 2015, p. 15, Jul. 2015.

[82] M. Khurshudyan, N. S. Mazhari, D. Momeni, R. Myrzakulov, and M. Raza, "Observational Constraints on Models of the Universe with Time Variable Gravitational and Cosmological Constants Along MOG," *Int. J. Theor. Phys.*, vol. 54, no. 2, pp. 484–505, Feb. 2015.

[83] J. Rayimbaev and P. Tadjimuratov, "Can modified gravity silence radio-loud pulsars?" *Physical. Rev. D*, vol. 102, no. 2, p. 024019, Jul. 2020.

[84] A. Tursunov, Z. Stuchlík, M. Kološ, N. Dadhich, and B. Ahmedov, "Supermassive Black Holes as Possible Sources of Ultrahigh-energy Cosmic Rays," *Astrophys. J*, vol. 895, no. 1, p. 14, May 2020.

[85] M. Bañados, J. Silk, and S. M. West, "Kerr Black Holes as Particle Accelerators to Arbitrarily High Energy," *Phys. Rev. Lett.*, vol. 103, no. 11, p. 111102, Sep. 2009.

[86] B. Turimov and S. Hayitov, "Black Holes as a Collider of High Energy Particles," *arXiv e-prints*, p. arXiv:2307.01919, Jul. 2023.

[87] J. D. Jackson and R. F. Fox, "Classical Electrodynamics, 3rd ed." *American Journal of Physics*, vol. 67, no. 9, pp. 841–842, Sep. 1999.

[88] P. A. M. Dirac, "Classical Theory of Radiating Electrons," *Proceedings of the Royal Society of London Series A*, vol. 167, no. 929, pp. 148–169, Aug. 1938.

[89] L. D. Landau and E. M. Lifshitz, *The Classical Theory of Fields, Course of Theoretical Physics, Volume 2.* Oxford: Elsevier Butterworth-Heinemann, 2004.

[90] A. Tursunov, M. Kološ, Z. Stuchlík, and D. V. Gal'tsov, "Radiation Reaction of Charged Particles Orbiting a Magnetized Schwarzschild Black Hole," *ApJ*, vol. 861, no. 1, p. 2, Jul. 2018.

[91] A. A. Tursunov, M. Kološ, and Z. Stuchlík, "Orbital widening due to radiation reaction around a magnetized black hole," *Astronomische Nachrichten*, vol. 339, no. 5, pp. 341–346, Jun. 2018.

[92] A. A. Shoom, "Synchrotron radiation from a weakly magnetized Schwarzschild black hole," *Phys. Rev. D*, vol. 92, no. 12, p. 124066, Dec. 2015.

[93] T. Damour and N. Deruelle, "Radiation reaction and angular momentum loss in small angle gravitational scattering," *Physics Letters A*, vol. 87, no. 3, pp. 81–84, Dec. 1981.

[94] T. Damour, "Gravitational Radiation Reaction in the Binary Pulsar and the Quadrupole-Formula Controversy," *Phys. Rev. Lett.*, vol. 51, no. 12, pp. 1019–1021, Sep. 1983.

[95] C. Cutler, D. Kennefick, and E. Poisson, "Gravitational radiation reaction for bound motion around a Schwarzschild black hole," *Phys. Rev. D*, vol. 50, no. 6, pp. 3816–3835, Sep. 1994.

[96] B. Turimov, H. Alibekov, P. Tadjimuratov, and A. Abdujabbarov, "Gravitational synchrotron radiation and penrose process in stvg theory," *Phys. Lett. B*, vol. 843, p. 138040, 2023.

[97] L. Manfredi, J. Mureika, and J. Moffat, "Quasinormal Modes of Static Modified Gravity (MOG) Black Holes," in *Journal of Physics Conference Series*, ser. Journal of Physics Conference Series, vol. 942, Dec. 2017, p. 012014.

[98] L. Manfredi, J. Mureika, and J. Moffat, "Quasinormal modes of modified gravity (MOG) black holes," *Physics Letters B*, vol. 779, pp. 492–497, Apr. 2018.

[99] L. Manfredi, J. Mureika, and J. Moffat, "Quasinormal Modes of Modified Gravity (MOG) Black Holes," *Journal of Undergraduate Reports in Physics*, vol. 29, no. 1, p. 100006, Jan. 2019.

[100] S. Capozziello, C. A. Mantica, and L. G. Molinari, "General properties of f(R) gravity vacuum solutions," *International Journal of Modern Physics D*, vol. 29, no. 13, p. 2050089, Jan. 2020.

[101] F. Bajardi, R. D'Agostino, M. Benetti, V. De Falco, and S. Capozziello, "Early and late time cosmology: the f(R) gravity perspective," *European Physical Journal Plus*, vol. 137, no. 11, p. 1239, Nov. 2022.

[102] J. W. Moffat and V. T. Toth, "Fundamental parameter-free solutions in modified gravity," *Classical and Quantum Gravity*, vol. 26, no. 8, p. 085002, Apr. 2009.

[103] M. Kološ, A. Tursunov, and Z. Stuchlík, "Radiative Penrose process: Energy gain by a single radiating charged particle in the ergosphere of rotating black hole," *Phys. Rev. D*, vol. 103, no. 2, p. 024021, Jan. 2021.

[104] B. Turimov, A. Nosirov, and A. Abdujabbarov, "Gravitational analogue of radiation reaction in STVG," *Phys. Dark Univ.*, vol. 42, p. 101375, 2023.

[105] E. Poisson, "The Motion of Point Particles in Curved Spacetime," *Living Reviews in Relativity*, vol. 7, no. 1, p. 6, May 2004.

[106] B. P. Abbott *et al.*, "Observation of Gravitational Waves from a Binary Black Hole Merger," *Phys. Rev. Lett.*, vol. 116, no. 6, p. 061102, 2016.

[107] E. Berti, V. Cardoso, and A. O. Starinets, "Quasinormal modes of black holes and black branes," *Class. Quant. Grav.*, vol. 26, p. 163001, 2009.

[108] B. F. Schutz and C. M. Will, "Black hole normal modes - A semianalytic approach," *apjl*, vol. 291, pp. L33–L36, Apr. 1985.

[109] H.-J. Blome and B. Mashhoon, "Quasi-normal oscillations of a schwarzschild black hole," *Phys. Lett. A*, vol. 100, no. 5, pp. 231–234, 1981.

[110] C. M. Bender and T. T. Wu, "Anharmonic oscillator," *Phys. Rev.*, vol. 184, pp. 1231–1260, 1969.

[111] T. Sulejmanpasic and M. Ünsal, "Aspects of perturbation theory in quantum mechanics: The BenderWu Mathematica ® package," *Comput. Phys. Commun.*, vol. 228, pp. 273–289, 2018.

[112] Y. Hatsuda, "Quasinormal modes of black holes and Borel summation," *Phys. Rev. D*, vol. 101, no. 2, p. 024008, 2020.

[113] T. Regge and J. A. Wheeler, "Stability of a Schwarzschild Singularity," *Physical Review*, vol. 108, no. 4, pp. 1063–1069, Nov. 1957.

[114] F. J. Zerilli, "Effective potential for even parity Regge-Wheeler gravitational perturbation equations," *Phys. Rev. Lett.*, vol. 24, pp. 737–738, 1970.

[115] S. A. Teukolsky, "Rotating black holes - separable wave equations for gravitational and electromagnetic perturbations," *Phys. Rev. Lett.*, vol. 29, pp. 1114–1118, 1972.

[116] C. V. Vishveshwara, "Stability of the schwarzschild metric," *Phys. Rev. D*, vol. 1, pp. 2870–2879, 1970.

[117] W. H. Press, "Long Wave Trains of Gravitational Waves from a Vibrating Black Hole," *apjl*, vol. 170, p. L105, Dec. 1971.

[118] J. R. Mureika, J. W. Moffat, and M. Faizal, "Black hole thermodynamics in MOdified Gravity (MOG)," *Physics Letters B*, vol. 757, pp. 528–536, Jun. 2016.

[119] M. A. Green, J. W. Moffat, and V. T. Toth, "Modified gravity (MOG), the speed of gravitational radiation and the event GW170817/GRB170817A," *Physics Letters B*, vol. 780, pp. 300–302, May 2018.

[120] M. F. Wondrak, P. Nicolini, and J. W. Moffat, "Superradiance in modified gravity (MOG)," *JCAP*, vol. 2018, no. 12, p. 021, Dec. 2018.

[121] X. Qiao, M. Wang, Q. Pan, and J. Jing, "Kerr-MOG black holes with stationary scalar clouds," *European Physical Journal C*, vol. 80, no. 6, p. 509, Jun. 2020.

[122] J. W. Moffat, "Modified gravity (MOG), cosmology and black holes," *JCAP*, vol. 2021, no. 2, p. 017, Feb. 2021.

[123] K. Düztaş, "Overspinning Kerr-MOG black holes by test fields and the third law of black hole dynamics," *European Physical Journal C*, vol. 80, no. 1, p. 19, Jan. 2020.

[124] A. G. Abac *et al.*, "GW250114: Testing Hawking's Area Law and the Kerr Nature of Black Holes," *Phys. Rev. Lett.*, vol. 135, no. 11, p. 111403, 2025.

[125] H. Beauchesne and A. Edery, "Black hole free energy during charged collapse: a numerical study," *Journal of High Energy Physics*, vol. 2012, p. 146, May 2012.

[126] I. Aref'eva and I. Volovich, "Complete evaporation of black holes and page curves," *Symmetry*, vol. 15, no. 1, 2023. [Online]. Available: https://www.mdpi.com/2073-8994/15/1/170

[127] R. A. Konoplya, "Quasinormal behavior of the d-dimensional Schwarzschild black hole and higher order WKB approach," *Phys. Rev. D*, vol. 68, p. 024018, 2003.